A NEW BIOMATERIAL FOR VACCINATION: AN AQUEOUS ZIF-8 CRYSTAL

GROWTH TO PRESERVE ANTIGENS AND ENHANCE THE IMMUNE ACTIVATION

by

Michael Andrew Luzuriaga

APPROVED BY SUPERVISORY COMMITTEE:

_____
Dr. Jeremiah J. Gassensmith, Chair

_____
Dr. Sheena D'Arcy

_____
Dr. Ronald Smaldone

_____
Dr. Jung-Mo Ahn

For my wife Erika Calubaquib, for understanding this difficult journey. To my family and friends, for sticking by me throughout the years.

A NEW BIOMATERIAL FOR VACCINATION: AN AQUEOUS ZIF-8 CRYSTAL

GROWTH TO PRESERVE ANTIGENS AND ENHANCE THE IMMUNE ACTIVATION

by

MICHAEL ANDREW LUZURIAGA. BS

DISSERTATION

Presented to the Faculty of

The University of Texas at Dallas

in Partial Fulfillment

of the Requirements

for the Degree of

DOCTOR OF PHILOSOPHY IN

CHEMISTRY

THE UNIVERSITY OF TEXAS AT DALLAS

December 2020

ACKNOWLEDGMENTS

A NEW BIOMATERIAL FOR VACCINATION: AN AQUEOUS ZIF-8 CRYSTAL

GROWTH TO PRESERVE ANTIGENS AND ENHANCE THE IMMUNE ACTIVATION

Michael Andrew Luzuriaga, PhD
The University of Texas at Dallas, 2020

Supervising Professor: Jeremiah J. Gassensmith

Biomaterials encompass a broad range of applications for medical treatment and can be on the macroscale, such as heart valves or hip implants, to the microscale and nanoscale, such as stitches, dental fillings or particles for drug delivery. For the last thirty years, biomaterials with sustained release properties have been investigated as a method to improve the delivery of vaccines. Vaccines are considered one of the most significant inventions in the human history, as it has prevented hundreds of millions of deaths since its invention and is the main cause for extending the human life expectancy. However, a major issue with current methods of vaccination is their low stability at room temperature and the requirement for multiple injections to produce an immune response strong enough to develop long-term memory. For these reasons, the "cold chain" infrastructure keeps them refrigerated from manufacturer to clinic, ensuring the epitopes in the proteinaceous vaccines do not unfold. Any failures in this process can lead to the loss of billions of dollars and, even with this system, the proteinaceous material will denature over time. On top of that, the necessity of multiple injections to provide immunity it is clear how heavily we rely on the cold chain. To solve these issues, biomaterials with sustained release properties has been

employed to "cage" proteins within a stabilizing polymer network that prevents conformational changes and enables storage at room temperature. Herein, methods to encapsulate proteinaceous material under aqueous conditions within zeolitic imidazole framework-8 (ZIF-8), a well-studied metal organic framework, is investigated for it's ability to activate the immune system in mice and protect vaccines from denaturation.

TABLE OF CONTENTS

LIST OF FIGURES

LIST OF TABLES

CHAPTER 1

SUSTAINED RELEASE BIOMATERIALS IN VACCINATION: A SINGLE DOSE DEFENSE AGAINST INFECTIOUS DISEASES

Authors – Michael A. Luzuriaga[†], Arezoo Shahrivarkevishahi, Fabian C. Herbert, Yalini H. Wijesundara, Jeremiah J. Gassensmith*

The Department of Chemistry and Biochemistry, BSB13.102

The University of Texas at Dallas

800 West Campbell Road

Richardson, Texas 75080-3021

1.1   Introduction

Every year, infectious diseases cause millions of deaths worldwide making it the third leading cause of death after cardiovascular disease (**Figure 1.1A-B**).[1] Presently, our society is dealing with the COVID-19 pandemic, which at the time of this writing has claimed 1 million lives and remains on a worrying trajectory as the pandemic continues. Efforts to control the pandemic have focused on developing prophylactic vaccines and every possible approach to create an effective drug is being pursued. This pandemic is unique in *recent* human history in its expanse and severity; however, some of the worst pandemics in human history have resulted in the deaths of millions of people worldwide and vaccines are credited with significantly extending human lifespans by reducing the voracity of disease spread.[2-4] Vaccination was first described in 1796 by Edward Jenner, who experimentally proved that immunity against the deadly disease smallpox was created by inoculating a person with cowpox—a similar, but less virulent virus.[5, 6] This discovery provided a pathway to produce other vaccines that have either greatly mitigated or eradicated several deadly diseases, including measles, tetanus, diphtheria, and poliovirus.[7] Still, 300 years after the first vaccination, vaccines continue to be complicated therapeutics to create and distribute. Vaccination relies of the production of a robust immunological response that is otherwise triggered by an actual invading organism and a key developmental hurdle is trying to engender that same immunological response with non-infectious agents that are both potent yet not reactogenic. Further, vaccines are some of the most thermally sensitive drugs on the planet and demand complex and expensive infrastructure that maintains cryogenic temperatures for their deployment from manufacturer to clinic. [8-12]
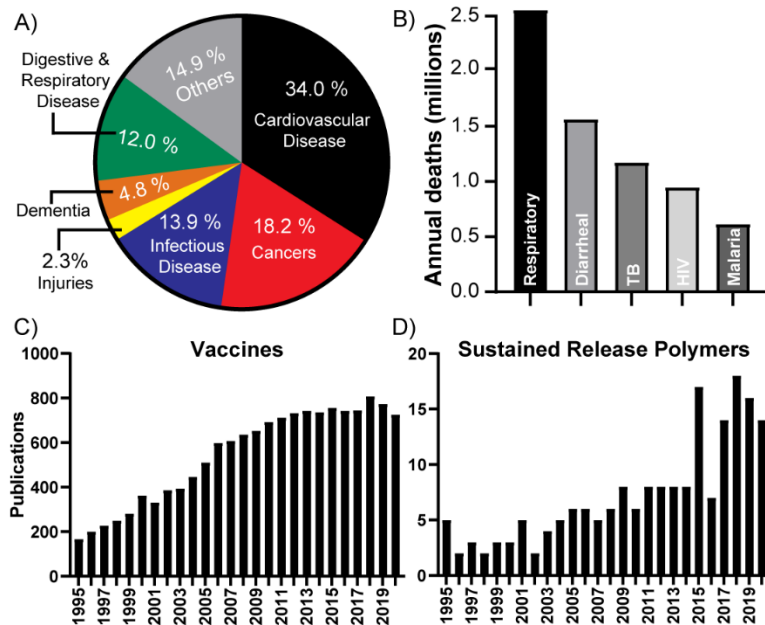
Figure 1.1: A pie chart showing in percentages the A) leading causes of death worldwide and B) the number of deaths by the leading causes of deaths by infectious diseases for 2017. The number of publications published from 1995 – 2020 with the key word being C) vaccine refined to journals, letters, and reports, with additional refinement for *in vivo* and D) polymer vaccine or sustained release vaccine refined to journals, letters, and reports, specifically regarding *in vivo* work. Note: 2020 publications were checked on October 15, 2020.

Vaccines protect individuals by developing immunological memory, so when the body encounters a foreign pathogen, an immediate and proportional adaptive response against that pathogen begins before it can reproduce and cause systemic damage. The immune response to an infectious agent follows two broadly defined phases: an initial innate response followed by an adaptive response. The initial response occurs when the cellular vanguards of the immune system—neutrophils, macrophages, monocytes, or immature dendritic cells—recognize pathogen-associated molecular patterns (PAMPs) on a foreign invader using pattern recognition receptors (PRRs) on their cellular surfaces. This allows these cells to verify that what it has encountered as potentially dangerous. If it is indeed a foreign substance, the cell will consume the material via phagocytosis and release signaling chemicals called chemokines and cytokines that recruit additional cells and induce the

physical symptoms of local inflammation to indicate infection. Some of these cells will differentiate into antigen presenting cells (APCs) and will migrate to the T-cell region of the draining lymph node, where they will initiate the second phase of the immune response, the adaptive response.[13, 14]

The adaptive response and development of immune memory for rapid response to previously vaccinated antigen depends upon an important interplay between T-cells and the rest of the immune system. CD4+ cells are only able to determine if an antigen is foreign or not if they were presented with the antigen by an APC that was activated in the initial infection or vaccination. From there, the activated CD4+ cells that have become memory CD4+ cells will no longer need activation from APCs during a second encounter with the infection, thus being able to mount a faster and stronger immune response. Clearing a pathogen, however, requires the immune system to respond in a number of different ways. The adaptive immunity is most commonly divided into two major systems: the first is the cellular-mediated response, which is characterized primarily by T helper 1 CD4+ cells, which activate cytotoxic CD8+ T-cells, and this system can police human cells that might be harboring infectious pathogens. It is thought that vaccines that target tuberculosis, cancer, and HIV will need to focus primarily on developing a strong cellular response. The other system produces a humoral response, characterized by T helper 2 CD4+ cells, which activate B-cells and plasma cells to secrete antibodies. There are several different types of antibodies, each serving specific purposes, but most vaccines focus on producing neutralizing IgG-type antibodies that can bind tightly to the surface of a pathogen to either block it from entering cells and/or to flag it as a foreign invader that should be destroyed. This latter route has been the focus of the vast majority of vaccines, including those for COVID-19 and urinary tract infections; indeed, most successful vaccine development has largely focused on this latter route.

Differentiating between foreign and self-proteins is one of the most critical parts of adaptive immunity, and this differentiation is often made by assessing the surface antigens that are displayed on the outside of a pathogen. Therefore, vaccine development has historically involved identifying the most immune stimulating aspect of a pathogen and presenting it to the immune system, with

the hope that the immune system will be able to mount the correct type of immune response. Three such formulations are frequently employed—live attenuated, inactivated, and subunit vaccines. Live attenuated vaccines are "living" relatives of the infectious organism that produce no or only mild symptoms yet are capable of instigating a protective immunity against a dangerous pathogen. At issue, however, is that live attenuated vaccine might replicate too rapidly for elderly or immune compromised patients and have the potential to mutate back to a virulent form, leading to severe complications.[15-18] The alternative to a live pathogen to use an inactivated pathogen that has been rendered non-reproductive (or dead) through either heat or chemical crosslinking. Alternatively, the exterior antigens can be removed or purified or genetically engineered onto the surface of a nanoparticle so as to fool the immune system into producing antibodies that bind specifically to that antigen. In both cases, inactivation or subunit vaccines are considered to be safer than inactivated vaccine systems[19-21] although both approaches frequently fail to induce a strong immune response on their own even after multiple injections, meaning they may not provide any protection against the actual disease and usually require an adjuvants in order to promote a robust immune response.[22, 23] The use of adjuvants have been a way to steer the type of response the immune system has. As the current method to determine how long a vaccine retains protection against a disease is whether the host still produces antibodies against the disease.[24-26] A better way to answer this question is to determine what immune cells need to be activated in the adaptive immune system to guarantee long-lasting protection.

The ideal 21st century vaccine should be a safe, patient-friendly, and stable enough such that it can be stored at ambient conditions and provide long-term immunity after one administration. Biomaterials have been investigated for the last three decades as strong candidates to enhance vaccinations and improve the stability of proteins. Several studies have been published that investigate biomaterials as a tool to preserve proteins for long periods of time at room temperature by either attaching[27, 28] functional groups that prevent water loss or by encapsulation[29-31] to prevent unfolding, which would eliminate the need for the cold chain. We found that, in the last 25 years, there have been a lot of publications for vaccinations that have or mention *in vivo* (**Figure 1.1C**) and it is clear from **Figure 1.1 D**, that biomaterials with sustained release for vaccinations is a new

area gaining traction. This review will focus on biomaterials that provide sustained release and have been mainly investigated *in vivo.*

1.2   Types of Biomaterials

Vaccine development has made remarkable progress since 1791, when Edward Jenner developed the first vaccine for smallpox.[32] Since then, safer vaccine designs have emerged. For example, inactivated/live-attenuated pathogens formulations,[33] subunit vaccines,[34] immunogenic epitopes,[35] and inclusion of different classes of adjuvants[36] have significantly improved long-term immunological memory by generating higher antibody titers, while reducing severe side effects.[37] However, many challenges remain associated with low stability, inefficient delivery, poor selectivity, and inability to translate into humans.[38] For the past three decades, biomaterial-based technologies such as synthetic and natural polymers, lipids, scaffolds, microneedles, and other particle-carriers have emerged rapidly to improve vaccine efficacy, safety, and stability.[39, 40] Biomaterials offer a unique design strategy of carrier/adjuvant for immune cargos loading, protection, modification, and administration to control targeted delivery, minimizing number of injections, and reducing systemic and local toxicity.[41-43] In this section, we discuss biomaterials with excellent biocompatibility, biodegradability, and chemical modifiability that make them ideal candidates for controlled release vaccine delivery system.

1.2.1   Synthetic biodegradable polymers

Synthetic polyesters including poly(lactic acid) (PLA), poly(lactic-co-glycolic acid) (PLGA), polyurethane (PU), and poly(ε-caprolactone) (PCL) are the most widely studied biodegradable polymers in the biomedical and vaccine field.[44-50] They have shown favorable physiochemical properties including high biocompatibility, tunable hydro/lipophilicity, high antigen loading, and sustained cargo release for *in vivo* applications.[42, 51, 52] They also can be designed in different shapes with various surface chemistries to provide selective cell targeting delivery (*e.g.* APCs) and showing switchable and stimuli responsive behavior in cargo release.[53-55] Flexibility of polyester

based vaccine platforms in method of antigen encapsulation (*e.g.* single and double emulsion solvent evaporation, nanopercipitation, and spray drying) and route of administration (*e.g.* dermal, intranasal and subcutaneous) provides a selection of formulations that can enhance the immune response activation. Among the polyester materials, PLGA copolymers are considered promising FDA approved sustained release vaccine delivery vehicles for both antigen and adjuvant thanks to their excellent safety profile.[56, 57] Although PLGA is one of the most studied biomaterials and has had several studies to understand the effects of surface charge,[58, 59] injection interval,[60] and administration route,[61] it wasn't until 2017 that particle size was considered in activating the immune system by the Guanghai lab.[62] PLGA (molar ratio for lactide/glycolide = 75:25, Mw ≈ 13000 Da) particles were formulated using an oil in water technique to obtain particle sizes at 500 nm, 900 nm, 2.1 µm and 4.9 µm, all having a similar negative surface charge (**Figure 1.2A**). Each particle was mixed with 25 µg of ovalbumin and injected intramuscularly twice at two-week intervals. While each size showed good cell viability, uptake, and overall good immune activation compared to the antigen alone, the 900 nm particle proved to perform the best in production of antibodies and cytokine compared to the other particle sizes owing to the enhanced uptake in macrophage. This study shows there are still many variables even for well-known materials to be tested in vaccine development, like surface charge, dosage, interval of injections, molecular weight or polymer ratio, in addition to particle size has on activating the immune system. Despite the successful immunization seen *in vivo*, PLGA particles along with other polyesters face several major limitations including production of local acidic environment following hydrolysis and using harsh synthesis condition such as toxic organic solvent and high temperatures. These limitation can lead to protein denaturation, reduction in encapsulation efficiency, and harm to patients when the organic solvent isn't removed before injection, which has led researchers to look towards alternative biomaterials.
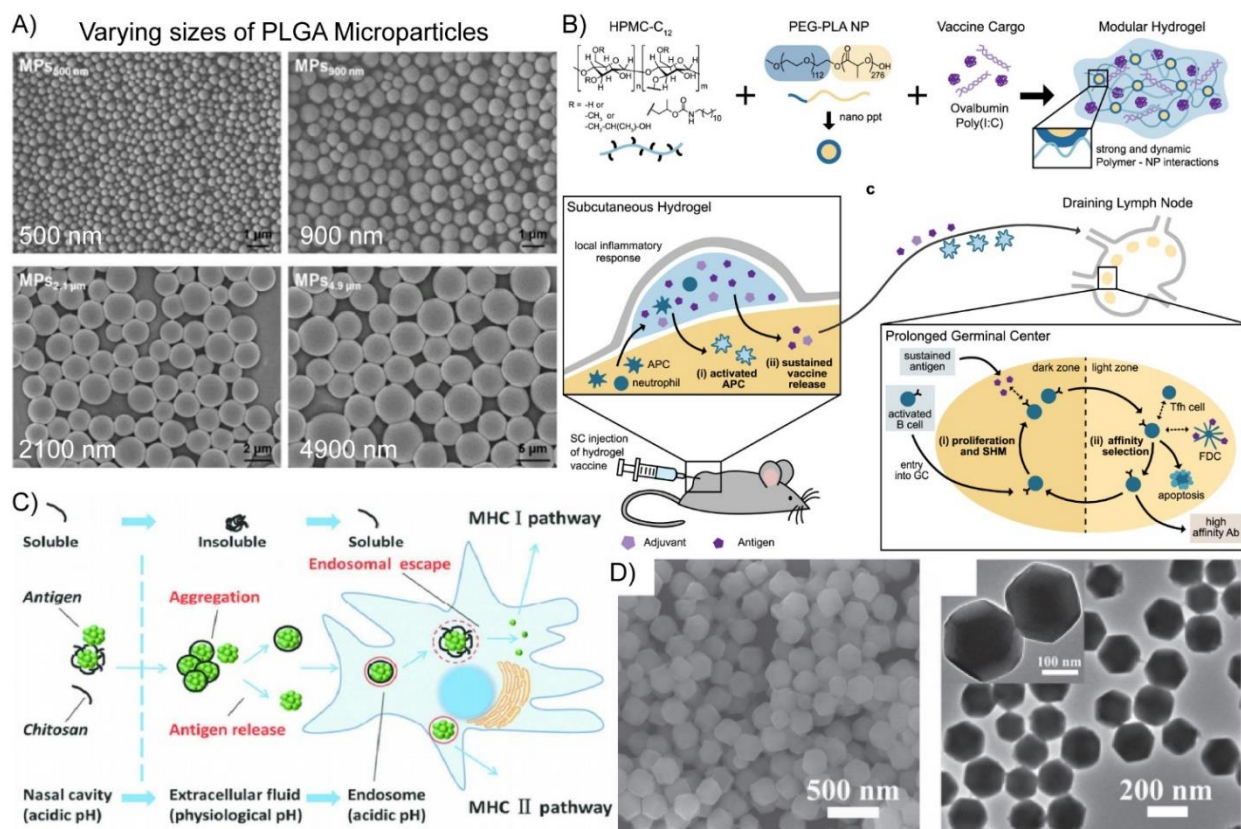
Figure 1.2: A) SEM images of different PLGA particle sizes tested by the Guanghai lab to determine the effects it has on activating the immune system. B) The Appel Lab formulated different hydrogels to tune the release and determine the activation of the germinal center in the draining lymph node. Reprinted from reference [62] and [63] with permission from American Chemical Society Copyright 2017 and Copyright 2020. C) The Xu lab investigate chitosan with antigen to evaluate it as a potential adjuvant and determine the mechanism of immune activation. Republished with permission from Royal Society of Chemistry for reference [64]; permission conveyed through Copyright Clearance Center, Inc. D) SEM and TEM images after ZIF-8 was grown in methanol to encapsulate ovalbumin stabilized with PVP + CPG, which the Qu lab showed can improve the immune activation compared to a bolus shot of ovalbumin + CPG. Reprinted with permission from John Wiley and Sons for reference [65] Copyright 2016.

1.2.2 Natural Material

Natural materials, such as chitosan,[66, 67] hyaluronic acid,[68] starch,[69] cellulose,[70] and alginate[71, 72] offer renewable resources for controlled vaccine delivery system. Major properties that have attracted researchers to natural materials are their good water solubility, ease of preparation, and simple chemical modification. In addition, these biologically assembled particles have led to development of effective oral and intranasal vaccine administration that have advantages over parenteral injection such as patient compliance and convenience of at-home self-care vaccination.[73, 74] Among the natural materials, chitosan has been studied heavily and evaluated in humans for the potential use in vaccination against infectious diseases owing to its high safety and ease of clearance.[75-77] Twenty years of research has shown chitosan significantly enhances APCs uptake through electrostatic interaction owing to its positively charged nitrogens and can be combined with other biomaterials (*e.g.* PLGA) to synergistically enhance immune activation.[78-80] However, the mechanism by which chitosan enhances an immune response wasn't investigated until 2016 by the Xu Lab.[64] For this study, they used hepatitis B antigen and mixed it with acid-soluble chitosan for *in vitro* and *in vivo* adjuvant mechanistic evaluation. Their study showed that the intranasal delivery of chitosan mixed with antigens involves a depot effect produced by insoluble chitosan at physiological pH found in the extracellular fluid, whereas in lower pH found in lysosomes they are able to facilitate escape of the encapsulated antigen, which is schematically shown in **Figure 1.2C**. This was corroborated *in vitro* with higher dendritic cell activation and *in vivo* with improved cell mediated activation. Again, this study shows the importance of understanding the biomaterial properties first. As it is possible that adjuvants may not even be needed for some of these sustained release biomaterials and could be sufficient alone with antigen to produce single shot vaccines.

1.2.3 Others

Hydrogels and metal-organic frameworks that are biocompatible are other biomaterials that have been used for drug delivery that fall in between both synthetically made and naturally produced materials.[81-85] A major advantage of these materials are their ability to self-assemble with antigens

under aqueous conditions as well as their availability for post-synthetic modifications.[86-88] Given the infancy of these materials in immunology, correlation between immunogenicity and parameters such as size or antigen dosage are yet to be addressed. In some cases, biomaterials have not been studied alone, meaning only with antigen and without any adjuvants, to determine any immune enhancement. Most studies will mix the biomaterial with adjuvant + antigen to show that the system all together can initiate a stronger immune response. For example, an excellent study by the Appel Lab investigated the encapsulation of ovalbumin and Poly(I:C), a toll-like receptor 3 agonist, using different formulated hydrogels.[63] The hydrogels were composed of PEG-PLA nanoparticles and hydroxypropylmethylcellulose derivatives at different ratios. The focus of the paper was to show an improve immunogenic response compared to free ova and adjuvant, showing the 2:10 slower delivery prolonged germinal center activation (**Figure 1.2B**) and produced a better overall humoral response compared to the bolus and 1:5 injections. However, the investigation of the hydrogel alone with ova without adjuvant was not tested, nor was the toxicity, dosage and length between each injection and the effects this could have on the immune response. In 2016, the Qu lab encapsulated ovalbumin within ZIF-8, then mixed it with a solution of CpG. The ZIF-8 was grown in methanol and PVP was used to help stabilize the ovalbumin under these conditions (**Figure 1.2D**).[65] They showed that ZIF-8 would release less than 20% of antigen when incubated in pH 7.4 PBS buffer and would release ~90 % of the antigen after 2 h when the pH went down to 6, stating the antigen would only release after endocytosis. They injected mice subcutaneously and showed their system could enhance the immune activation compare to free ovalbumin + CpG, but did not look at ovalbumin encapsulated within ZIF without CpG. Further research by the Gassensmith lab showed a method to encapsulate a whole virus within ZIF-8 under aqueous conditions and the antigen could be released when incubated in serum.[89, 90] The subcutaneous injection corroborates the slow release in serum that ZIF slowly release particles from within to develop a strong humoral response. This study was interesting because they showed a more stable method to encapsulate antigens and showed that the biomaterial could enhance the immune system without the need of the adjuvant. However, ZIF-8 formulations have not been studied to determine how particle size, dosage, and surface modification affect the immune activation. The dissection of these biomaterials and newly developed polymer system that

offer sustained release attributes need to be further investigated, specifically on the tuning of size, charge, dosage, and frequency of injections the biomaterial itself has on the activation of the immune system.

1.3 The Interaction between Antigen and Biomaterial

Weak immunogenicity and short-term stability are some limitations associated with subunit antigens, where a common solution to overcome these is to use biomaterials as delivery/protection vehicles.[91-93] Biomaterials can be a host that stabilizes antigens against denaturing conditions (*e.g.* absence of refrigeration), can be tailored to achieve different types of release profiles (*e.g.* sustained and pulsatile), can augment the desired immune activation, and in some cases can provide lifetime immunity from a single dose.[94] However, a major challenge associated with their usage is formulation of antigen/biomaterial to achieve optimal therapeutic efficacy. **Figure 1.3** portrays several antigen/biomaterial interaction approaches developed over the years. Below, we discuss some of the forces driving such interactions and their performance when injected in murine models.
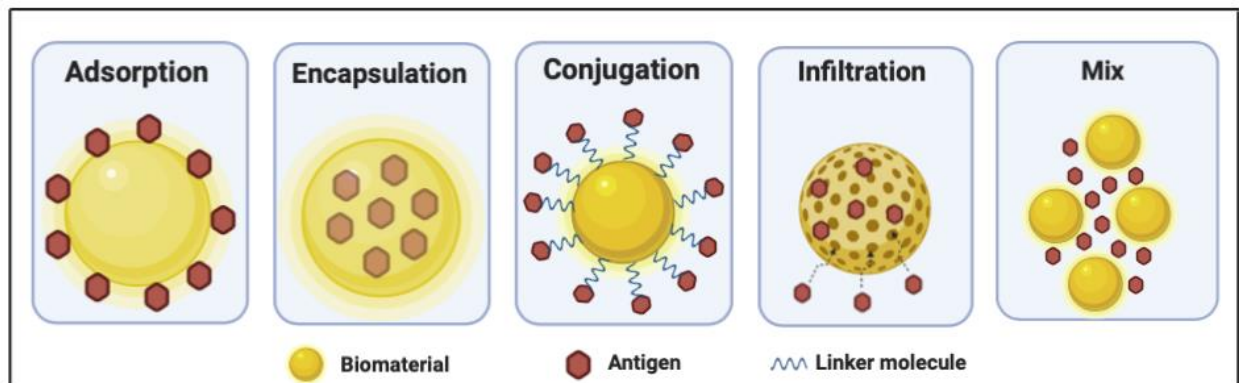
Figure 1.3: A schematic of different ways biomaterials interact with antigens

1.3.1 Interaction and Release

The interaction between the antigen and biomaterial can be broadly classified into five categories; surface adsorption, mixing, encapsulation, conjugation, and infiltration.[95] Surface adsorption for example, is fully driven by electrostatic or hydrophilic/hydrophobic interactions leading to weak attachment of the antigen to the surface of the biomaterial. Thus, when tested *in vivo,* the composite readily dissociates exhibiting a burst release kinetics profile.[96] Differently, conjugation relies on chemical crosslinking of the antigen to the biomaterial. Release is achieved through biomaterial decomposition either intracellularly or extracellularly. Further, this interaction is mostly used to improve immunogenicity.[97] Encapsulation is achieved through mixing the antigen and precursors of the biomaterial during synthesis.[98] Antigens encapsulated get gradually released *in vivo* through biomaterial degradation or when taken up by cells and digested in low pH compartments. For sustained release kinetic profiles, adsorption and encapsulation interactions are currently the most investigated interactions for improving vaccines.[99-102] While adsorption studies have focused more on the uptake of the biomaterial rather than a slow release of antigen,[103] most *in vivo* studies for sustained release use encapsulation as it offers both long-term stability and slow release for single injection vaccinations.[55, 104] For the development of single injection vaccinations, slow or consistent release has been most studied *in vivo* and has shown significant stimulation of the immune system. [105, 106] A concern articulated by some researchers has been that antigen persistence can lead to immune cell exhaustion and lower antibody affinity to antigens.[107-110] Instead, pulsatile release seems to be a better alternative as it mimics a single injection followed by several booster shots.[111] For example, the Langer Lab investigated 16 different formulations of PLGA and took three formulations that exhibited pulsatile release profiles.[112] The goal of this study was to show the pulsatile release could develop a humoral response identical to a single injection, followed by two booster shots. They focused on the biomaterial and future studies will look at further tuning the material to elongate the pulse from two weeks to two months to mimic better the injections schedule of current vaccines.

1.3.2 Antigenicity and Long-term Stability

Biomaterials play a pivotal role in vaccine development, as they can improve the stability of the antigens encapsulated within. Thus, it is important that the antigenicity and epitope stability be monitored over a long period of time. Stability *in vitro* has only been investigated for short periods of time ranging from 1 – 12 months and using circular dichroism, western blot, or enzyme-linked immunosorbent assay (ELISA) to determine the stability of model proteins, such as ovalbumin.[60, 113] However, biomaterial usage in vaccine development is still an area of ongoing investigation; long-term stability should be assayed using antigens other than ovalbumin, which is known to be a quite robust protein. Additionally, translation to actual subunit proteins should be investigated and verified *in vivo* as these studies are rare, only short-term, or just mentioned as a possibility.[114-118] The Tiyaboonchai lab encapsulated Pasteurella multocida within alginate microparticles for subcutaneous injections. Key to this study was a 6 month storage test were antigenicity was investigated in samples kept either at 4 or 37 °C. [119] Results revealed that mice injected with either formulation elicited an immune response similar to freshly encapsulated antigens. Further, the work done by Tiyaboonchai lab provides an ideal experimental template for single dose vaccination investigations. Future investigations should focus on long-term stability and researchers should test the antigenicity at RT for at least six months or longer for these systems to be able to replace the cold chain infrastructure.

1.4   Biomaterial Immune Activation

The investigation of biomaterials for the delivery of vaccines against infectious diseases offer new strategies to engineer specific immune responses. As discussed in section 3, determining the antigenicity of antigens within a biomaterial will ensure that the immune activation will be produced for the correct epitope. To further verify this, the biomaterials discussed above needs to be studied *in vivo* to understand their role for long-term immunity from single or multi shots to any associated toxicity. Since most investigations of biomaterials tend to be short-term, [74, 120] experiments need to be developed to ensure this field is being advanced. The following section focuses on biomaterials studied *in vivo* and provides an analysis of some examples in the literature,

which focus primarily on the production of antibodies, cytokines, immune cells, and survival studies.[121]
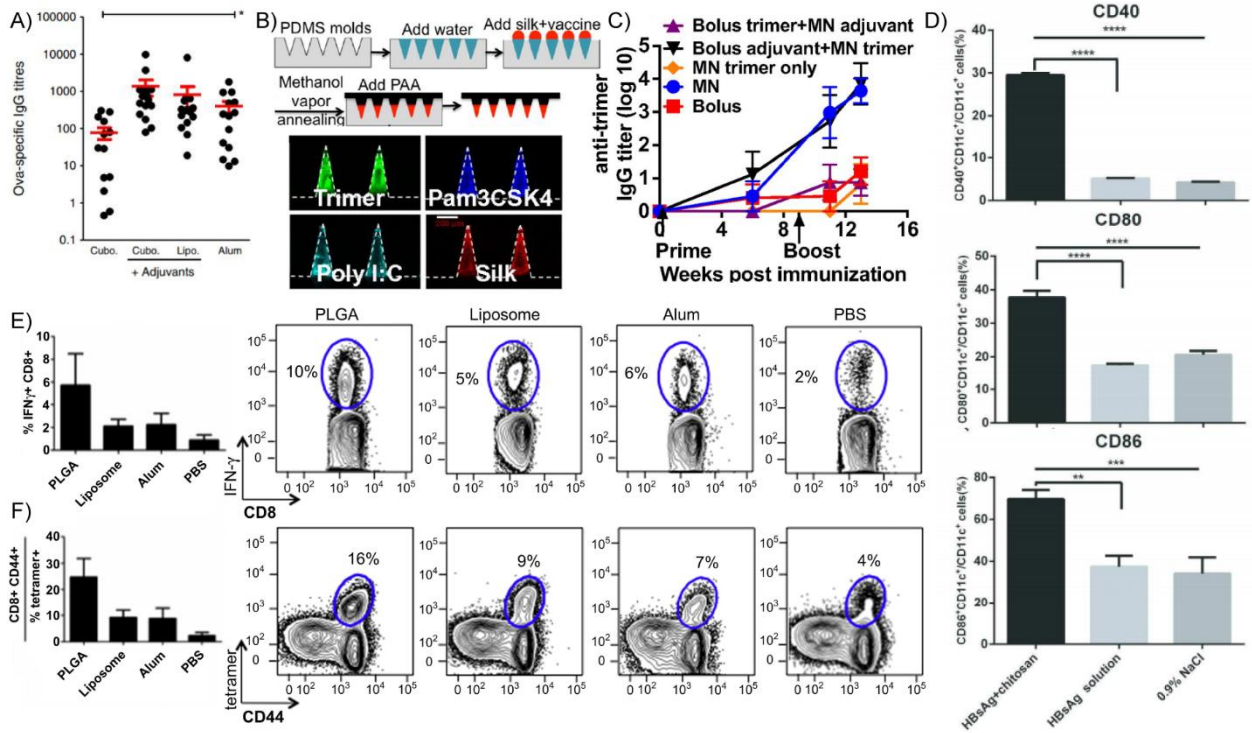
Figure 1.4: A) The comparison of ovalbumin antibodies that have been encapsulated inside of a cubosome polymer with and without adjuvant has similar production compared to alum. Reprinted from reference [122], with permission from Elsevier. An image of a B) the steps to develop silk loaded microneedle tips, containing HIV trimer along with adjuvants and when delivered into mice models, C) the microneedle containing trimer and adjuvant produced the highest amount of antibodies. Reprinted from reference [123], with permission from PNAS. D) The Xu lab shows that chitosan nanoparticles have a higher upregulation in CD40, CD 80, and CD 86 in bone marrow dendritic compared to a bolus shot of the hepatitis B antigen. Republished with permission from Royal Society of Chemistry for reference [64]; permission conveyed through Copyright Clearance Center, Inc. The Fahmy lab compares the slow release of PLGA, Liposome, and alum for release of ova and show that PLGA stimulates a higher population of cytotoxic T cells producing E) IFN-γ and F) activated specifically to ovalbumin. Reprinted from reference [124], with permission from Elsevier.

1.4.1 Antibodies:

From 1995 to 2005 the main experiment conducted to determine the immune response of an antigen + biomaterial was based on the production of antibodies. The main biomaterial investigated was PLGA with a plethora of antigens, such as diptheria, tetanus toxoid, and hepatitis B, used to determine it's effectiveness in animal models.[125-128] The goal of those studies was to show that a single dose of PLGA, slowly releases the antigen from within and can produce a humoral response similar to 3 injections of the antigen alone.[129] With the emphasis that higher antibody production means improved formulation of the biomaterial and this has been the approach for most investigations. More recent studies go beyond just antibodies and develop experiments to determine the increase in antibodies. For example in 2013, the Hook Lab showed that cubosomes, a lipid based nanocarrier, could prime T cells more efficiently because they can encapsulate a higher amount of antigen compared to liposomes.[122] In this study, they use ovalbumin as their subunit antigen and delivered 15 µg of ovalbumin, 150 µg imiquimod, and 14 µg of monophosphoryl lipid A—imiquimod and MPL are toll-like receptor agonists and used as adjuvants. As can be seen from **Figure 1.4A**, the Cubosome with adjuvant produced the highest amount of antibodies when compared to Liposome with adjuvant and alum. More Recently in 2019, the Irvine Lab fabricated microneedles with silk fibroin protein tips and encapsulated HIV envelope trimer within as shown in **Figure 1.4B**.[123] In addition, mixed within the tips they added TLR2 agonist pam_3CSK_4 and TLR3 agonist Poly I:C as adjuvants to recruit immune cells to the skin. They showed clearly that the mice vaccinated with MNs containing the trimer and adjuvant had the highest production of anti-trimer IgG titers compared to the mice receiving bolus injections (**Figure 1.4C**). Both studies showed that the biomaterial developed an immune response without the need of an adjuvant, but the inclusion of an adjuvant provided a higher response. However, both studies were short-term, lacked the type of antibodies produced, and could have investigated if the slow release improved binding affinity, which would have provided more information on how effective the biomaterial is at enhancing the humoral response.

1.4.2   Immune cell activation

It is understandable to just look at antibody production, as the current method to determine if a vaccine is still active is to test whether a patient is still producing antibodies. However, to get a better understanding of how well a formulation works it is necessary to investigate the activation of immune cells. For antigen presenting cells (APCs), researchers mainly focus on macrophage and dendritic cells and for the activation of the adaptive immune system they look at T-cells and B-cells found in secondary lymphoid organs—the lymph nodes and spleens. For example, the Xu lab investigated the mechanism of chitosan as an adjuvant, with hepatitis B as the model antigen.[64] They showed that the insolubility of the chitosan particles enabled the formation of a sustained release depot and enhanced the uptake of antigens by bone marrow dendritic cells. It was clear that the chitosan particles containing hepatitis B improved the maturation of DCs as can be seen from the upregulation of CD 40, CD 80, and CD 86 (**Figure 1.4D**). However, an interesting study would have been to test if the chitosan particle improved T cell activation. More recent studies to determine if a biomaterial can activate immune system is by directly looking at the draining lymph nodes and spleen for activation markers on DCs and T-cells.[130] The Fahmy lab[124] showed that liposome and PLGA nanoparticles improve the T cell activation owing to sustained release antigens. They mention that most vaccine focus on developing neutralizing antibodies, even though a defense against viruses and intracellular bacteria would benefit more from a cellular immune response. Thus, they show that the PLGA and Liposome nanoparticle not only enhance antibodies, but also enhance the cytotoxic immune cells (CD8+) and these activated T cells (CD8+,CD44+) are specific to ovalbumin (tetramer) as seen in (**Figure 1.4E-F**). Future studies should investigate the activation of memory T and B cells that activate specifically to the pathogen epitope.
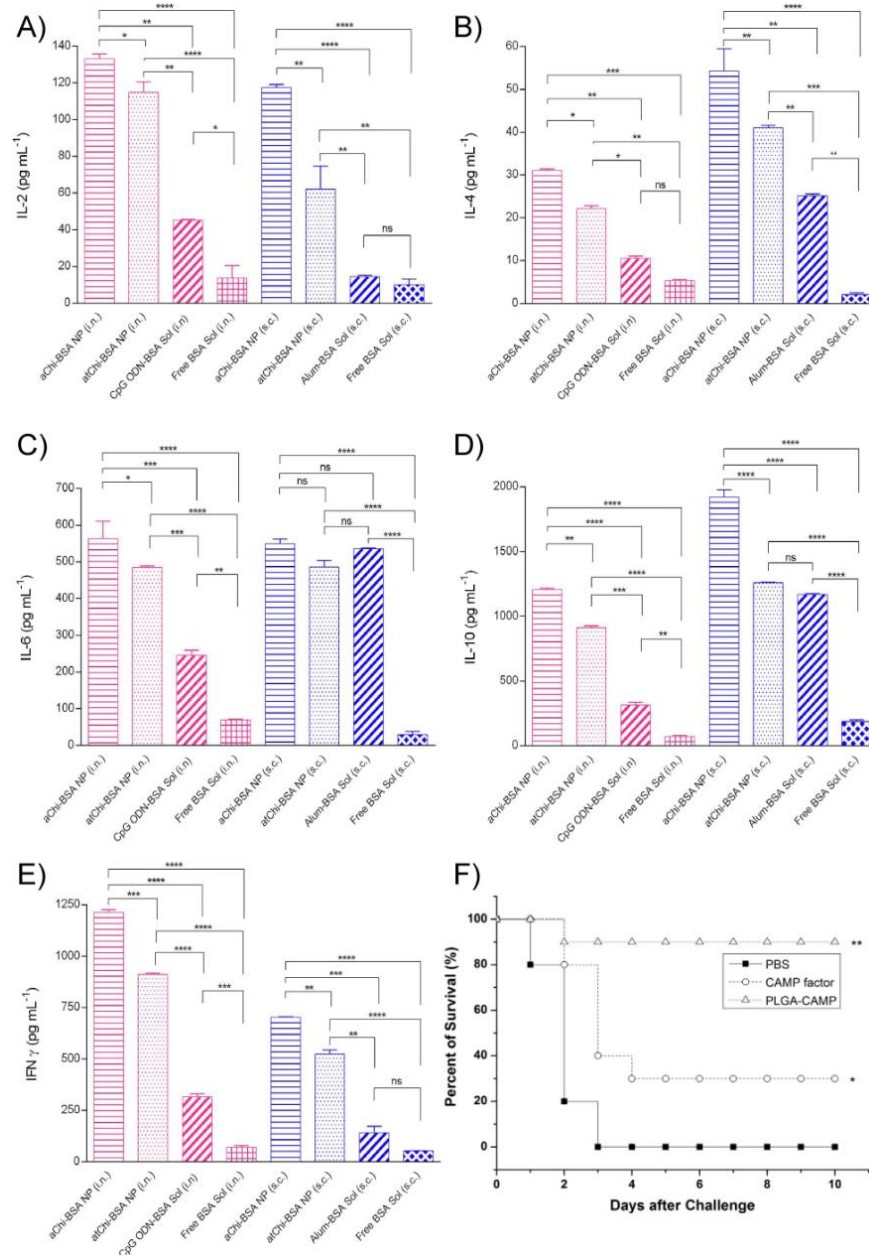
Figure 1.5: The Cevhar lab investigates chitosan activation of the immune system when different administrations are used and compare the cytokine production of A) IL-2, B) IL-4, C) IL-6, D) IL-10, and E) IFN-γ. Reprinted from reference [131], with permission from Elsevier. F) The Han Lab vaccinated mice with PLGA containing a subunit protein CAMP found in Toxoplasma *gondii*, which improve the survival rate of mice compared to a bolus shot of the subunit protein alone. Reprinted from reference [132], with permission from Elsevier.

1.4.3   Cytokines (Type of response)

Cytokines as additional experiments to test the biomaterial ability to activate the immune system *in vivo* did not start to pick up until 2006. In addition to immune cell activation, the cytokines produced can indicate whether the immune response is Th1, Th2 or both and can distinguish how size, adjuvant, dosage, and other attributes can affect this response.[62] Th 1 is an intracellular or cell-mediated response and Th 2 tends to focus on extracellular pathogens and reducing inflammation. The Ainslie lab chemically modified a naturally occurring polysaccharide to have acid-cleavable acetal groups and silyl groups.[133] They showed that extending the alkyl chain or mixing the inulin and dextran polysaccharides at different ratios could shorten or extend the release of antigens from within. They mention an ongoing challenge with subunit vaccines is incorporating adjuvants that safely stimulate and activates both a Th1 and Th2 immune response. They used a solvent evaporation technique to encapsulate ovalbumin within dextran microparticles to show that their particle could target APCs more efficiently and would obtain a more balanced cellular and humoral response. They vaccinated mice subcutaneously with 50 μg of ovalbumin and showed that their biomaterial produced antibodies similar to ova+alum. In addition, they looked at the amount of TNF-α produced by macrophage *in vitro* and the IFN-γ produced by splenocytes restimulated with SIINFEKL—a peptide sequence of ovalbumin. With the same supernatant collected from the splenocyte restimulation, they could have looked at the IL-4, IL-6, IL-12, and IL-10 to corroborate the high production of antibodies and show a balanced Th1/Th2 response. In fact, the Cevhar lab did a thorough investigation[131] to show that their chitosan particles could activate a balanced Th1/Th2 immune response. The focus of this paper was to show that their aminated chitosan and aminated plus thiolated chitosan provide a balanced Th1/Th2 response when delivered intranasally and compared this to mice vaccinated subcutaneously (**Figure 1.5A**). The results obtained from spleens harvested at day 253 show that intranasal injections of 20 μg of BSA encapsulated within the chitosan formulations have a similar Th2 response when compared to mice vaccinated subcutaneous based on the IL-6, IL-4, and IL-10 cytokine productions (**Figure 1.5B-D**). The cell mediated response for mice vaccinated with chitosan was actually higher compared to subcutaneous injections and controls using CPG as an adjuvant based on the IFN-γ and IgG2a antibodies (**Figure 1.5E**). This was a great study that compared injection routes and

18

compared their chitosan formulation to current adjuvants used in vaccinations. The only issue with cytokines is that different immune cells can produce these cytokines, therefore just measuring cytokines gives an idea of the type of response, but not specifically what cells are producing the cytokines. In order to truly understand the immune activation and the type of response would be to do intracellular staining to determine the cytokine being produced by T helper cells. This staining method along with an antigen-specific marker for the TCR would without a doubt determine how balanced of an immune response these biomaterials are creating.

1.4.4   Survival Studies

Survival studies for Biomaterials with an encapsulated antigen was first found in 2004 to provide protection against tumors.[134] Most survival studies with biomaterials tends to focus on how long their biomaterial can keep mice alive after inoculation with tumor cells.[83, 101, 135, 136] The earliest experiment that looks at survival against infectious diseases using a sustained release polymer was conducted by the Zhu lab using PLGA as the biomaterial.[137] They encapsulated subunit proteins, rROP18 and rCDPK6 from an intracellular parasite called Toxoplasma *gondii* (*T. gondii*) within PLGA microparticles to generate a long-lasting immune response. The mice were vaccinated subcutaneously and immune response was measured by lymphocyte proliferation, cytokine expression, and antibody production. In addition, they challenged the vaccinated mice six weeks after the last injection with live *T. gondii* and their survival was recorded daily until all mice were dead. The mice vaccinated with PLGA and rROP18 subunit protein survived the longest. Similarly, the Han lab entrapped[132] a subunit protein, CAMP factor, from streptococcus agalactiae within PLGA to develop single-dose vaccines that provide protection against diseases. Mice were vaccinated by an intraperitoneal injection and six weeks later were challenged with a lethal dose of *S. agalactiae* ($LD_{50} = 2\times10^8$ CFU). Mice were monitored for 10 days for mortality and the CAMP-PLGA vaccinated group had the highest chance of survival as shown in **Figure 1.5F**. It is fitting that PLGA was the first biomaterial to be investigated as a single dose vaccination treatment to test survival efficiency as it has been studied the longest. As researchers continue to investigate biomaterials for vaccination, survival experiments should be kept in mind to determine how well they can provide protection against infectious diseases.

1.5   Conclusion and Perspective

This review summarizes how far we have come in understanding the use of sustained release biomaterials as a tool to improve vaccination. However, there are still questions that need to be answered for biomaterials to become a new method of vaccination. Researchers need to report the protein loss during integration with these polymer systems, along with the antigenicity. The binding affinity between the polymer system and antigen needs to be investigated to understand the antibody production occurring in vivo, followed by determining whether the antibodies produced have a strong affinity to the antigen. As some studies have shown that the continuous release of antigens could reduce the binding affinity of the antibodies produced against it and induce immune exhaustion.[107, 109, 110] It is clear that more thorough studies have to be done with biomaterials without adjuvants to understand the effects that the type of release, size, charge, dosage, and injection intervals has on activating the immune system *in vivo*. In addition, understanding the specific immune activation of T-cells and B-cells need to be further investigated. Specifically, by looking at TCR and BCR that are antigen specific and determining the population of effector cells and memory cells during the study with biomaterials will give us a better understanding of how well they induce an immune response. Correlating all this with survival studies can give us a more quantitative answer on the level of response from the immune system that is needed to provide protection against infectious diseases. As newer biomaterials with improved properties are being engineered, investigators should keep these experiments in mind. The application of sustained release biomaterials to infectious diseases is still in its infancy and will require strong collaborative efforts between researchers in diverse fields. Ultimately, the field of sustained release biomaterials offers new tools that could be used to manipulate the immune system to develop improved vaccines that protect against infectious diseases after a single injection and could provide long-term stability for antigens at ambient temperatures.

CHAPTER 2

ENHANCED STABILITY AND CONTROLLED DELIVERY OF MOF-ENCAPSULATED VACCINES AND THEIR IMMUNOGENIC RESPONSE IN VIVO

Authors – Michael A. Luzuriaga[†], Raymond P. Welch[†], Madushani Dharmarwardana, Candace E. Benjamin, Shaobo Li, Arezoo Shahrivarkevishahi, Sarah Popal, Lana H. Tuong, Chayton T. Creswell, Jeremiah J. Gassensmith*

The Department of Chemistry and Biochemistry, BSB13.102

The University of Texas at Dallas

800 West Campbell Road

Richardson, Texas 75080-3021

2.1   Introduction

Proteinaceous therapeutics are moving to the forefront of medicine for their specificity in treatments, favorable side effect profiles, and their potential in personalized medicine.[138, 139] Unfortunately, many of these proteins are structurally metastable[140] and they can undergo drastic conformational changes at elevated temperatures, in organic solvents, and at pHs different from physiological conditions.[141, 142] These problems limit proteins to short-term low-temperature storage that require costly infrastructure in place to keep them stable throughout shipping. Researchers have been motivated by these limitations and have begun to develop new methods that can enhance protein stability.[10, 27, 143-147]

Metal organic framework (MOF) encapsulation has been shown[29] to stabilize enzymes,[148, 149] viruses,[150, 151] and antibodies[152] while providing structural and chemical protection. MOFs are highly porous crystalline materials made of metal ion clusters linked by organic ligand struts[153, 154] that have shown promise for use in gas storage[155] and separation,[156, 157] catalysis,[158, 159] sensing,[160] and small molecules drug delivery.[161-164] Recently, researchers have been shown that MOFs can immobilize[165, 166] and stabilize[167, 168] biomacromolecules. In particular, coating proteins in zeolitic imidazolate framework-8 (ZIF-8) is proving to be a promising method for protection against conditions normally adverse to proteins, and there have been many promising advancements in this area.[31, 167, 169-171] In particular, biomimetic mineralized growth[149, 150, 166] of ZIF-8 directly on to the surface of a protein has emerged as a means to encapsulate enzymes and insulin using only protein, zinc salts, and methylimidazole directly in water.[172, 173] Because ZIF-8 can grow on protein surfaces of different sizes, charge states, and morphologies, this process is quite "agnostic" to the biomolecule host inside the ZIF.[151, 170] This differs from other equally

elegant methods that use bespoke MOFs with tuned[174-176] pore sizes to encapsulate specific biomolecules or polymer encapsulated proteins coated with ZIF and formed in organic protic solvents.[65, 177] For instance, our lab biomimetically encapsulated Tobacco Mosaic Virus (TMV) within a ZIF-8 shell (TMV@ZIF) and found the encapsulation process to be high yielding and promoted by a modest affinity for zinc ions toward the proteinaceous surface.[151] This affinity leads to high local concentrations of zinc, which promotes a mineralization process that results in either core-shell or monolithic crystals of bionanoparticles.[149, 178] It is unclear, however, how—or if— the nucleation and growth affects the secondary or tertiary structure at the protein surface. If the protein surface of a therapeutic protein is altered as a result of the nucleation process, unwanted immunological reactions may occur as human proteins wouldn't be recognized as "self" and antigens for encapsulated vaccines would raise antibodies against a misfolded protein rendering this strategy moot.[139, 179, 180] Because an articulated aim[166] of thermally stabilizing proteins is to improve the global distribution of vaccines, which depend upon the fidelity of their folded structure, we were drawn to determine if changes in the immunogenicity of a viral nanoparticle would emerge following encapsulation and administration.

We chose TMV, a 300 nm × 18 nm tubular RNA plant virus, as a model vaccine biomacromolecule owing to extensive data on its *in vivo* performance as a carrier for engineered and chemically conjugated[181-183] epitopes in vaccine development (**Figure 2.1**). This chemical modifiability, which can occur on both interior and exterior surfaces independently, has given TMV a unique appeal beyond vaccine development as the structure tolerates attachment of dyes,[184] sensors,[185, 186] contrast agents,[187] and bioactive molecules.[188, 189] The multivalent nature of TMV comes from its 2130 identical coat proteins arranged helically around a 4 nm central pore where the viral RNA is

located. This allows many bioconjugations to the same virus particle, increasing local concentration of active sites and immobilizing them, which is one reason it is thought to be such a useful platform for vaccine development.[181-183]
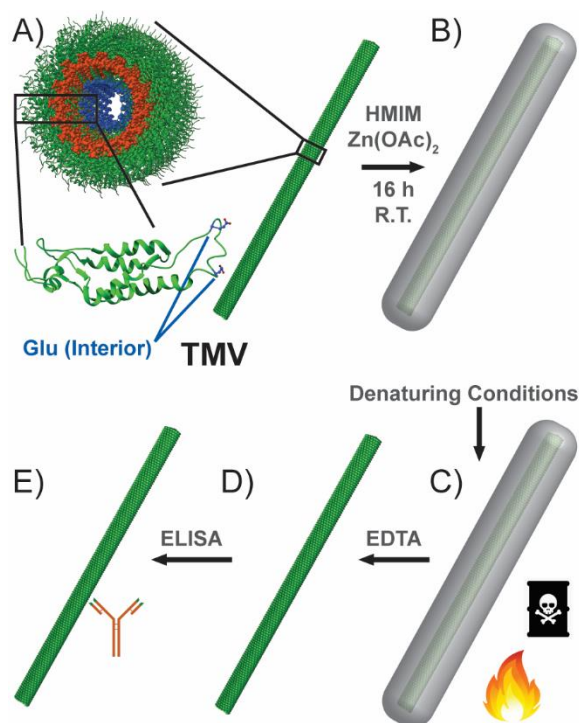
Figure 2.1: Schematic for analyzing surface effects from encapsulation and stressing: TMV contains glutamate residues, shown in blue, on the interior pore modifiable with EDC chemistry. The viral RNA, shown in orange, is embedded inside the TMV pore. A) Native TMV is incubated with 2-methylimidazole and zinc acetate to form B) TMV@ZIF. C) TMV@ZIF is subjected to denaturing conditions such as heat and organic solvents. D) Stressed TMV@ZIF is exfoliated with EDTA. E) Recovered TMV surface integrity is characterized by ELISA.

Since TMV is an established pre-clinical vaccine platform, it is a reasonable model to test the efficacy of thermal protection when encapsulated inside ZIF-8. While it is possible to remove the ZIF-8 shell to obtain pristine TMV, we wondered if this additional step was unnecessary. Indeed, it had occurred to us that the dissolution of ZIF-8, which happens slowly in biological media, may

present a method to formulate 'slow release' agents for proteins—an area of active research interest.[190, 191] We thus sought to determine if we could simply leave the TMV inside the protective ZIF-8 shell and inject this composite subcutaneously in a mouse model as a method to slowly release TMV, producing an immune response similar to injecting native TMV subcutaneously. We can quantify changes to the surfaces of TMV as a result of ZIF-8 growth and removal using anti-TMV antibodies measured in an enzyme-linked immunosorbent assay (ELISA). A damaged or unfolded protein at the virus surface will not interact strongly with their complementary antibodies and this loss of affinity will manifest as a diminished ELISA response. The TMV@ZIF composite was subjected to stressors, including heat and denaturing solvents, the ZIF shell was removed, and the recovered protein was examined by ELISA to confirm surface intactness. Tobacco plant infection and *in vivo* studies further demonstrate the viability of ZIF-8 as a protective shell. Finally, we conducted longitudinal *in vivo* studies to ascertain the toxicity and immunogenicity of the TMV@ZIF-8 when implanted subcutaneously. Our results show that this strategy has considerable potential to operate concurrently as a substrate to stabilize proteins at above-ambient conditions as well as deliver them effectively intact and in a more linear dose.

2.2   Results and Discussion

TMV@ZIF can be prepared in a number of different morphologies[151] ranging from bulky rhombic dodecahedra containing hundreds of viruses to discrete rod-shaped core-shell bionanoparticles with a shell thickness tunable from 10 to 40 nm. Each of these morphologies have different colloidal and dispersion characteristics and for this study the following criteria were considered: i) the composite made had to be dispersible in solution for easy *in vivo* injection, and ii) the kinetics of shell dissolution should allow for complete dissolution of all *in vivo* administered ZIF-8 by the

end of our one-month study. When we attempted to suspend rhombic dodecahedra, they settled out of solution too quickly and clogged the syringe. This is in line with literature reports that particles larger than 1000 nm tend to settle rather quickly, making them a difficult material for injection.[30, 192] We chose to continue forward with rods, as the ~350 nm particle size allow for them to be easily dispersed into solution and the shell exfoliates more rapidly than the larger rhombic dodecahedra. We thus set out to determine whether the ZIF-8 shell would increase the stability of TMV and if it could be delivered *in vivo*. The encapsulation of TMV into ZIF-8 crystals was obtained by mixing TMV (0.111 mg) with an aqueous solution of 2-methylimidazole (400 mM, 3.0 mL), followed by an aqueous solution of zinc acetate (20 mM, 1.5 mL) (**Figure 2.1**). After 16 h, the TMV@ZIF particles were collected by centrifugation at 4300 $\times g$ and the shell diameter and rod-like morphology were verified by scanning electron microscopy (SEM) (**Figure 2.2A**). The morphology of TMV@ZIF is clearly different from the common rhombic dodecahedral native ZIF-8 crystals.
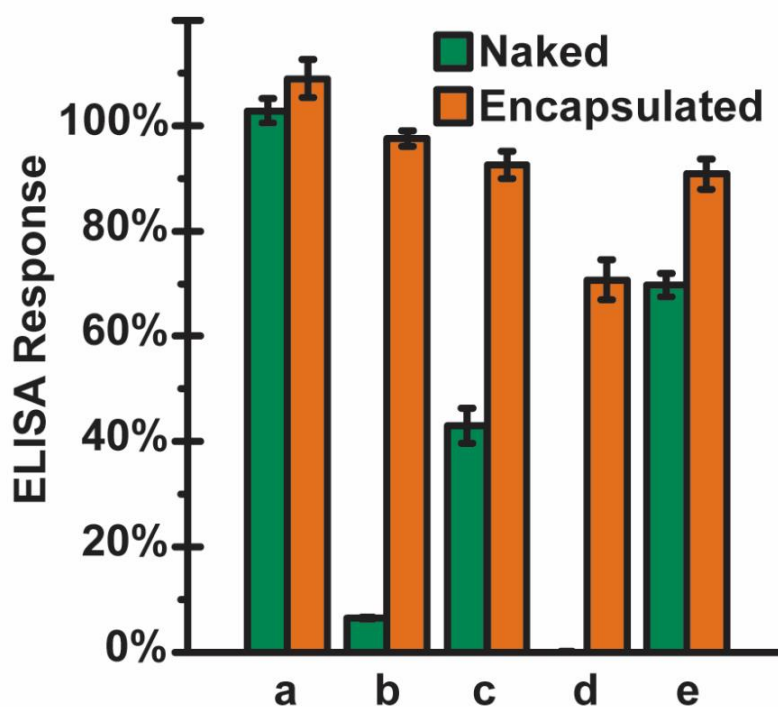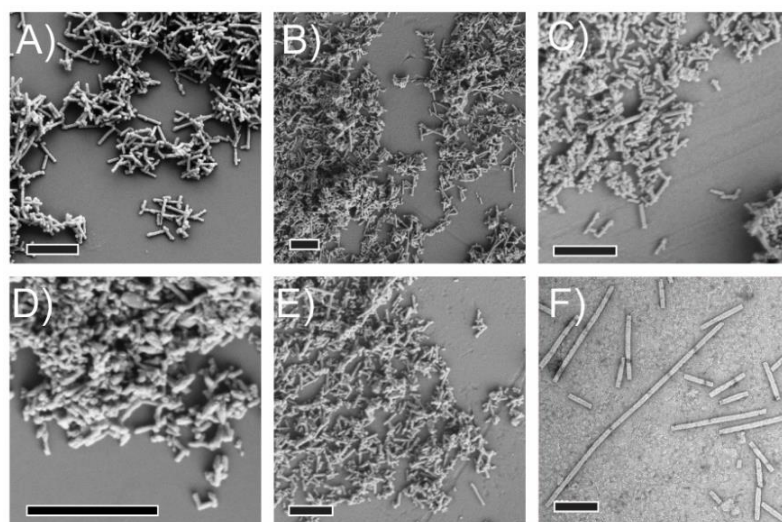
Figure 2.2: Top: SEM images of TMV@ZIF A) non-stressed, B) heating at 100 °C for 20 min, and after soaking overnight in C) methanol, D) 6 M guanidinium chloride, and E) ethyl acetate. Scale bars represent 1 µm. F) TEM image of exfoliated non-stressed TMV. Scale bar is 200 nm. Bottom: The ELISA response of naked and encapsulated TMV subject to no stress (a), heating (b), methanol (c), 6 M guanidinium chloride (d), and ethyl acetate (e). These labels correlate to the SEM images A-E above. The percentages range from buffer blank (0% TMV) to a separate internal control of non-stressed naked TMV (100% TMV).

TMV@ZIF was then stressed under various conditions to determine the stability of the encapsulated virus surface. Stability versus various solvents was tested: soaking in methanol, ethyl acetate, and 6 M guanidinium chloride—a common protein denaturant[193]—overnight. Thermal stability was tested by heating TMV@ZIF to 100 °C for 20 min. After stressing, samples retained their rod-like morphology, as seen in SEM (**Figure 2.2B-E**), and the ZIF-8 shells retained their crystallinity, as seen in PXRD (**Figure A.2**). The post-stressed composites were exfoliated in EDTA, desalted, and resuspended in 0.1 M sodium phosphate buffer. The protein concentrations were then determined by Lowry assay, and all samples were diluted to 5.0×10^{-4} mg/mL and ELISA response determined. Since changes in the viral proteins surface are being investigated, the ELISA results were normalized to naked non-stressed TMV (100%), and buffer blank (0%) for comparison between the two. We were pleased to discover that the process of the shell formation and exfoliation did not significantly alter the protein surface and that the shell confers considerable protection to TMV when exposed to high temperatures. For instance, the percent difference between naked TMV and TMV@ZIF when heated to 100 °C for 20 min was 165.0% (**Figure 2.2 bottom, Table A.1**). Likewise, the percent difference between protected and unprotected exposure to the strongly denaturing guanidinium chloride was 199.2% (**Figure 2.2 bottom**). We were also able to demonstrate that the ZIF was able to confer protection against other denaturing organic solvents (**Table A.1**).
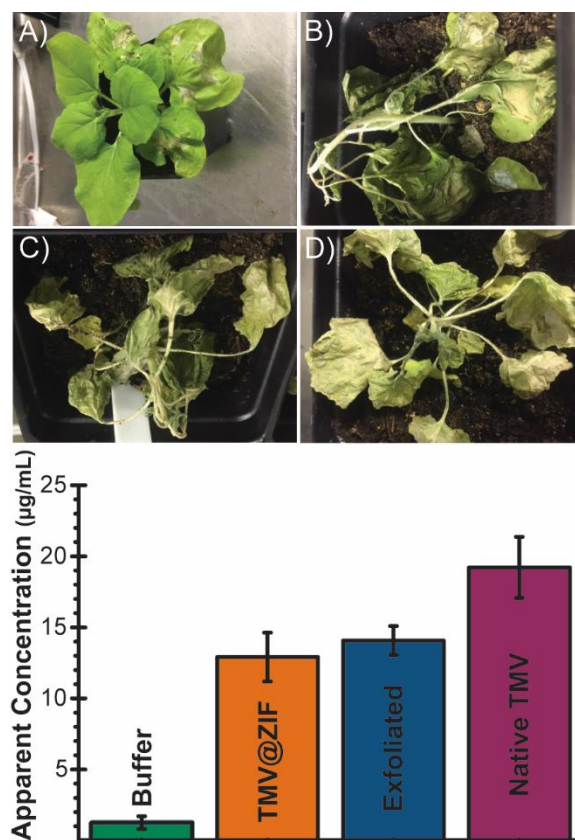
Figure 2.3: Top: *N. benthamiana* plants 10 days after inoculation with A) 0.1 M pH 7.4 potassium phosphate buffer as a negative control, B) TMV@ZIF, C) exfoliated TMV@ZIF, and D) native TMV as a positive control. Bottom: A bar graph showing the viral recovery of TMV from 1 g of harvested leaves measured by ELISA. Leaves were inoculated with buffer as a negative control, TMV@ZIF, exfoliated TMV@ZIF, and native TMV as a positive control.

We then set out to determine whether encapsulating TMV would damage the RNA. To assess the protection that TMV@ZIF has on the RNA of TMV, *Nicotiana benthamiana* plants were inoculated with phosphate buffer as a negative control, TMV@ZIF, TMV@ZIF exfoliated with EDTA, and native TMV as a positive control. The infection of *N. benthamiana* depends on the disassembly of the capsid to liberate the intact viral RNA and begin replication. Consequently, any damage to the RNA will reduce viral load in plants.

Inoculated leaves were collected after 10 days post infection. Visually, the control plants remained green and the other plants withered (**Figure 2.3A-D**). ELISA was performed on 1 g of of leaves macerated in 10 mL of extraction buffer and centrifuged to remove the large plant matter. Since the relative amount of TMV present in the leaf matter was being investigated, the ELISA results were fit to a standard curve of native TMV and results reported as apparent TMV concentration in µg/mL. The TMV@ZIF, exfoliated TMV@ZIF, and native TMV plants showed a clear increase in ELISA response compared to the buffer-inoculated plants, with percent differences of 164.32% (a 10-fold increase), 167.01% (an 11-fold increase), and 175.29% (a 15-fold increase), respectively (**Figure 2.3 bottom**). This indicates that the TMV remains virulent and that the RNA survives the encapsulation and exfoliation process.
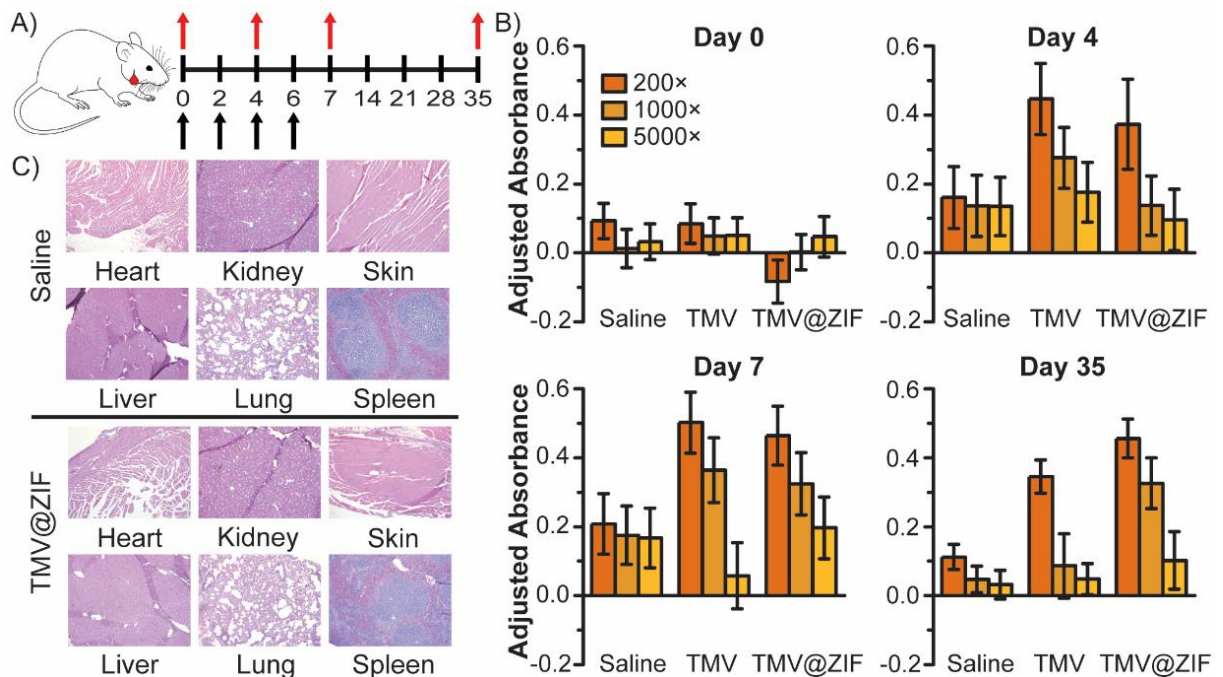
Figure 2.4: a) Time schedule showing the days the mice were injected (black arrows) and submandibular blood withdrawals were performed (red arrows). Serum samples were diluted 200×, 1000×, and 5000×. b) ELISA response for each time point, buffer blank subtracted. c) hematoxylin & eosin Y staining of saline and TMV@ZIF injected mice.

We next turned our attention to *in vivo* studies on murine models to determine i) whether the virus would release from the protective ZIF shell *in vivo*, ii) how the antiTMV IgG production against subcutaneously administered TMV@ZIF compares to native TMV, and iii) the biocompatibility of TMV@ZIF composite. In order to determine relative antibody production and optimize serum dilutions, 2 groups (n = 4) of BALB/c test mice were either non-injected or injected subcutaneously with native TMV and blood drawn after 10 days. In the test mice, there was a clear antiTMV ELISA response in mice injected with native TMV compared to non-injected mice after 10 days, and an optimal serum dilution range of 200× to 5000× was found (**Figure A.3**). To continue our investigation, 12 BALB/c mice were divided into three groups (n = 4) and subcutaneously injected on day 0, 2, 4, and 6 with saline, native TMV, or TMV@ZIF. Multiple injections were administered to enhance the antibody production levels in mice. We hypothesized that the TMV@ZIF would protect the encapsulated TMV in the body for as long as native TMV and result in a similar antibody production level. Submandibular blood draws were conducted on day 0, 4, 7, and 35 (**Figure 2.4A**). The ELISA response, which measures the production of mouse antibodies against TMV, shows that the TMV@ZIF elicits an antibody response comparable to naked TMV (**Figure 2.4B**). Antibody production typically depends upon successful uptake by antigen presenting cells (APCs)—for instance macrophages and dendritic cells—in the body. This means that the shell is being removed before or during APC uptake. Exactly what is happening requires further study; however, there is literature precedent[169] that ZIF-8 can dissolve in the presence of cell media and it is not unexpected that ZIF-8 would dissociate in the interstitial fluids of the subcutaneous region prior to cellular uptake. The antibody levels that were detected for the composites were comparable to that of naked TMV, confirming that the TMV@ZIF does not need

31

to be exfoliated before administration. Five days after the last blood withdrawal, hematoxylin and eosin Y (H&E) stained images were taken on various organs for each mouse to further evaluate TMV@ZIF biocompatibility. No visual difference could be determined between mice injected with saline and with TMV@ZIF (**Figure 2.4C**). This confirms the biocompatibility of TMV@ZIF, following multiple subcutaneous injections with no apparent toxicity or behavioral changes in the mice. While some literature has shown *in vitro* toxicity,[169, 194] our study has concluded that these results may not translate *in vivo*.

Our method depends upon the slow degradation of ZIF-8 *in vivo* by physiological salts and macromolecules, suggesting that encapsulation and protein-ZIF composite formation may be an intriguing way to prolong a linear dose of protein-based drugs. This could be especially useful for the administration of insulin and vaccines, which typically require multiple injections over time to achieve a sustained effect.[195] Histology of the tissue at the subcutaneous site of administration at the conclusion of the study—which consisted of four consecutive TMV@ZIF injections—did not uncover any residual material, tissue damage, or scarring, which lead us to suspect that the full dose was being absorbed into the animal, as shown in **Figure 2.4C**. To better understand the rate at which TMV@ZIF was taken up by the mouse, we conducted time dependent *in vivo* imaging using TMV labeled on its interior with the red-emitting fluorophore Cy5 (Cy5-TMV, **Figure A.4**). The Cy5-TMV concentration was determined by NanoDrop to be 12.59 mg/mL and the apparent Cy5 concentration by UV-Vis was 37.44 µM (**Figure A.5**). Calculating the number of moles of Cy5 and TMV present in the Cy5-TMV (TMV M.W. $= 4.08 \times 10^7$ g/mol, Cy5 M.W. $= 746.97$ g/mol), the average number of Cy5 molecules per TMV rod was determined to be 12.13. This labeled TMV was encapsulated inside ZIF-8, which caused a quenching of the red fluorescence

(**Figure A.6**). This fluorescence of Cy5-TMV was restored in full when the shell was removed, providing a clear indication of shell removal. For this study, 6 BALB/c mice were divided into two groups (n = 3), shaved to remove the hair on their torso and limbs, and injected subcutaneously with either un-encapsulated Cy5-TMV or Cy5-TMV@ZIF and imaged over two weeks. The images shown in **Figure 2.5B** show that, prior to injection, the only fluorescence comes from the hairs near the head. As shown in the series of images in **Figure 2.5C**, subcutaneous injection of Cy5-TMV decayed slowly over a period of 120 h. In contrast, the Cy5-TMV@ZIF fluoresced weakly at first, followed by an increase then gradual decay. After 288 h, the fluorescence at the injection site for the encapsulated material returned to baseline (**Figure 2.5A**).
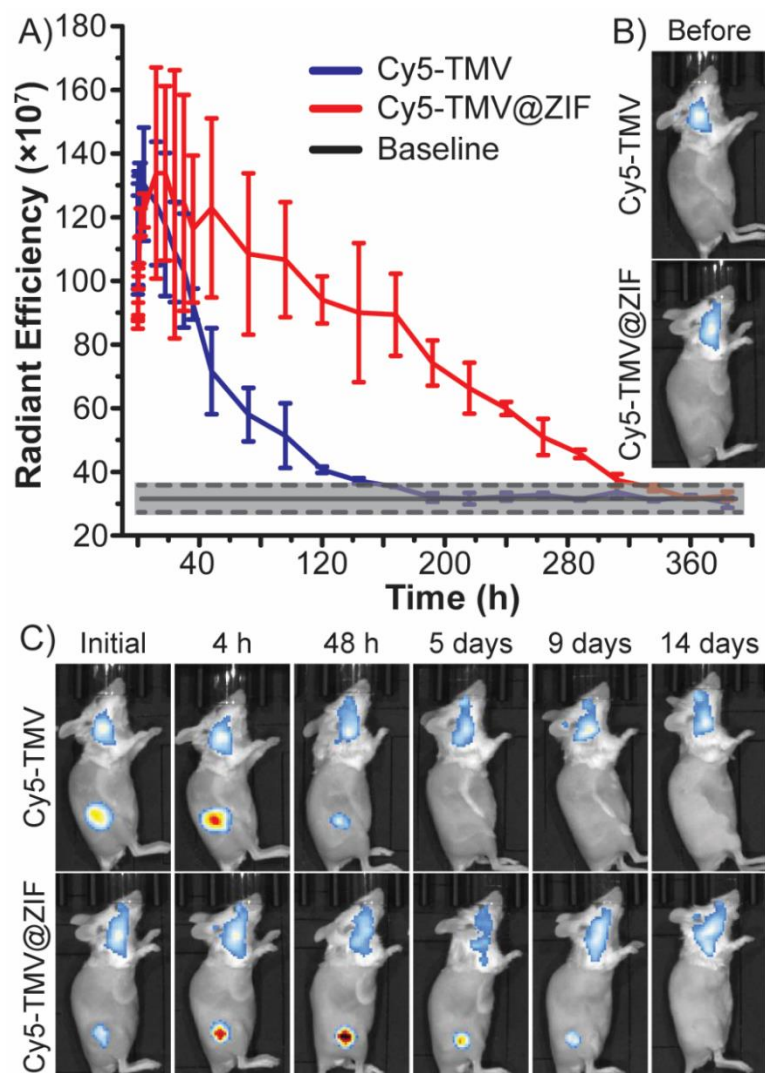
Figure 2.5: a) Fluorescence intensity over time. The baseline is the average fluorescence intensity of 4 mice before injection. The dashed line represents the error of the baseline. b) Images of the mice prior to injection of Cy5-TMV or Cy5-TMV@ZIF. The mice were shaved and the only initial fluorescence comes from the hairs on the head. c) After injection and time point images of Cy5-TMV or Cy5-TMV@ZIF.

2.3   Conclusions

The results of this study strongly indicate that ZIF-8 coatings not only provide protection against denaturing solvents and heat, but the nucleation and growth of the crystalline lattice does not alter the secondary or tertiary structure of protein and protein ensembles. Further, the shell does not

significantly damage the viral RNA. The ZIF-8 shells are exceptionally easy to synthesize on proteins, their composites are formed in a few seconds, and are ready to use within hours. It is clear from histology data that prolonged exposure to ZIF-8 does not alter tissue morphology at either the injection site or distal organs. Qualitatively, we saw no behavior changes in mice following administration, nor did any mice become ill or die as a result of prolonged exposure to TMV@ZIF composites. On the other hand, *in vivo* data clearly suggest that the administration of equal quantities of immunogenic protein yielded identical antibody responses, showing that the release of the protein from the ZIF shell occurs to completion. This was further corroborated with time-dependent *in vivo* imaging studies, which showed a time-delayed release of the injection over the course of 14 days—a property of ZIF-8 we aim to exploit in subsequent studies. Taken together, these data strongly suggest ZIF-8 based shells may provide a method to concurrently protect and deliver proteinaceous drugs safely.

All Supplementary Information can be found in Appendix A.

CHAPTER 3

ZIF-8 DEGRADES IN CELL MEDIA, SERUM, AND SOME—BUT NOT ALL—

COMMON LAB BUFFERS

Authors – Michael A. Luzuriaga, Candace E. Benjamin, Michael W. Gaertner, Hamilton Lee,

Fabian C. Herbert, Snipta Mallick, Jeremiah J. Gassensmith*

The Department of Chemistry and Biochemistry, BSB13.102

The University of Texas at Dallas

800 West Campbell Road

Richardson, Texas 75080-3021

3.1   Introduction

Over the preceding two decades, metal-organic frameworks (MOFs) have been proposed for a number of industrial applications in catalysis,[158, 159] and separations[156, 157, 196] and have more recently emerged as promising materials for biological sensing[197] and drug delivery.[161-163] The applications for drug delivery have run from proposed systematic delivery of small molecules to the slow release of proteins *in vivo*.[10, 164] A significant number of these MOFs in drug delivery have focused on two hydrolytically stable systems based on either zeolitic imidazole framework-8 (ZIF-8),[30, 162, 163] a coordination polymer composed of methyl-imidazole (HMIM) ligands bound to zinc that self-assembles into a zeolitic topological net, or zirconium-based systems, which use inorganic $Zr_6O_4(OH)_4$ polynuclear clusters as secondary building units typically linking benzodicarboxylic acid struts.[175, 198, 199] While these systems are both well-known for their hydrolytic stability, biological milieu can be quite complex and for *in vivo* or *in vitro* work, a number of aqueous buffered systems are used routinely. Of concern is that several of these buffers contain inorganic anions that can form kinetically trapped complexes with transition metals and MOF stability in buffers has been relatively unexplored.[200] In particular, buffers based on phosphates and bicarbonate are fairly ubiquitous and these salts comprise a significant portion of cell media like Dulbecco's Modified Eagle's Medium (DME) as well as derivations of that media (DMEM, EMEM, etc). Further, serum contains a substantial amount of albumin, which is a 66.5 kDa protein covered in solvent exposed thiols from externally facing cysteine residues.[201] These residues are well known binders to metals and are a component of metal transport in blood.[202-204] Our interest in MOFs as potential drug delivery systems has focused on slow-release of large proteins for vaccine or therapeutic delivery by injecting the drug either subdermally or

intramuscularly.[89] Our approach has been to grow ZIF-8 non-specifically onto the surface of the proteins,[150, 151] which not only thermally stabilizes the inlayed protein but also creates a "slow release" mechanism for the protein to escape after implantation while protecting the protein from biological degradation by elevated temperatures or proteolytic enzymes.[89] In this context, the slow dissolution of the ZIF is a critical component of drug release in that, over time, as the ZIF dissolves, it releases proteins that were "biomimetically" integrated into the framework.

Because our MOF work frequently takes us both *in vivo* and *in vitro,* aqueous buffered solutions and cell media are frequently employed; thus, we sought to determine the stability of ZIF-8 in the most common laboratory buffer systems as well as cell media, serum, and "whole cell media" which is a mixture of cell media and serum. Our investigation revealed that neither phosphate nor carbonate-based buffers are innocent and induce almost immediate morphological changes as well as new and altered reflections in the PXRD pattern following exposure to these buffers. Beyond buffers, we found that serum "burrows" holes into ZIF-8 crystals, the effects of which are imperceptible by PXRD, but cause cargo embedded in the crystalline matrix to leak out. In the context of controlled protein delivery *via* subdermal or intramuscular implantation, neither of these issues are problematic—in contrast, they help explain the protein release we have already observed.[89] On the other hand, *in vitro* cell delivery and systemic delivery of small drugs may be complicated by these observations and the experimentalist should take care to interpret their results in light of these issues.

3.2   Results and Discussion

As described in the supporting information and **Figure B.1**, we prepared ~ 1 µm sized ZIF-8

crystals by optimizing the final concentration of zinc acetate and HMIM solutions. Our ZIF-8

sample purity was confirmed by infrared spectroscopy (IR), scanning electron microscopy (SEM),

and powder x-ray spectroscopy (PXRD). The crystals were not activated with organic solvent, but

they were held under dynamic vacuum to remove excess wash water to dry them out for easier

handling. These crystals were then weighed out into individual 15 mL falcon tubes and dispersed

in different common lab buffers, which were buffered above pH 7.4. Additionally, we tested

unbuffered 0.9% saline, which was measured to be mildly acidic from dissolved carbon dioxide.

All samples were placed on a laboratory rotisserie to ensure proper mixing. Several buffers

investigated had minimal effect on the apparent morphology of ZIF-8. Specifically, the 0.9%

saline, 0.05 M Tris, and 0.025 M HEPES buffered solutions, (**Figure B.3**) yielded little apparent

changes over 24 hours by SEM while 1X PBS (phosphate buffered saline), 10X PBS, produced

mild changes after several hours. On the other hand, within the first 10 mins, morphological

changes—in some cases, significant ones—were apparent by SEM on ZIF-8 that had been placed

in 0.1 M bicarbonate buffer, 0.1 M KP buffer, the cell media additive DMEM, bovine serum, and

whole cell growth media, which is typically a combination of growth medium (DMEM in our case)

with 10% serum. These morphological changes became even more obvious over time as can be

seen in **Figure 3.1** and continued until the end of our 24 hours experiment (**Figure B.2**). The

changes observed when incubated with DMEM—a commonly used buffered cell growth

medium—make sense, as these solutions contain 0.665 mM phosphate and 60.6 mM bicarbonate.
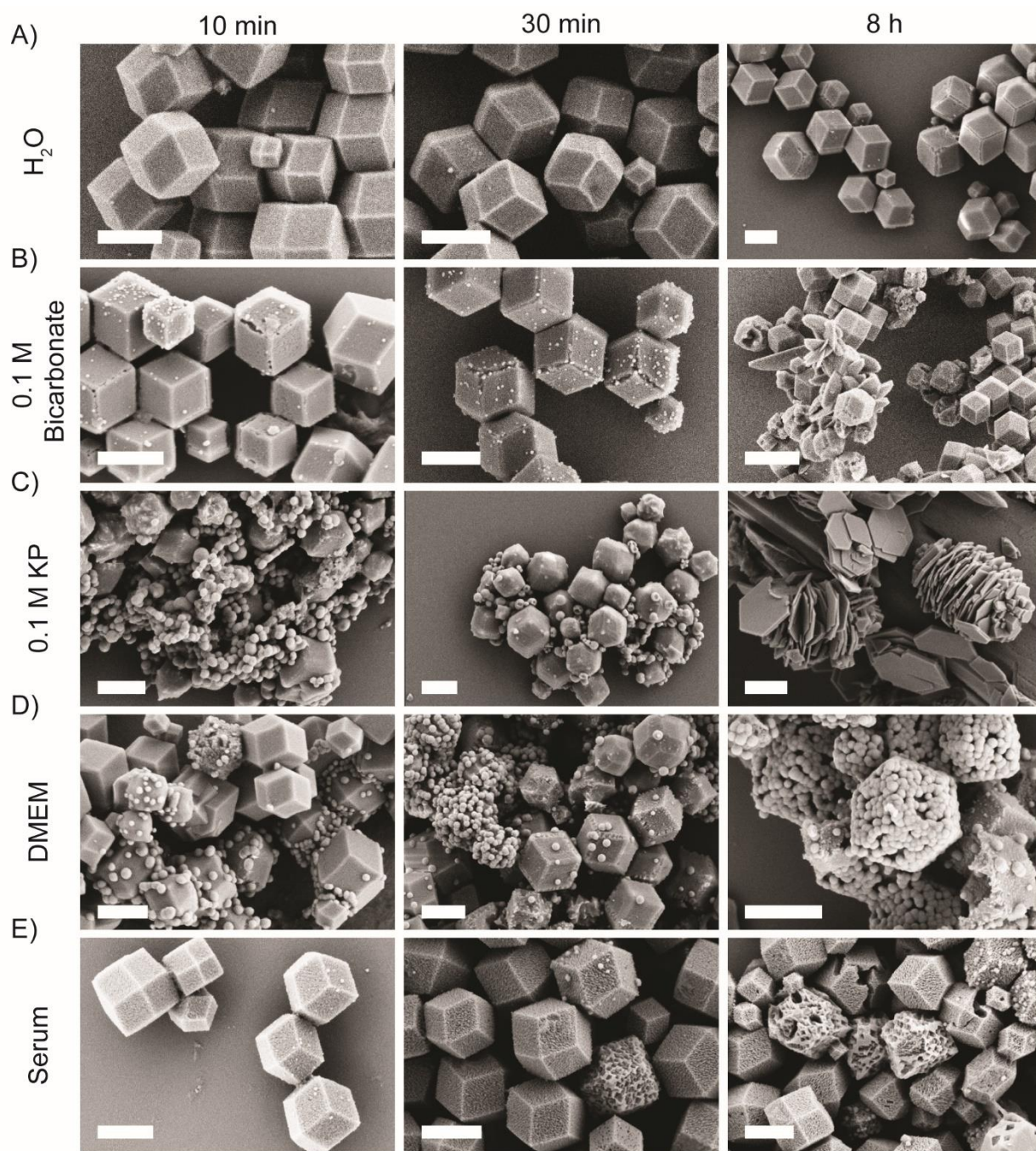
Figure 3.1: Time-resolved SEM micrographs of ZIF-8 incubated in A) water pH 7.8, B) 0.1 M Bicarbonate buffer (pH 9.5), C) 0.1 M KP Buffer (pH 7.4), D) DMEM (pH 7.6), and E) Serum (bovine serum, pH 7.9). At each time point an aliquot of the ZIF-8 was taken and washed three times with water, dried, and imaged by SEM. (Scale bar: 1 µm)

In addition to morphological analysis, all ZIF-8 samples were analyzed by PXRD and EDX. Prior to this, solutions in their respective buffers and media were centrifuged at 4300 $\times g$ for 10 min at room temperature. The supernatant was pipetted off, its pH was measured, and free Zn content was analyzed by ICP-MS (**Table B.1 and Table B.2).** The remaining pellet was washed three times with water and dried under vacuum for analysis. Changes to the bulk crystals were obvious by PXRD for all the phosphate and bicarbonate containing buffers and media—including DMEM. Because DMEM contains a significant amount of bicarbonate salts (60.6 mM), it is not surprising that incubation in DMEM and bicarbonate show similar PXRD reflections—11.04°, 18.96°, and 23.92° 2θ—in addition to the known ZIF-8 reflections (**Figure 3.2A**).
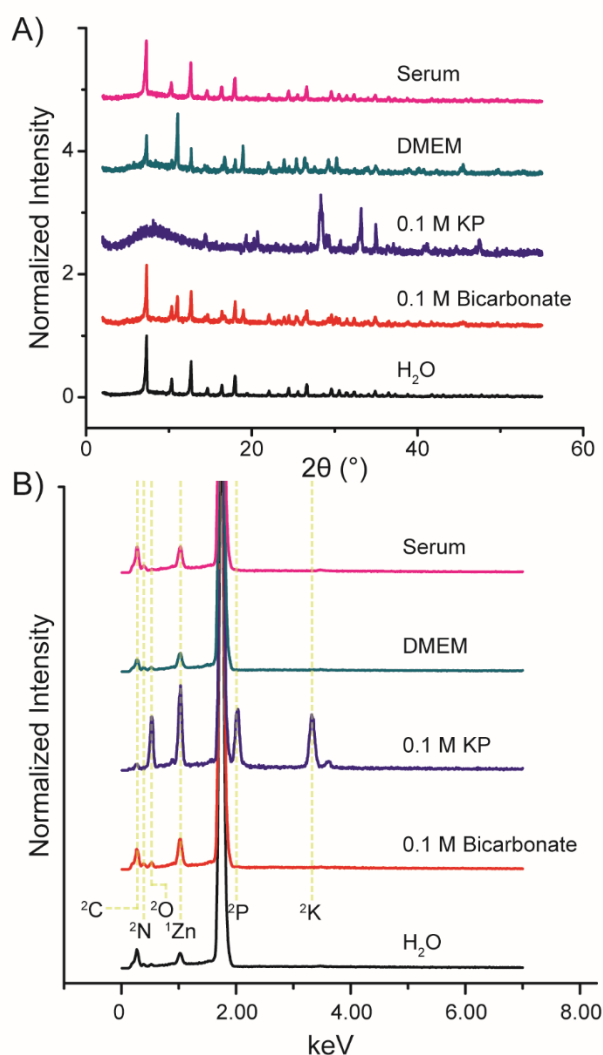
Figure 3.2: A) PXRD and B) EDX of ZIF-8 after 24 h of incubation with water, 0.1 M bicarbonate buffer, 0.1 M KP buffer, DMEM, and serum. (superscript 1 are L shell electrons and superscript 2 are k shell electrons).

The 0.1 M potassium phosphate buffer (KP), on the other hand, completely eradicated the ZIF-8 replacing it with a different crystalline material altogether. Energy-dispersive X-ray (EDX) spectroscopy shows the resulting constituent crystals to likely be zinc and potassium phosphate salts with little HMIM remaining on the surface as noted by the lack of carbon or nitrogen (**Figure 3.2B and B.5**). Considering the extensive changes with KP buffer, we were surprised that the PBS buffered solutions, which stands for "phosphate buffered saline" showed markedly less changes in

the PXRD spectra (**Figure B.4**). While the standard laboratory "recipe" for 1X PBS buffer uses an order of magnitude less phosphate, the 10X PBS buffer has the same phosphate concentration as 0.1 M KP buffer, yet 10X PBS buffers affects were clearly more mild over the same period of time as shown by PXRD (**Figure B.4**). Tentatively, we ascribe this to the high NaCl concentration, which seems to suppress the release of free zinc into solution per inductively coupled mass spectrometry (ICP-MS) data presenting in **Table B.2**.

Surprisingly, despite the apparent morphological changes to crystals left in bovine serum, the PXRD for these samples remained largely unaffected, indicating that the crystallinity of the sample was not significantly altered (**Figure 3.2A**). The other buffers that had ZIF-8 were measured by PXRD and had no obvious changes in the spectrum, meaning that the buffers did not change the crystal (**Figure B.4**). It is clear from ICP-MS data in **Table B.2** that serum was dissolving and solubilizing the Zn into solution, the most likely culprit being albumin.

Finally, we wondered how these changes to the crystal composition and morphology would affect entrapped biomolecules with the assumption that some of the buffers that cause profound changes to morphology would lead to leaking. For the following study, green fluorescent protein (GFP)— a 27 kDa and barrel-shaped protein: 4.2 nm in length and 2.4 nm in diameter [205]—was biomimetically mineralized within ZIF-8 (**Figure 3.3A**) and the synthesized crystal was characterized by PXRD and FTIR (**Figure B.6 and B.7**). The crystal conditions were tuned such that the final crystal sizes were similar to the ones created for the preceding work as shown by DLS measurements (**Figure B.8**).[31, 206] GFP@ZIF was individually incubated in the buffers mentioned above and ultrapure water and aqueous 0.5M EDTA—which completely dissolves the ZIF-8—were used as controls. Separate samples were pelleted at 1 h, 4 h, and 24 h by

centrifugation and fluorescence measurements of the supernatant were taken. Surprisingly, the only significant release of protein occurred in the serum, while, in all other cases, only a very small release occurred close to the lower limit of detection. The exact amount of GFP released from the crystals can be found in **Table B.3** (**Figure 3.3B and B.9**). The observed marginal release of GFP from ZIF-8 incubated in KP, DMEM and 0.1 M bicarbonate with the observed changes in morphology and crystal composition, suggests a double displacement reaction between salts in solution with the ZIF-8 that proceeds with one component—either the ZIF-8 or the salt—always remaining in the solid phase. In other words, even at very small scales, the salt exchange reaction appears to be completely heterogeneous. On the other hand, the GFP leaking from serum is attributable to the fact that, unlike the salts, the Zn is solubilized by serum proteins, thus the ZIF is literally dissolving into solution. This is corroborated by ICP-MS data that shows the supernatant obtained from serum had half the zinc concentration of the supernatant from an EDTA solution, which fully dissolves the ZIF-8. This dissolving of ZIF-8 by blood proteins causes approximately 40% of the GPF to be released within 24 h.
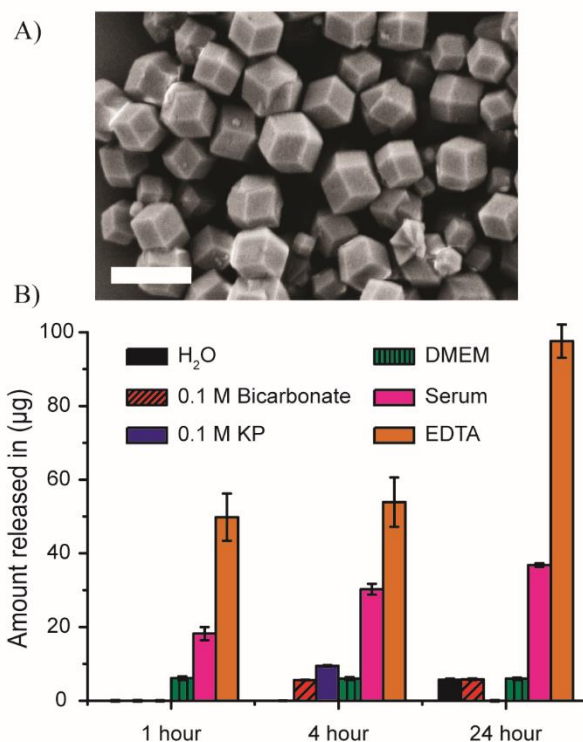
Figure 3.3: An SEM micrograph of A) GFP@ZIF (scale bar: 1 µm) and Time resolved fluorescence study showing B) the release of GFP from ZIF after 1 h, 4 h, and 24 h incubation with water, 0.1 M bicarbonate buffer, 0.1 M KP buffer, DMEM, serum, and EDTA as a control.

3.3   Conclusions

This study shows that ZIF-8 is not stable in certain buffers, even though they are all above pH 7, and that PXRD and electron microscopy studies are both needed together to fully demonstrate this. We have summarized our results to indicate the buffer and cell prep formulations that are "compatible", "should be used with caution", and "not compatible" with ZIF-8 in **Table 3.1**. The stability seems to be a competition between the coordination bonds of zinc and 2-methylimidazole against strong inorganic and proteinaceous zinc binders, which include bicarbonate and phosphate and surprisingly serum proteins as well. That said, only serum seem to degrade ZIF-8 in such a way that allows significant quantities of GFP to escape. These experiments provide insight on the importance of buffer choice for *in vitro* and *in vivo* studies, storage, and drug delivery formulation.

45

Table 3.1: Buffer compatibility chart.
✓ compatible, O caution × not compatible

Buffer	No Surface Change	ZIF-8 Reflections	Not Leaky
H_2O	✓	✓	✓
0.9% saline	✓	✓	✓
0.025 M HEPES	O	✓	✓
0.05 M Tris	O	✓	✓
0.1 M Bicarb	×	×	O
1X PBS	✓	✓	✓
DMEM	×	O	✓
Serum	×	✓	×
Cell Media	×	✓	O
10X PBS	×	O	✓
0.1 M KP	×	×	✓

Further, we are beginning to understand how ZIF-8 fully dissolves at physiological pH *in vivo* and it is clear that blood proteins, will play an important component. We caution that these effects may change when using different sized proteins and we are not sure how translatable these results are to Zr-based MOFs; however, it is worth pointing out that, under mimicked physiological conditions, the Zr MOF UiO-66 seems to show analogous behavior.[207]

Finally, the changes in surface chemistry from the interactions with cell media clearly suggest that cells are likely not interacting with the surface of ZIF-8—rather, they are interacting with a complicated surface of different formed salts and plasma proteins, this surface composition and morphology clearly depends upon incubation time and cell media choice. Consequently, we recommend experimental controls that include—as appropriate—cell media, buffers, and common plasma proteins to demonstrate morphological and chemical stability for projects that use MOFs for *in vitro* and *in vivo* applications.

CHAPTER 4

A WHOLE CELL METAL-ORGANIC FRAMEWORK ENCAPSULATED VACCINE AGAINST SEPTICEMIC UPEC INFECTIONS

Authors – Michael A. Luzuriaga, Fabian C. Herbert, Olivia R. Brohlin, Arezoo Shahrivarkevishahi, Yalini H. Wijesundara, Kavya Veera, Candace E. Benjamin, Sarah Popal, Michael D. Burton, Molly A. Ingersoll, Nicole J. De Nisco, Jeremiah J. Gassensmith*

The Department of Chemistry and Biochemistry, BSB13.102

The University of Texas at Dallas

800 West Campbell Road

Richardson, Texas 75080-3021

4.1 Introduction

Development of vaccines against bacterial infection is an ongoing challenge. Globally disseminated antimicrobial resistance (AMR) and the difficulty of developing of antimicrobial agents lacking serious side effects has compelled researchers to look to different strategies to prevent pandemic spread of AMR organisms. AMR is so widespread that treatment of even routine bacterial infections, such as urinary tract infection (UTI), has become problematic.[208] UTIs are the second most common adult bacterial infection worldwide, with ~80% of all community-acquired UTIs caused by uropathogenic *Escherichia coli* (UPEC).[209] Indeed, half of all women will develop a UTI in their lifetime, and more than 40% of these individuals will experience a recurrent infection.[210, 211]

The incidence and recurrent nature of infection take on more urgency given that 10–25% of uncomplicated UTI patient isolates are resistant to trimethoprim/sulfamethoxazole[212, 213] (TMP/SMX), a common antibiotic treatment regimen for UTI. When antibiotic treatment fails, bacteria persist in the bladder, increasing the cost of care and morbidity for the patient.[214] Left untreated, lower UTI can ascend to the kidneys progressing to the more severe diseases of pyelonephritis and urosepsis, which have a global mortality rate of 40%.[215, 216] Given the ubiquity of UTI and the high likelihood of recurrence, the societal cost is estimated to be over $5 billion each year in the US alone.[217] A prophylactic vaccine would be an ideal first line of defense against UTIs but there are no FDA-approved vaccines for this disease.[218] Indeed, no approved vaccine against infection caused by any pathogenic *E. coli* exists.

UPEC presents a unique challenge for the development of vaccines owing to the incredible genetic diversity of UPEC strains, which span the four major phylogenetic groups of *E. coli* (A, B1, B2, D).[219] To create a subunit vaccine, which typically incorporates pathogen surface proteins, the selection of antigens inducing broad protection against all UPECs would be exceedingly difficult. Additionally, subunit vaccines must be conjugated to a carrier to mimic the multivalence found in or on pathogens and require several booster shots to induce a robust immune response.[22, 23] Inactivated, whole cell vaccines would bypass the need for specific antigen selection required for subunit vaccines. The primary hurdle for the development of inactivated whole cell bacterial vaccines is the weak immune response they elicit because of their short half-life within the body, poor uptake by antigen presenting cells, and surface antigen degradation by harsh fixation methods.[220-222] In the present study, we have developed a method to gently inactivate whole cell bacteria by encasing them in a crystalline metal-coordination polymeric matrix called zeolitic imidazolate framework-8 (ZIF-8). This process occurs within minutes in water, uses inexpensive and biocompatible reagents, occurs at ambient temperatures, and most importantly, greatly improves survivability following systemic bacterial infection compared to standard inactivated formulations.

4.2   Results and Discussion

To develop a whole cell vaccine capable of inducing durable immune responses, we tested whether porous metal-coordination polymers, more commonly known as metal organic frameworks (MOFs), protect surface proteins from denaturation and prolong the release of bacterial antigens. MOFs are low density, crystalline metal-coordination polymers formed from metal nodes that coordinate organic ligands in a highly repeating and ordered matrix (**Figure 4.1A and B**). These

materials are useful in catalysis, separations, sensors, and recently, as non-toxic vehicles for drug delivery.[156-163, 207] We and others have described a specific type of MOF called ZIF-8,[151, 166] composed exclusively of zinc metals interconnected by methylimidazole ligands, that crystallize "biomimetically" on a variety of biomacromolecules including soluble proteins, polysaccharides, viruses, and whole cells. [31, 65, 150, 169, 223-225]

For this study, we used CFT073, a model urosepsis strain of UPEC frequently employed in the development of new vaccines.[226] Gram-negative *E. coli* has an outer membrane containing embedded polysaccharides and proteins,[227-229] which support ZIF-8 growth (**Figure 4.1C**). We resuspended CFT073 in a saline solution containing 2-methylimidazole (HMIM) and zinc acetate and after washing to remove excess zinc and HMIM, analyzed the resulting encapsulated bacteria, called CFT@ZIF, by scanning electron microscopy (SEM), powder X-ray diffraction (PXRD), and energy dispersive X-ray (EDX) spectroscopy. ZIF-8 growth occurred exclusively on the surface of the bacteria (**Figure 4.1D**). The PXRD of CFT@ZIF confirmed the shell was crystalline ZIF-8 (**Figure 4.1E**) and EDX confirmed the presence of zinc and phosphorus, indicating the presence of both bacteria and ZIF-8 (**Figure C.1**).

An initial challenge was the formation of free or empty ZIF-8 crystals. To find conditions that reduced the number of empty ZIF-8 particles (**Figure 4.1C**, white arrows), we tested a time course of incubation and a range of salinity in the encapsulation solution. We observed that an encapsulation time of 20 minutes and a final concentration of 100 mM NaCl yielded crystal growth primarily on the bacteria (**Figure C.2**). Using these parameters to generate CFT@ZIF, we then tested whether we could remove the shells from the encapsulated bacteria, in a process called exfoliation. We observed by transmission electron microscopy (TEM) that the bacteria

remained intact after dissolving the ZIF-8 shell in mildly acidic (pH 5) sodium acetate buffer and

no obvious debris from lysed bacteria were seen (**Figure 4.1D**).
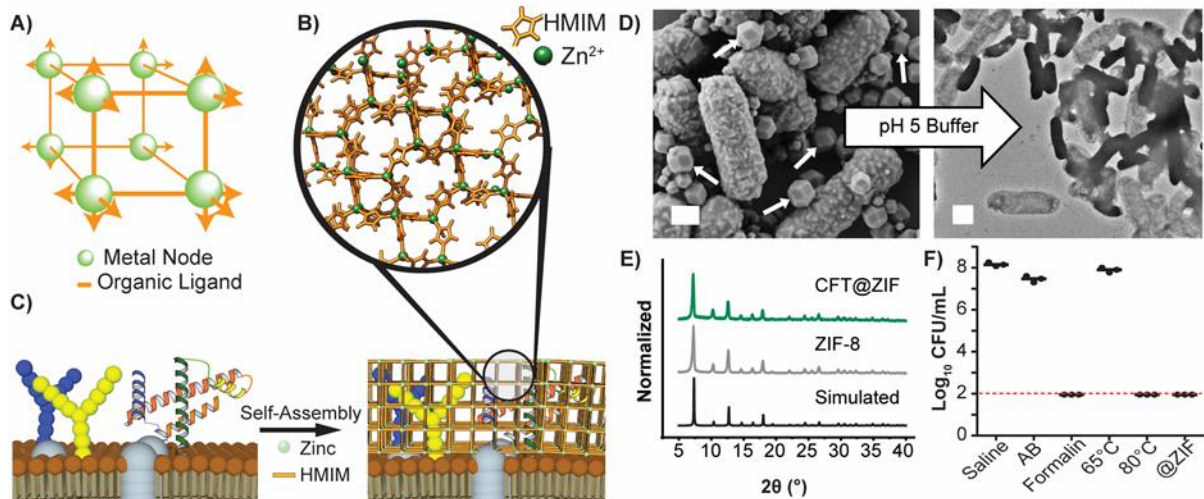
Figure 4.1: A) Simplified schematic of a metal organic framework composed of metal nodes and organic ligands that can expand infinitely in all directions. B) The crystalline super structure of ZIF-8 is illustrated. C) Conceptualization of the synthetic process shows that the surface of an E. coli external membrane can initiate ZIF-8 growth on and around membrane-bound biomacromolecules following incubation with Zn2+ and 2-methylimidazole (HMIM). D) Scanning electron micrograph of ZIF-encapsulated UPEC strain CFT073 (CFT@ZIF) (left), which can be removed gently in sodium acetate buffer (AB) at pH 5 to reveal whole bacteria, as seen in the transmission electron micrograph (right). White scale bars are 1 µm and white arrows are free ZIF crystals. E) Powder X-ray diffraction of CFT@ZIF compared to pristine/empty ZIF-8, showing the measured data matches simulated PXRD spectra of pristine ZIF-8. F) Bacteria growth assay shows CFT@ZIF is not viable after exfoliation, similar to formalin fixation or heat treatment, and can be used as a method to inactivate bacteria. The dashed line indicates the detection limit of 100 CFU/mL.

To assess the stability of the CFT@ZIF, we introduced a plasmid encoding small near-infrared

fluorescent protein (smURFP) to CFT073 and monitored smURFP fluorescence of CFT@ZIF and

unencapsulated CFT073 during heating (**Figure C.3A**). In addition to finding that thermal stress

did not lyse bacteria or induce changes in the CFT@ZIF morphology, we observed that smURFP

fluorescence was preserved in CFT@ZIF compared to unencapsulated CFT073 (**Figure C.3B**).

We and others reported that ZIF-8 thermally protects proteins immobilized in the ZIF-8 matrix

from denaturation,[148-150, 194] likely by limiting conformational mobility within the framework; however, to the best of our knowledge, an example of a protein within a microorganism being protected has not been reported.

A challenge in whole-cell vaccine formulation is that the bacteria must be inactivated with minimal damage to the surface epitopes, including delicate membrane-bound proteins and complex oligosaccharides. We tested whether ZIF encapsulation inactivates CFT073. Following formation of the ZIF shell, immobilized CFT073 was incubated for 30 min at room temperature and exfoliated with 500 mM sodium acetate buffer. Unencapsulated CFT073 was inactivated using formalin or heating as described for other whole-cell bacterial vaccines,[230-232] and bacterial viability was measured for each condition by colony forming unit (CFU) assay, and compared to naked CFT073 incubated in 0.9% saline. Bacterial growth was observed for unencapsulated CFT073 incubated in saline or in the sodium acetate buffer but not for bacteria that were formalin-fixed, heat-inactivated, or, importantly, exfoliated from the ZIF shell (**Figure 4.1F**). These results support that the ZIF-shell growth process itself inactivates bacteria, which is in line with previous observations that overexposure to zinc causes bacterial cell death.[233-235]

Having established that CFT073 was encapsulated, intact, and inactivated, we turned to immunological studies. A humoral response depends on the activation of antigen-specific B cells to differentiate into antibody-producing plasma cells.[236] We hypothesized that the ZIF shell would induce higher antibody titers by protecting immunogenic surface antigens. We first compared the time-resolved fluorescence of smURFP-expressing CFT-Fixed, CFT@ZIF, and free ZIF-8 and confirmed that emission was from smURFP within the CFT073 and that formalin fixing did not alter fluorescence *in vivo* (**Figure C.3C**). Mice were then injected with saline, formalin-fixed

CFT073 (CFT-Fixed), or CFT@ZIF subcutaneously and monitored over a period of 12 days until

fluorescence levels returned to baseline (**Figure 4.2A**). Images collected during this period show

that intact CFT@ZIF remained at the injection site 4 days longer than CFT-Fixed (**Figure 4.2B**).

Figure 4.2: Mice (n=4) were injected with smURFP-expressing CFT073 that was inactivated with formalin (CFT-Fixed) or by encapsulation (CFT@ZIF). A) The graph shows fluorescence change at the site of injection over time. The baseline is the average fluorescence of four mice before and after injecting with saline. The dashed line represents the error of the baseline. B) Representative images of mice prior to injection with CFT-Fixed or CFT@ZIF and after injection were monitored over a course of 12 days. After injection, images were taken at 15, 30, 60, 120, 240, and 480 min, then every 12 h for 12 days. C) Vaccination schedule for mice injected with either saline, CFT-Fixed, CFT@ZIF, CFT-Heat, or CFT@ZIF-Heat. Black arrows are vaccinations and red arrows are blood draws. D) At day 21 and 42, blood was drawn and measured by ELISA to determine the antibody production. E) IL-6 in serum at day 14. F) H&E staining of organs at day 42. Error bars represent the mean±SD. Statistical significance was calculated using an ordinary one-way ANOVA with Tukey's multiple comparison post-test (*$p < 0.05$, **$p < 0.01$, ***$p < 0.0005$, ****$p < 0.0001$).

We next measured antibody titers in mice injected with saline, CFT-Fixed, thermally inactivated

CFT073 (CFT-Heat), CFT@ZIF, or thermally-treated CFT@ZIF (CFT@ZIF-Heat) according to

the vaccination and blood sampling schedule in **Figure 4.2C**. Serum from days 21 and 42 post-injection was serially diluted and the amount of anti-CFT073 IgG produced was determined by ELISA against CFT073. Mice immunized with CFT@ZIF produced the highest levels of anti-CFT073 IgG at day 21 and 42 compared to all other groups (**Figure 4.2D**). Remarkably, even the thermally stressed CFT@ZIF-Heat induced more anti-CFT073 IgG compared to unstressed CFT-Fixed (**Figure 4.2D**). As expected, the thermally-inactivated CFT-Heat formulation induced the lowest antibody production, in line with the observation that high temperatures lead to thermal denaturation of proteinaceous and sugar-based epitopes.[10] As IL-6 promotes plasma cell production of immunoglobulins,[237] we diluted serum from day 14 and measured IL-6 production by ELISA. IL-6 levels were highest in CFT@ZIF, which correlated with enhanced production of antibodies in mice injected with this formulation (**Figure 4.2E**). The increase in CFT073-specific antibodies from mice injected with CFT@ZIF supports the hypothesis that ZIF encapsulation protects immunogenic epitopes. Elevated antibody production may also be a result of the prolonged presence of CFT@ZIF in the tissue compared to unencapsulated bacteria.

Throughout the experiment, mice were monitored daily and showed no signs of pain or changes in behavior, indicating the CFT@ZIF vaccine did not induce acute toxicity. At day 42, the mice were euthanized, and the spleen, liver, kidney, injection site, lung, and heart were collected, fixed in formaldehyde, and stained with H&E for pathological analysis. Organs displayed no signs of toxicity and H&E-stained organ sections showed no abnormal lesions, aggregation, or change in tissue compared to mice injected with saline (**Figure 4.2F**).
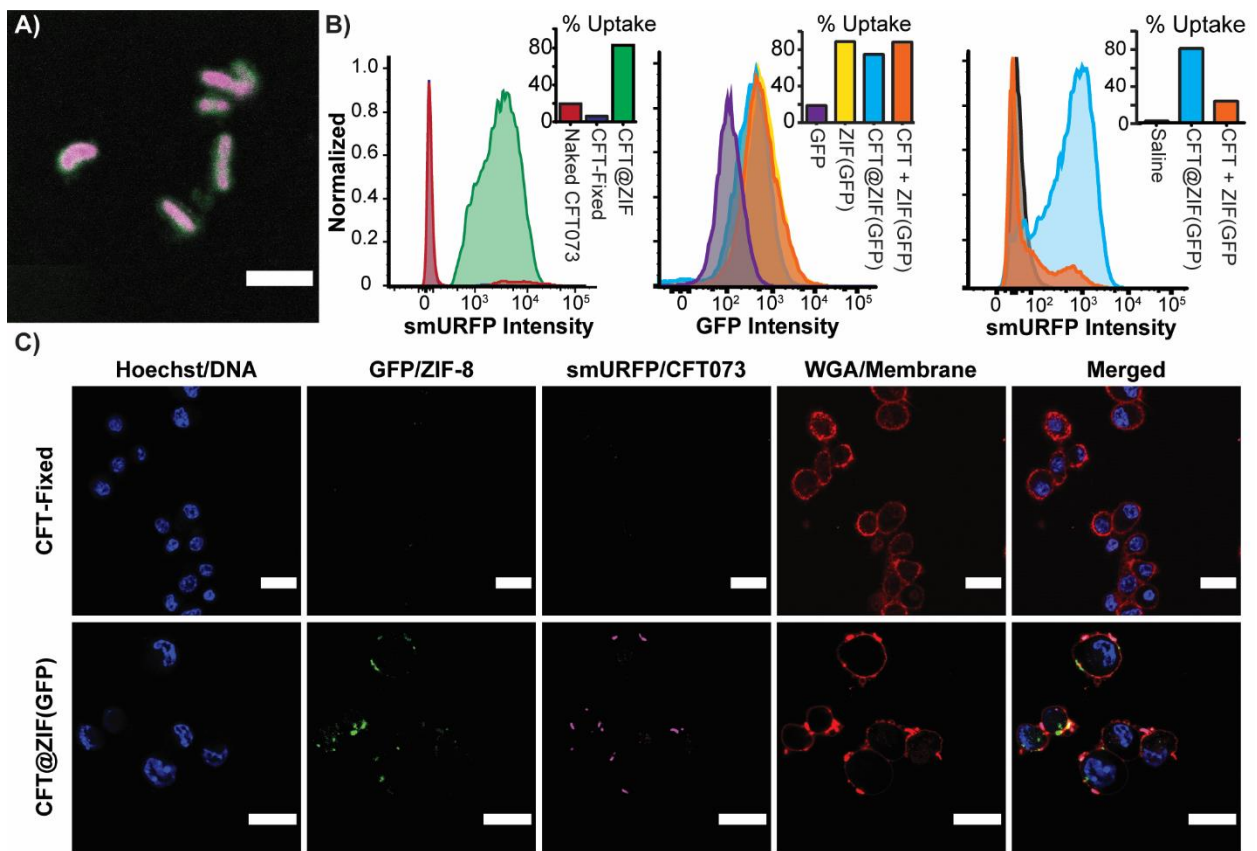
Figure 4.3: A) Confocal micrograph of CFT@ZIF(GFP). The outer shell fluoresces green from trapped GFP while the encapsulated bacteria fluoresce red. Scale bar = 5 µm. B) Representative histograms show smURFP or GFP fluorescence, for the indicated bacterial preparations and controls. C) Confocal live cell images of smURFP expressing CFT-Fixed and CFT@ZIF(GFP) incubated with RAW 264.7 macrophages after 4 h. Scale bar = 20 µm.

Antigen persistence via a "depot effect" is correlated with a strong adaptive immune response, as demonstrated above. However, a second mechanistic explanation for the greater antibody response may be increased uptake by professional phagocytes. We hypothesized that coating *E. coli* in a charge-neutral metal-organic framework would promote phagocytosis. ZIF-8 dissolves in the acidic compartments of phagosomes, endosomes, and lysosomes, [30, 238-240] which would free surface epitopes in a manner similar to our exfoliation process in acidic buffer. To test this, we performed ZIF-8 shell growth on smURFP-expressing CFT073 in a solution with GFP to make

CFT@ZIF(GFP). The rapid shell formation around the CFT073 serendipitously captured solvated GFP within the crystalline matrix, which created a fluorescent "core-shell" composite that allowed us to monitor the bacteria separately from the ZIF shell (**Figure 4.3A**). CFT073, CFT-Fixed, and CFT@ZIF(GFP) were incubated for four hours with RAW 264.7 macrophages. Flow cytometry analyses showed a four-fold increase in uptake of ZIF formulations of CFT073 over naked CFT073 and more than an order of magnitude increase over formalin-fixed CFT (**Figure 4.3B**). Confocal microscopy images revealed that GFP was taken up by the cells, which strongly indicates that the ZIF-shell was intact during bacterial uptake (**Figure 4.3C**). To rule out that the presence of ZIF-8 in the media promoted macrophage phagocytosis, a mixture of CFT073 and ZIF-8 crystals (CFT+ZIF(GFP)) was incubated together with the macrophages, which did not result in greater CFT073 uptake compared to naked CFT073. Taken together, these data demonstrate that the ZIF encapsulation is correlated with increased uptake of CFT073. This, in addition to the depot effect, likely accounts for the strong antibody response observed in **Figure 4.2D**.

Activation of a cell-mediated immune response is a vital aspect of vaccine development to promote long-term memory.[124, 241] To determine whether CFT@ZIF promotes a cell-mediated immune response, we measured TNF-α, an immunostimulatory cytokine mainly produced by macrophages and T_h1 (Type 1 T helper) CD4$^+$ T cells, and IFN-γ, a cytokine produced mainly by T_h1 T cells and dendritic cells promoting a cell-mediated response by stimulating cytotoxic T lymphocytes.[242, 243] We employed the vaccination schedule depicted in **Figure 4.2C**, and on day 21, re-stimulated splenocytes collected from each group with CFT073. We measured TNF-α (**Figure 4.4A**) and IFN-γ expression (**Figure 4.4B**) levels by ELISA, observing that mice immunized with CFT@ZIF had higher levels of both cytokines compared to CFT-Fixed treated mice following re-stimulation.

Taken together, our data indicate a more robust cell mediated response in mice treated with CFT@ZIF compared to CFT-Fixed-vaccinated mice.
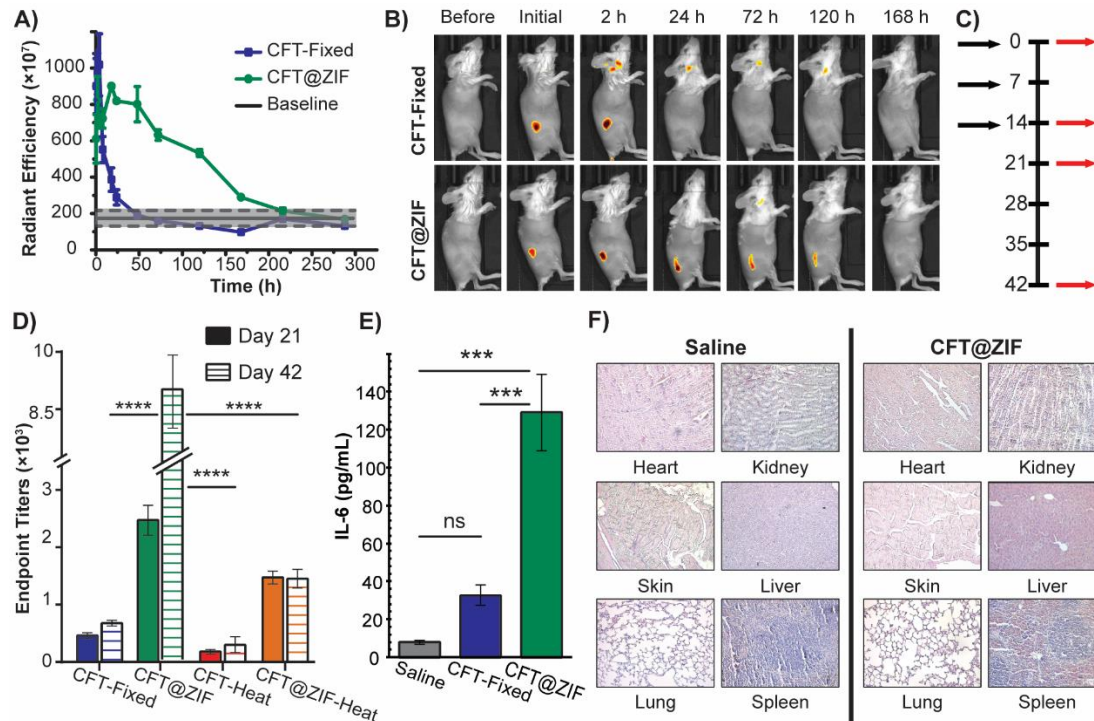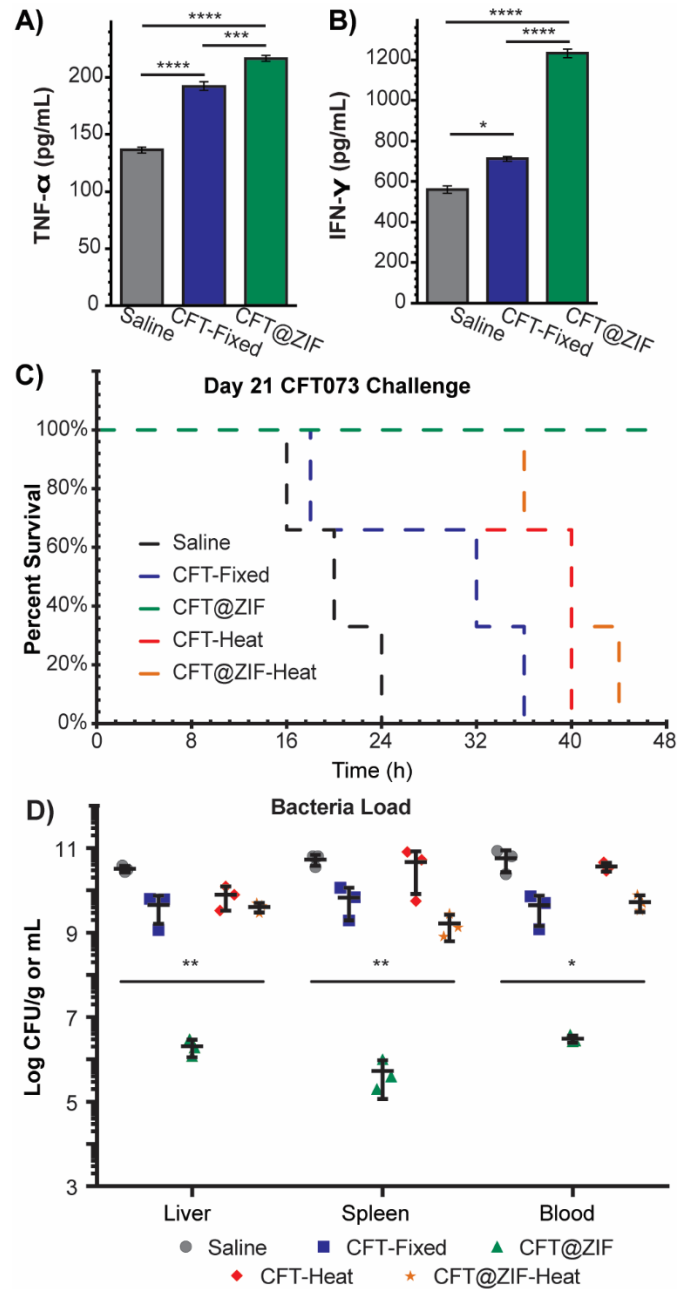

Figure 4.4: Mice (n=4) were injected with CFT073 that was inactivated with formalin (CFT-Fixed) or by encapsulation (CFT@ZIF). At Day 21, splenocytes were collected from immunized mice and incubated with 10 µg/mL of naked CFT073 for 48 h. After 48 h, the supernatant was tested for A) TNF-α and B) IFN-γ. A second cohort of mice following the vaccination schedule

in **Figure 4.2C** were injected interperitoneally with a lethal dose of CFT073 at day 21 and monitored for 48 h. C) Survival for each group over the course of 48 h. D) When the mice became moribund or by the end of 48 h were assessed for the bacteria loads in the liver, spleen, and blood. Error bars represent the mean±SD. Statistical significance was calculated using an ordinary one-way ANOVA with Tukey's multiple comparison post-test (*$p < 0.05$, **$p < 0.01$, ***$p < 0.0005$, ****$p < 0.0001$).

Mice vaccinated with CFT@ZIF had increased antibody production and increased expression of multiple key cytokines at day 21 compared to other CFT formulations. To determine whether these responses would be protective, we used a uro-sepsis model. We vaccinated as above with either saline, CFT-Fixed, CFT-Heat, CFT@ZIF, or thermally stressed CFT@ZIF. On day 21, we administered a lethal dose[15] of CFT073 and mice were monitored over the course of 48 hours and euthanized when they became moribund, defined by lack of movement for over 15 minutes, shaking in place, and a decrease of body temperature. All CFT@ZIF-vaccinated mice survived after 48 hours compared to the other treated groups, which all succumbed to challenge (**Figure 4.4C**). After euthanasia, blood, spleens, and livers were collected, homogenized, and CFUs were enumerated (**Figure 4.4D**). Bacterial load in the blood, spleens, and livers of CFT@ZIF-vaccinated mice were four orders of magnitude lower than all the other groups. This lower bacterial load may be attributed to the 5-fold higher anti-CFT073 IgG that CFT@ZIF promotes over CFT-Fixed. Notably, the thermally stressed CFT@ZIF formulation promoted longer survival, which hints at a possible thermally protective effect of the ZIF-8 shell, an observation that is with considerable precedence.[31, 89, 206]

4.3   Conclusions

In this work, we demonstrated that ZIF-8 effectively inactivated a urosepsis strain of UPEC, creating a persistent vaccine formulation that considerably outperformed current whole cell

inactivation methods in nearly every regard. This method of inactivation avoids the use of toxic formaldehyde, and is faster, more convenient, and yields superior results. Only CFT@ZIF-vaccinated mice survived a lethal dose of CFT073, which we attribute to the five-fold increase in IgG and superior uptake by phagocytes as compared to CFT-Fixed-vaccinated mice. Furthermore, this reduction in bacterial load and survival exceeds the efficacy of published subunit vaccine strategies for CFT073.[214, 244, 245] The results showing improved survival even after thermally stressing the vaccine formulation are in line with published data showing that ZIF protects surface epitope structure. Finally, the biomimetic growth strategy that we employed here is likely generalizable across a number of different organisms, presenting an enormous opportunity for a generalizable approach toward whole-cell vaccine formulation. Formulation of the inactivated bacteria does not use dangerous or toxic compounds, involves the mixture of only three components, and the total reaction time is under 30 minutes. Our ecologically friendly and low-cost approach makes it an ideal platform for rapid vaccine production from patient isolate UTIs. This creates an opportunity to produce rapidly patient-specific prophylactic and therapeutic vaccine formulations for those suffering from recurrent UTI in a truly personalized medicine approach.

CHAPTER 5

CONCLUSION AND FUTURE WORK

5.1　Conclusions

The development of materials for healthcare treatment is essential for curing diseases. Chemistry offers a vast amount of synthetic approaches to tune biomaterials to serve specific needs, such as cell targeting, tracking, and stimuli response. However, to fully understand the safety of these biomaterials for patient care will involve collaborations with immunologist, biologist, and pathologist from other fields. The areas of biomaterials and colloidal chemistry were used to develop formulations for physiologically safe microparticle that could be used to deliver antigens encapsulated within to patients and showed that serum would develop holes that would release the antigens over time. The joining of the areas of immunology and material science have introduced a simple one-pot method under aqueous conditions to preserve vaccines at ambient conditions during shipping without refrigeration and eliminate the world's reliance on the cold chain. In addition, this novel vaccine protection platform has the potential to activate the immune system after a single injection owing to the sustained release.

5.2　Future Directions

There are still a lot of studies before ZIF-8 can be used as a biomaterial for vaccination and multiple directions can be followed from this work. The most beneficial study would be to determine the type of immune response ZIF-8 helps activate. The current experiments done above seem to lean more towards a Th2 type response but investigating the cytokines CD4+ helper T cells produce

after vaccination with ZIF-8 containing antigens and ZIF-8 without antigens would verify the mechanism of immune activation. Other minor, but beneficial studies would be to determine the effects of number of injections, dosage, crystal size, and adjuvants have in developing adaptive immune memory. The studies of ZIF-8 as a biomaterial for vaccination should move away from whole viruses and bacteria to safer subunit/inactivated vaccines to determine if it can initiate an immune response for the proteins inlayed within. This would be novel because a major issue with subunit vaccines is their inability to produce a long-lasting, protective immune response and this would show that ZIF-8 cab be both an adjuvant and thermal protection carrier. Either way ZIF-8 has the potential to encapsulate multiple components during crystal growth, which could be used to encapsulate multiple antigens with adjuvant or multiple antigens at once. Animal models that can test this multiple antigen presenting system against an infectious disease would further confirm ZIF-8 as a generalizable method for prophylactic vaccines. The immune response should be tested for the type of antibodies produced and immune cell activation in the lymph node, spleen, blood and area of vaccination. The testing of known subunit proteins that the immune system develops against, during the actual infection, can be used to look at T cell and B cell activation specific to that antigen. Survival studies can be done and correlated to the cell mediated response and humoral response to correlate what led to survival would be a very novel experiment to do. Finally, the formulation that provides long-term protection at ambient condition, produce long-lasting immune memory after a single injection, and prevents infections/death should be tested in clinical trials.

APPENDIX A

EXTENDED DATA FOR CHAPTER 2

MATERIALS

Acetic acid, acetic anhydride, acetone, bovine serum albumin, 6-bromohexanoic acid, 1-butanol, chloroform, o-dichlorobenzene, diethanolamine, egg albumin, ethyl acetate, 1-ethyl-3-(3-dimethylaminopropyl)carbodiimide (EDC), ethylenediamine, ethylenediaminetetraacetic acid (EDTA), guanidinium chloride, hydrazinobenzene sulfonic acid hydrates, hydrochloric acid, hydroxybenzotriazole (HOBt), 4-(2-hydroxyethyl)piperazine-1-ethanesulfonic acid (HEPES), iodomethane, magnesium chloride, malonaldehyde bis(phenylimine) monohydrochloride, β-mercatoethanol, methanol, 3-methyl-2-butanone, 2-methylimidazole, paraformaldehyde, p-nitrophenylphosphate, potassium hydroxide, potassium phosphate dibasic, potassium phosphate monobasic, poly(ethylene glycol) 8000, poly(vinylpyrrolidone) 40k (PVP 40k), 2-propanol, pyridine, sodium azide, sodium bicarbonate, sodium carbonate, sodium chloride, sodium hydroxide, sodium phosphate dibasic, sodium phosphate monobasic, sodium sulfite, sucrose, Triton X-100, Tween-20, and zinc acetate dihydrate were purchased from Sigma-Aldrich (St. Louis, MO, USA), Thermo Fisher Scientific (Waltham, MA, USA), Chem-Impex Int'l (Wood Dale, IL, USA), or VWR (Radnor, PA, USA), and used without further modification.

Lowry assay was performed using a Pierce Modified Lowry assay kit (Thermo Fisher Scientific).

ELISA was performed using a TMV ELISA kit (Agdia Inc. Elkhart, IN, USA).

Rabbit antiTMV IgG and Rabbit antiTMV-alkaline phosphatase IgG were provided with the ELISA kit. Goat antimouse-alkaline phosphatase IgG was purchased from Sigma-Aldrich.

Cy5-COOH was synthesized according to a literature protocol.[185]

Ultrapure water was obtained from an ELGA PURELAB flex 2 system with resistivity measured to at least 18.2 MΩ-cm.

ELISA Buffers

ELISA buffers were prepared according to documentation provided with the TMV ELISA kit.

Coating buffer: pH 9.6 Sodium carbonate/bicarbonate with sodium azide

Wash buffer: 0.1 M pH 7.4 PBS with 0.2% Tween-20

Sample Extraction buffer: Wash buffer with PVP 40k, sodium sulfite, chicken egg albumin, and sodium azide

Conjugate buffer: Wash buffer with bovine serum albumin, PVP 40k, and sodium azide

Substrate buffer: 1 M pH 9.8 diethanolamine with magnesium chloride and sodium azide

INSTRUMENTATIONS

UV-Vis

UV-Vis spectra were taken using a UV-1601PC UV-Vis-NIR Spectrophotometer (Shimadzu, Kyoto, Japan), Tecan Spark 20M plate reader (Tecan, Männedorf, Switzerland), or Biotek Synergy H4 hybrid reader (Biotek, Winooski, VT, USA). NanoDrop UV-Vis measurements were performed on a Thermo Scientific NanoDrop 2000 Spectrophotometer.

Fluorescence

Fluorescence measurements were taken using a Tecan Spark 20M plate reader.

Scanning Electron Microscopy

SEM was performed on a ZEISS Supra 40 Scanning Electron Microscope (Zeiss, Oberkochen, Germany) with an accelerating voltage of 2.5 kV and a working distance of 6.7 to 15.3 mm. Samples were sputtered with a 37 Å layer of gold.

Transmission Electron Microscopy

Transmission electron micrographs were taken on a JEOL JEM-1400+ (JEOL, Tokyo, Japan) at 120 kV with a Gatan 4k × 4k CCD camera. 5 µL of the ~0.1 mg/mL desalted sample was placed on a 300 mesh Formvar/carbon-coated copper grid (Electron Microscopy Sciences, Hatfield, PA, USA), allowed to stand for 30 seconds, and wicked off with Whatman #1 filter paper. 5 µL of 2% uranyl acetate (SPI Supplies, West Chester, PA, USA) was placed on the grid, allowed to stand for 30 seconds, wicked off as before, and the grid allowed to dry completely in air.

In vivo Fluorescence Imager

Fluorescent animal imaging was taken with IVIS Lumina III (PerkinElmer, Waltham, MA, USA) at an excitation of 620 nm and emission at 670 nm with a 0.5 s exposure.

METHODS

Propagation and Isolation of TMV

TMV particles were isolated from *Nicotiana benthamiana* plants from a previously published method.[150] The tobacco plants were grown, infected, and collected after 10 d of infection and stored at -80 °C until needed. Approximately 100 g of leaves were blended in pulses with 1000 mL of ice cold extraction buffer (0.1 M pH 7.4 potassium phosphate (KP) buffer, 0.2% (v/v) β-mercaptoethanol) followed by being pulverized with a mortar and pestle. The mixture was filtered through cheesecloth to remove the plant solids, and the filtrate centrifuged at 11,000 $\times g$ for 20 min at 4°C. The supernatant was filtered through cheesecloth again, and an equal volume of 1:1 chloroform/1- butanol mixture was added and stirred on ice for 30 min. The mixture was centrifuged at 4500 $\times g$ for 10 min. The aqueous phase was collected, followed by the addition of NaCl to a final concentration of 0.2 M, 8% (w/w) PEG 8000, and 1% (w/w) Triton X-100 surfactant. The mixture was stirred on ice for 30 min and stored at 4 °C for 1 h. The solution was

centrifuged at 22,000 $\times g$ for 15 min at 4 °C. The supernatant was discarded, and the pellet

resuspended in 0.1 M pH 7.4 potassium phosphate (KP) buffer at 4 °C overnight. The supernatant

was carefully layered on a 40% (w/v) sucrose gradient in 0.01 M KP buffer (with at least one

freeze-thaw cycle) in ultraclear tubes and centrifuged in a swing bucket rotor for 2 h at 96,000 $\times g$.

The light-scattering region was collected and centrifuged at 360,562 $\times g$ for 1.5 h. The supernatant

was discarded, and the pellet resuspended in 0.01 M pH 7.4 KP buffer overnight. The solution was

portioned equally into microcentrifuge tubes and centrifuged at 15,513 $\times g$ for 15 min. The

supernatant was collected as the final TMV solution. UV-Vis measurements were taken with

NanoDrop at 260 nm (RNA) and 280 nm (protein). A ratio of A_{260}/A_{280} around 1.23 indicates

intact TMV. Using the Beer-Lambert Law with $\varepsilon = 3$ as reported,[150] the solution concentration was

determined.

Synthesis

Cy5-COOH was synthesized according to literature protocol[246] and is reproduced below from

reference [185].

Scheme A.1. Synthesis of Cy5-COOH, reproduced from reference [185].
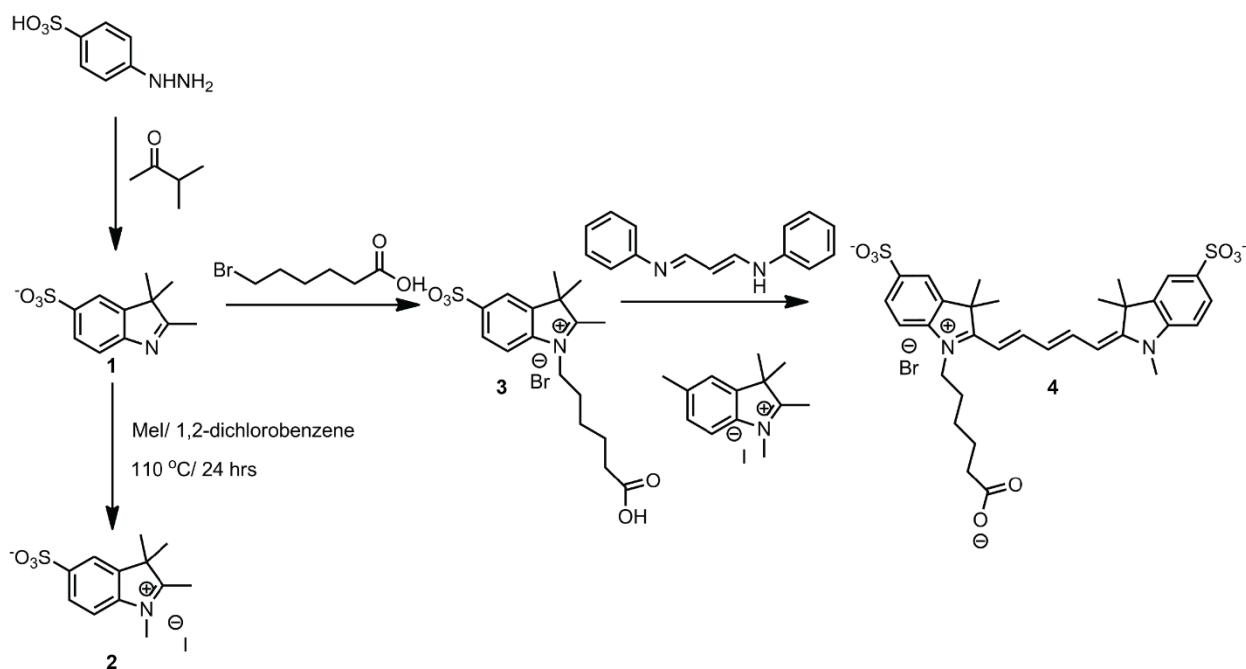
Synthesis of 3H-Indole-2,3,3-trimethyl-5-sulfonic Acid, Potassium Salt (1)

Hydrazinobenzene sulfonic acid hydrates (1.50 g, 7.60 mmol) and 3-methyl-2-butanone (2.52 mL, 23.4 mmol) were dissolved in acetic acid (4.5 mL). The mixture was heated to reflux at 110 °C for 3 h and acetic acid was removed. A solution of crude sulfonic acid in methanol (10 mL) was added dropwise to a stirred solution of potassium hydroxide (0.500 g) in 2-propanol (10 mL). The resulting mixture was stirred at 25 °C for 24 h and filtered through a paper filter. The residue was dried under reduced pressure to provide the crude compound (1.02 g, 4.49 mmol, 59.1% yield) (**1**). ^{1}H-NMR (600 MHz, D$_2$O) δ ppm 1.237 (s, 6H), 2.259 (s, 3H), 7.494 (d, J=8.02, 1H), 7.764 (d, J=8.09, 1H), 7.792 (s, 1H).

*Synthesis of 3H-Indolium, 1-Methyl-2,3,3-trimethyl-5-sulfonate (**2**)*

A slurry of crude **1** (0.900 g, 3.24 mmol) in iodomethane (3.5 mL, 0.20 mol) under N$_2$ was heated to reflux for 24 h and cooled down to 25 °C. The liquid phase was decanted, and the residue was washed with acetone (3 × 50 mL), filtered with a paper filter, and dried under reduced pressure at

40 °C to afford the crude compound (0.440 g, 1.25 mmol, 38.7% yield) (**2**). ^{1}H-NMR (600 MHz, D$_2$O) δ ppm 1.522 (s, 6H), 2.153 (s, 3H), 3.971 (s, 3H), 7.777 (d, J=8.25, 1H), 7.963 (d, J=8.80, 1H), 8.026 (s, 1H).

Synthesis of 3H-Indolium, 1-(5-Carboxypentyl)-2,3,3-trimethyl-5-sulfonate (3)

3H-Indole-2,3,3-trimethyl-5-sulfonic Acid, Potassium Salt (1.02 g, 3.70 mmol) and 6-bromohexanoic acid (0.827 g 4.33 mmol) were suspended in *o*-dichlorobenzene (5 mL). The suspension was stirred at 110 °C for 19 h, then allowed to cool to room temperature, and the supernatant was removed to afford 3H-Indolium, 1-(5-Carboxypentyl)-2,3,3-trimethyl-5-sulfonate (1.10 g, 2.73 mmol, 73.80% yield) (**3**). ^{1}H-NMR (600 MHz, D$_2$O) δ ppm 1.378 (m, 2H), 1.586 (s, 6H), 1.601 (m, 4H), 1.904 (t, J=7.65, 2H), 2.301 (t, J=7.14, 2H), 4.433 (t, J=7.41, 2H), 7.818 (d, J=8.58, 1H), 7.945 (d, J=8.64, 1H), 7.952 (s, 1H).

Synthesis of 3H-Indolium, 2-[5-[1-(5-Carboxypentyl)-1,3-dihydro-3,3- dimethyl-5-sulfo-2H-indol-ylidene]-1,3-pentadien-1-yl]-1-methyl-3,3-dimethyl-5-sulfonate (4)

A suspension of 1-methyl-2,3,3-trimethyl-3H-indol-1-ium-5-sulfonate (**2**) (0.253 g, 1.00 mmol) and malonaldehyde bis(phenylimine) monohydrochloride (0.235 g, 1.10 mmol) in acetic acid (5 mL) and acetic anhydride (5 mL) was refluxed at 110 °C for 4 h. Solvent was removed under reduced pressure and the resultant solid was dissolved in pyridine (10 mL) under N$_2$. The mixture was then treated with compound (**3**) (0.353 g, 1.00 mmol) at 25 °C. Reaction mixture was stirred at 60 °C for 4 h, cooled down to 25 °C, and agitated a heterogeneous mixture by addition of ethyl acetate (10 mL). Resulting mixture was filtered through a paper filter, and the residue was dried under reduced pressure and purified with reverse flash chromatography to yield (**4**) as a dark blue solid (0.150 g, 0.234 mmol, 23.4% yield). ^{1}H-NMR (600 MHz, D$_2$O) δ ppm 1.372 (m, 2H), 1.539

(m, 14H), 1.716 (p, J=4.90, 4H), 2.294 (t, J=7.50, 2H), 3.518 (s, 3H), 3.964 (m, 2H), 6.0474 (t, J=14.03, 2H), 6.376 (t, J=12.19, 1H), 7.259 (t, J=6.78, 2H), 7.741-7.779 (m, 3H), 7.871 (t, J=12.72, 2H).

Preparation of TMV@ZIF composites

TMV@ZIF

TMV@ZIF was prepared according to literature protocol.[150] 0.111 mg of native TMV was added to a 20 mL scintillation vial, followed by 3 mL of 400 mM 2-methylimidazole in 3 1 mL aliquots. 3×500 µL aliquots of 20 mM zinc acetate dihydrate were rapidly added to the virus-ligand solution, and the vial capped and swirled for 20 sec. Flocculates appeared within the first few seconds of zinc addition. The solution was left to incubate on the benchtop at R.T. for 16 to 18 h. The ripened solution was then transferred to a 15 mL Falcon tube and centrifuged at $4300 \times g$ for 20 min at 4 °C. The supernatant was discarded, and the pellet washed with ultrapure water twice. The final TMV@ZIF powder was then ether used as-is or dried in air.

Bioconjugation

Interior-modified Cy5-TMV was prepared according to a previously reported method.[185] The interior surface of TMV was modified with ethylenediamine (EA) using an EDC coupling reaction. 200 µL of a TMV solution (10 mg/mL) was diluted to 2 mg/mL with 574 µL of 0.1 M pH 7.4 HEPES buffer at R.T. followed by the addition of 130 µL of 0.1 M EA, 3 mg of HOBt, and 96 µL of 0.1 M EDC. The reaction mixture was incubated at R.T. for 24 h, purified with a PD MidiTrap G-25 column, and the solution was washed three times with 0.1 M KP buffer and concentrated to 10 mg/mL with a 10K MWCO Pierce™ Protein Concentrator to yield *in*EA-TMV. Cy5-COOH was then attached by the EDC reaction. 200 µL of the *in*EA-TMV solution (10 mg/mL) was diluted

to 2 mg/mL with 574 µL of 0.1 M pH 7.4 HEPES buffer at R.T. followed by the addition of 130 µL of 0.1 M Cy5-COOH, 3 mg of HOBt, and 96 µL of 0.1 M EDC. The reaction mixture was incubated at R.T. for 24 h, purified with a PD MidiTrap G-25 column, and the solution was washed three times with 0.1 M KP buffer and concentrated to 10 mg/mL with a 10K MWCO Pierce™ Protein Concentrator to yield Cy5-TMV.

Cy5-TMV@ZIF

Cy5-TMV@ZIF was prepared using the same protocol as TMV@ZIF, except using Cy5-TMV instead of native TMV.

EDTA Exfoliation

Exfoliation buffer was prepared by adding EDTA to 0.1 M in a 0.1 M potassium hydroxide solution. Solid potassium hydroxide pellets were added until the EDTA was fully dissolved, then the pH adjusted to 7.0 with HCl.

TMV@ZIF composites were exfoliated by reducing the solvent level to a minimum or drying out, then adding 1 to 2 mL of EDTA Exfoliation buffer and left on a rotisserie at 37 °C. Wet samples became water-clear within the first few minutes. Resuspended dried samples became cloudy and required a longer time to clear up, up to overnight. Samples were then buffer exchanged with a 10K MWCO Pierce™ Protein Concentrator.

TMV@ZIF Stressing

Three batches of TMV@ZIF were combined and either left as is (non-stressed), soaked in 1 mL of methanol, ethyl acetate, or 6 M guanidinium chloride overnight, or heated to 100 °C in a water bath for 20 min. Naked TMV samples were stressed in the same manner, with 0.333 mg of TMV soaked in 1 mL solvent overnight, or heated to 100 °C for 20 min. Encapsulated samples were

collected via centrifugation at 4300 $\times g$ for 20 min, rinsed with ultrapure water, and exfoliated in EDTA overnight. Exfoliated and naked samples were buffer exchanged into 0.1 M pH 7.4 sodium phosphate buffer in a centrifugal filter for concentration determination by Lowry assay and then diluted to 5×10^{-4} mg/mL for ELISA measurements.

ELISA

Stressed TMV

Stressed TMV@ZIF samples were exfoliated, then both exfoliated stressed TMV@ZIF and stressed naked TMV samples were desalted with a 10K MWCO Pierce™ Protein Concentrator and resuspended in 0.1 M pH 7.4 sodium phosphate buffer. Protein concentrations were then determined by Lowry assay before being diluted to 5×10^{-4} mg/mL for ELISA.

Rabbit anti-TMV IgG in coating buffer was added 100 µL per well to a 96-well plate and incubated at R.T. for 4 h or overnight at 4 °C. The plate was emptied and washed 3× with wash buffer. Samples and standards—concentrations determined by Lowry assay—were diluted to 5×10^{-4} mg/mL with sample extraction buffer, added 100 µL per well with additional wells filled with 100 µL per well with just sample extraction buffer as the buffer blank, and incubated for 2 h at R.T. or overnight at 4 °C. The plate was emptied and washed 8× with wash buffer. Alkaline phosphatase-conjugated rabbit anti-TMV IgG in conjugate buffer was added 100 µL per well and incubated for 2 hours at R.T. The plate was emptied and washed 8× with wash buffer. 1 mg/mL *p*-nitrophenylphosphate in substrate buffer was added 100 µL per well and the plate developed for 45 min at R.T. The plate was read at 405 nm, 420 nm, and 450 nm, and the absorbance values of buffer blank wells averaged and subtracted from the entire plate. Experiments were performed in 4 replicates and the values were normalized between that of naked non-stressed TMV (100%) and

that of the buffer blank (0%). The internal control ensures data comparability between separate

ELISA experiments. Percent difference was calculated according to the equation: $\dfrac{|V_1 - V_2|}{\left(\dfrac{V_1 + V_2}{2}\right)}$

where V_1 and V_2 are values expressed in percentages. The percent differences are listed below in

Table A1.

Table A.1: ELISA values of stressed TMV, stressed TMV@ZIF, and their percent differences

Stress	Naked	Encapsulated	Percent Difference
Non-Stressed	$102.8 \pm 2.3\%$	$108.9 \pm 3.6\%$	3.9%
Heated	$6.447 \pm 0.188\%$	$97.53 \pm 1.52\%$	165.0%
Methanol	$43.02 \pm 3.26\%$	$92.49 \pm 2.63\%$	55.42%
6 M Guanidine HCl	$0.09033 \pm 0.08277\%$	$70.70 \pm 3.78\%$	199.2%
Ethyl Acetate	$69.72 \pm 2.25\%$	$90.81 \pm 2.84\%$	18.33%

Plant Infection

Nicotiana benthamiana plants were divided into 4 groups (n = 6 plants) and inoculated with 0.01

M pH 7.4 KP buffer as a negative control, TMV@ZIF in ultrapure water, TMV@ZIF exfoliated

with EDTA and buffer exchanged into 0.01 M pH 7.4 KP buffer, and native TMV in 0.01 M pH

7.4 KP buffer as a positive control. Solutions were prepared such that 50 µL of solution delivered

5 µg of TMV, and 50 µL per leaf was used. To ensure no cross contamination each group was

placed in different trays and watered and handled separately. After 10 d, the plants were collected

into separate bags and stored at -80 °C until needed. Frozen leaves were coarsely ground and

approximately 1 g of recovered plant matter per group was macerated using a mortar and pestle in

10 mL of sample extraction buffer per 1 g of leaves. The plant pulp was allowed to extract

overnight at 4 °C, then centrifuged to remove large plant matter, and the supernatant collected as

samples for ELISA.

Mouse Serum

Rabbit anti-TMV IgG in coating buffer was added 100 µL per well to a 96-well plate and incubated at R.T. for 4 h or overnight at 4 °C. The plate was emptied and washed 3× with wash buffer. The collected plant extraction solutions were added 100 µL per well in 1×, 10×, and 50× dilutions, and incubated for 2 h at R.T. or overnight at 4 °C. The plate was emptied and washed 8× with wash buffer. Alkaline phosphatase-conjugated rabbit anti-TMV IgG in conjugate buffer was added 100 µL per well and incubated for 2 h at R.T. The plate was emptied and washed 8× with wash buffer. 1 mg/mL *p*-nitrophenylphosphate in substrate buffer was added 100 µL per well and the plate developed for 45 min at R.T. The plate was read at 405 nm, 420 nm, and 450 nm, and the absorbance values of buffer blank wells averaged and subtracted from the entire plate. Experiments were performed in 4 replicates, a best-fit line was fit to the blank-subtracted averaged standard values, sample values were calculated from the equation, dilutions were back-calculated and averaged, and values reported as the average ± standard deviation of the apparent sample concentrations in µg/mL.

Test Mice

8 BALB/c mice were divided into two groups (n = 4) and either left uninjected or injected subcutaneously with 100 µg of native TMV in saline. Blood was drawn submandibularly after 10 d, centrifuged to remove erythrocytes, and relative antiTMV IgG levels determined by ELISA as per the above procedure. Serum was serially diluted by factors of 2 from 20× to 10240× in order to determine relative ELISA responses and optimal serum dilution levels for subsequent ELISAs.

Mouse Time Study

All mice studies were approved by the Institutional Animal Care and Use Committee at the University of Texas at Dallas (Protocol # 17-05). 12 BALB/c mice were divided into three groups

(n = 4) and injected with saline, native TMV in saline, or TMV@ZIF suspended in saline. TMV solutions were prepared such that 200 µL delivered 10 µg of TMV. Doses of 200 µL of saline, TMV, or TMV@ZIF were administered subcutaneously on day 0, 2, 4, and 6 and blood was withdrawn submandibularly on day 0, 4, 7, and 35. The blood was centrifuged to remove erythrocytes, and the antiTMV IgG content of the resultant serum was determined by ELISA as described above. At the end of the study, the mice were sacrificed for histological analysis on the spleen, liver, kidney, lung, heart, and the skin at the administration site. The mice were sacrificed by carbon dioxide asphyxiation, the organs harvested, and fixed in 4% formaldehyde overnight. The fixed organs were moved to a 70% ethanol solution and processed with an ASP300 S tissue processor (Leica Biosystems, Buffalo Grove, IL) for dehydration into paraffin. The organs were then embedded into paraffin wax using a HistoCore Arcadia C and H paraffin embedding station (Leica Biosystems, Buffalo Grove, IL). Each organ was sliced into 4 µm sheets using a RM2235 manual microtome (Leica Biosystems, Buffalo Grove, IL) and imaged with a DMi1 optical microscope (Leica Biosystems, Buffalo Grove, IL) at 40× magnification.

Mouse Imaging

Ten BALB/c mice were fed a non-fluorescent diet and shaved once the mice showed no abdominal autofluorescence. The mice were anaesthetized with isoflurane and injected with 200 µL of saline (n = 4), Cy5-TMV (n = 3), or Cy5-TMV@ZIF (n = 3). The TMV-containing solutions were prepared such that 200 µL delivered 10 µg of TMV. A series of time points were taken at 1, 5, 10, and 30 min, with additional time points at 1, 2, 4, 8, 12, 18, 24, 30, 36, 48, and every 24 h thereafter until the fluorescence decayed back to the average level of the saline injected mice.

SUPPLEMENTARY FIGURES
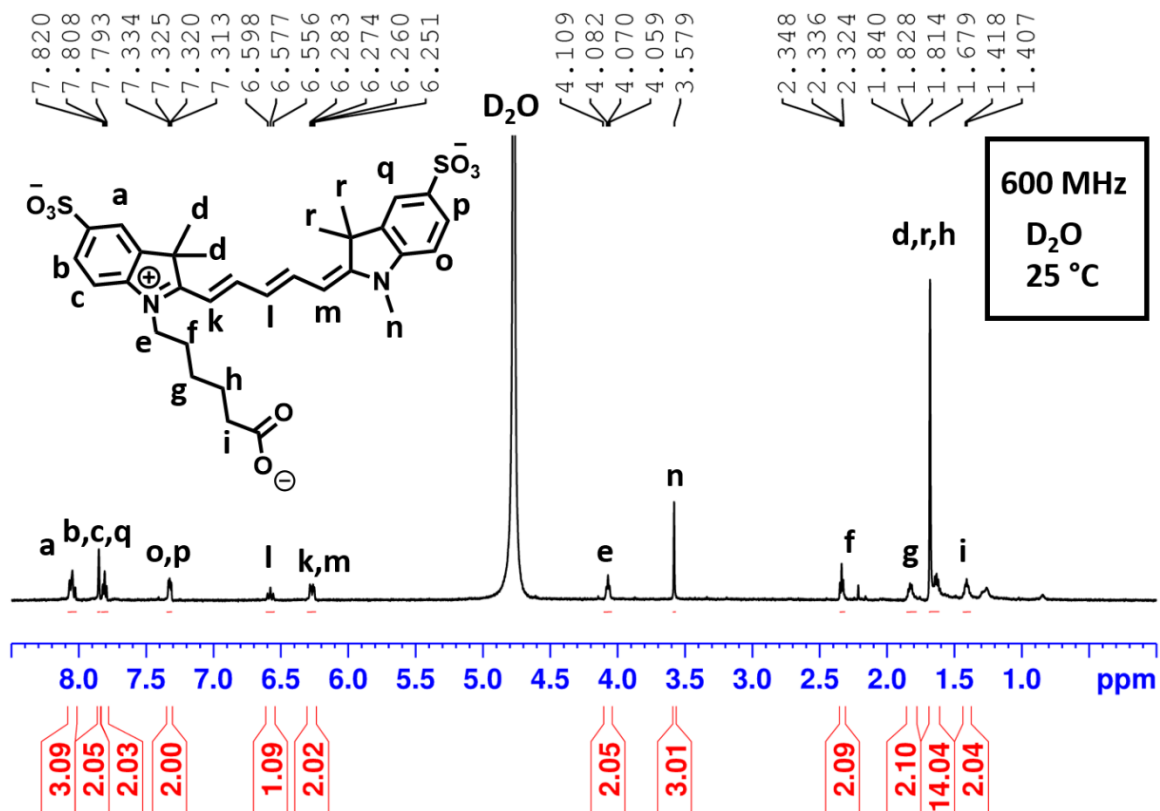
Figure A.1: ^{1}H NMR spectra of (**4**)
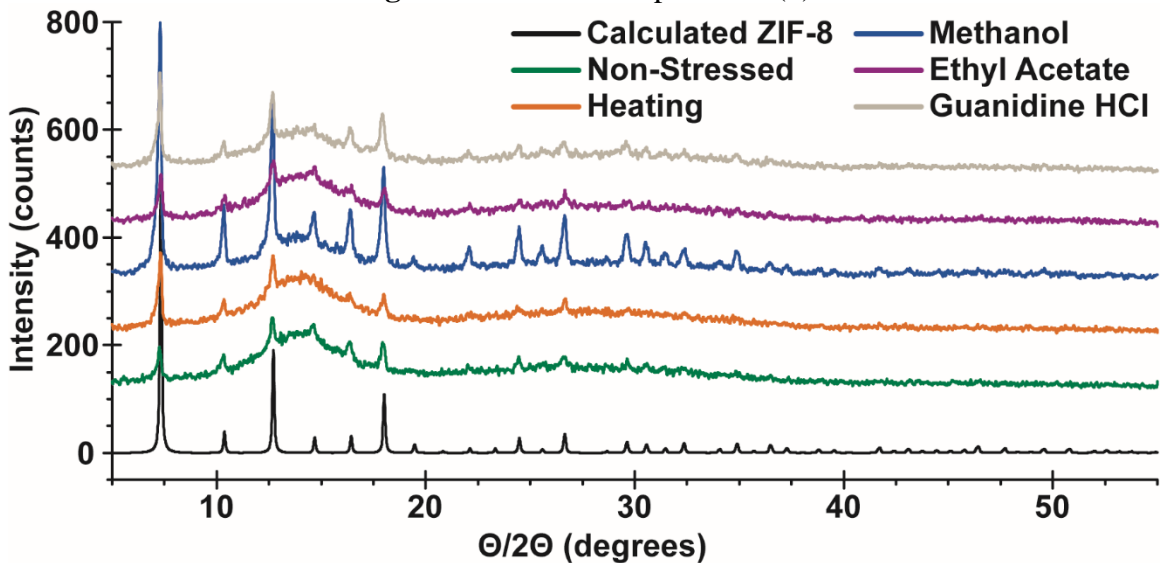
Figure A.2: PXRD spectra of stressed TMV@ZIF samples.
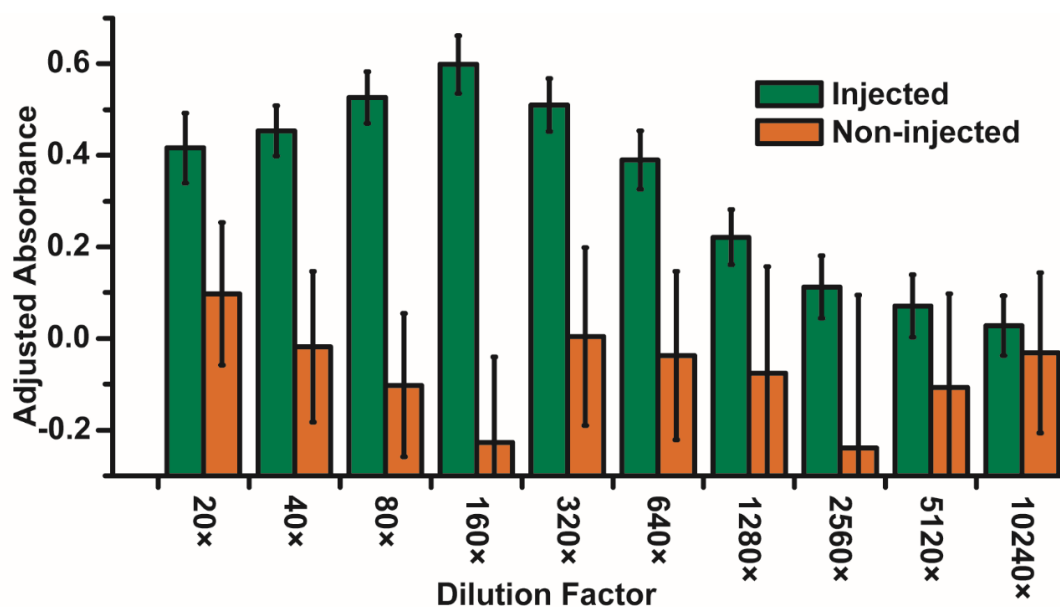
Figure A.3: ELISA response of test mice after 10 days.
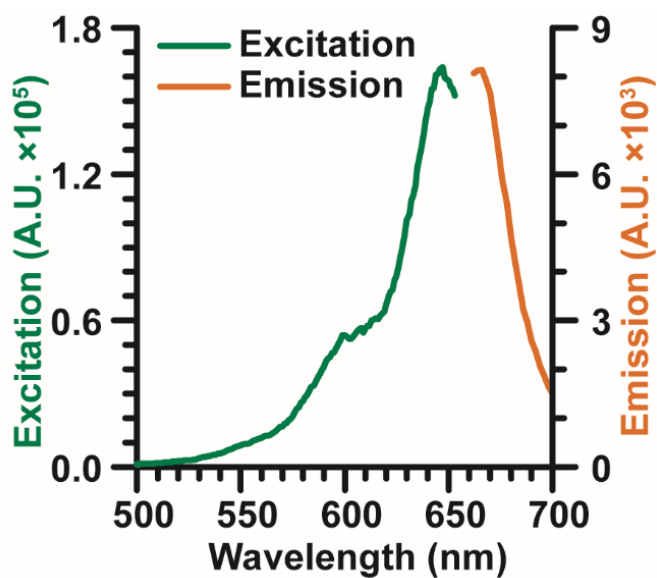
Figure A.4: Excitation and emission spectra of Cy5-TMV. Excitation λ_{max} = 647 nm; Emission λ_{max} = 666 nm
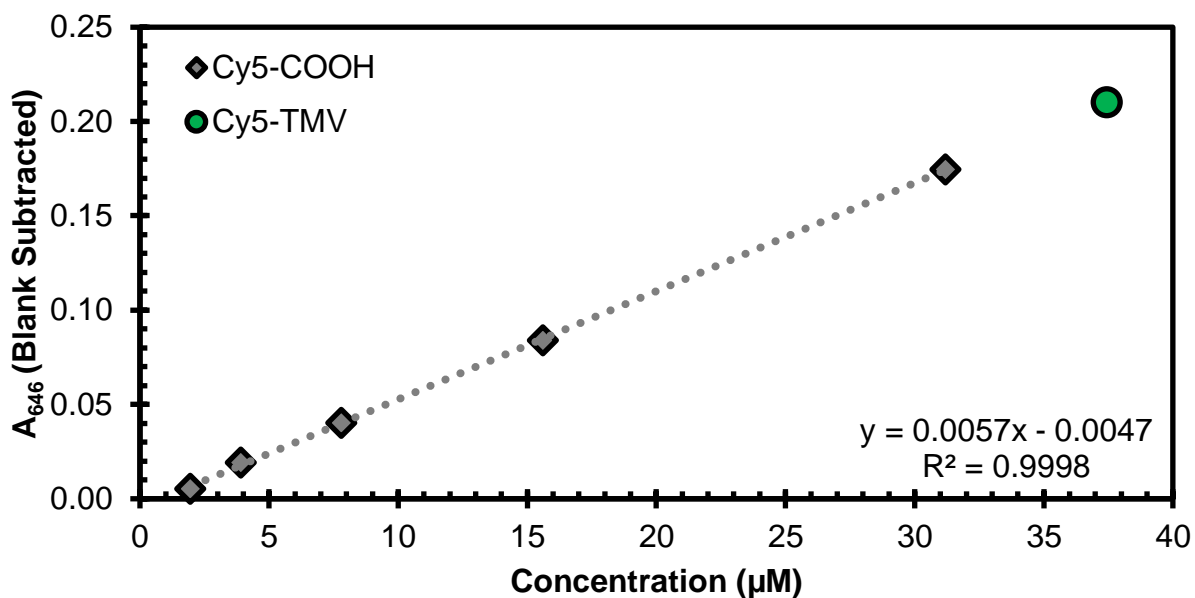
Figure A.5: UV-Vis absorbance at 646 nm of Cy5-COOH in solution and Cy5-TMV.
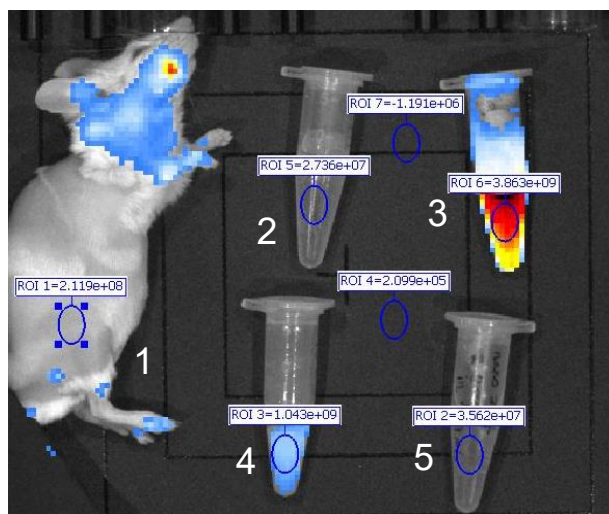
Figure A.6: Regions of interest and their and their radiant efficiencies ($\times 10^7$): 1) Mouse skin: 21.2, 2) Saline: 2.7, 3) Cy5-TMV: 386.3, 4) Cy5-TMV@ZIF: 104.3, and 5) ZIF-8 in water: 3.6. It should be noted that the quantity of Cy5-TMV in tubes 3 and 4 are the same, however, the ZIF shell attenuates the fluorescence.

APPENDIX B

EXTENDED DATA FOR CHAPTER 3

MATERIALS

Dulbecco's Modified Eagle's Medium (6429), ethylenediaminetetraacetic acid (EDTA), FB essence, hydrochloric acid, 4-(2-hydroxyethyl)piperazine-1-ethanesulfonic acid (HEPES), methanol, 2-methylimidazole, potassium chloride, potassium phosphate dibasic, potassium phosphate monobasic, sodium bicarbonate, sodium carbonate, sodium chloride, sodium hydroxide, sodium phosphate dibasic, sodium phosphate monobasic, Tris Base, and zinc acetate dihydrate were purchased from Sigma-Aldrich (St. Louis, MO, USA), Thermo Fisher Scientific (Waltham, MA, USA), Chem-Impex Int'l (Wood Dale, IL, USA), Research Product International (Mt Prospect, IL, USA) or VWR (Radnor, PA, USA), and used without further modification.

Ultrapure water was obtained from an ELGA PURELAB flex 2 system with resistivity measured to at least 18.2 MΩ-cm.

INSTRUMENTATION

UV-Vis

UV-Vis spectra were taken using a UV-1601PC UV-Vis-NIR Spectrophotometer (Shimadzu, Kyoto, Japan), Tecan Spark 20M plate reader (Tecan, Männedorf, Switzerland), or Biotek Synergy H4 hybrid reader (Biotek, Winooski, VT, USA). NanoDrop UV-Vis measurements were performed on a Thermo Scientific NanoDrop 2000 Spectrophotometer.

Fluorescence

Fluorescence measurements were taken using a Tecan Spark 20M plate reader.

Scanning Electron Microscopy

SEM was performed on a ZEISS Supra 40 Scanning Electron Microscope (Zeiss, Oberkochen, Germany) with an accelerating voltage of 2.5 kV and a working distance of 6.7 to 15.3 mm. Samples were sputtered with a 37 Å layer of gold.

Powder X-Ray Diffraction

Powder X-Ray Diffraction (PXRD) was taken on a Rigaku SmartLab diffractometer with CuKα (1.54060 Å) at 40 kV and 30 mA. The scans were performed for 2θ from 5° to 55° with a step size of 0.02°.

ICP-MS

All samples were boiled in aqua regia for a minimum of 2 hours and diluted in water before measurement. Each sample was analyzed for Au using both No Gas and Helium mode and compared against prepared zinc standards ranging from 31.25 ppb to 1000 ppb (Inorganic Ventures, Christiansburg, VA, USA), and analyzed 10 times each using an Agilent 7800 ICP triple Quadrupole MS.

METHODS

Preparation of Buffers

Buffers

0.9 % Saline: Made by adding 900 mg into 100 mL of ultrapure water. The solution was measured to have a pH of 5.8.

0.025 M HEPES: Made a 1 M Hepes buffer by adding 11.91 g of HEPES into 80 mL of ultrapure water. Added NaOH pellets until a pH of 7.00 was obtained and diluted to 100 mL with ultrapure water. This solution was then diluted to obtain 0.025 M HEPES buffer.

0.05 M Tris: Made 1 M tris buffer by adding 12.11 g of Tris base into 80 mL of ultrapure water. The solution was adjusted to a pH of 7.4 before diluting to 100 mL with ultrapure water. This solution was then diluted to obtain 0.05 M Tris buffer solution.

0.1 M Bicarbonate: Made by adding 0.623 g of sodium bicarbonate and 0.274 g of sodium carbonate into 80 mL of ultrapure water. The solution was adjusted to a pH of 9.50 before diluting to 100 mL with ultrapure water.

1X PBS: Made by taking 10 mL of 10X PBS and diluting to 100 mL with ultrapure water.

DMEM: Dulbecco's Modified Eagle's Medium used as is and measured to have a pH of 7.63.

Serum: FB essence used as is and measured to have a pH of 7.92.

Cell Media: Made by taking 9 mL of DMEM and 1 mL of serum. Made fresh on the day of use and measured to have a pH of 7.87.

10X PBS: Made by adding 80.00 g of NaCl, 2.00 g of KCl, 14.4 g of Na_2HPO_4, and 2.4 g of KH_2PO_4 into 900 mL of ultrapure water. The solution was adjusted to a pH of 7.60 before diluting to 1000 mL with ultrapure water.

0.1 M KP: Made by adding 12.12 g of K_2HPO_4 and 4.14 g of KH_2PO_4 into 900 mL of ultrapure water. The solution was adjusted to a pH of 7.40 before diluting to 1000 mL with ultrapure water.

EDTA exfoliation buffer: Exfoliation buffer was prepared by adding EDTA to 0.1 M in a 0.1 M potassium hydroxide solution. Solid potassium hydroxide pellets were added until the EDTA was fully dissolved, then the pH adjusted to 7.0 with HCl. It should be noted that EDTA exfoliation was only used for the ICP-MS and GFP release studies.

Preparation of ZIF-8

ZIF-8

ZIF-8 was prepared according to literature protocol.[151] Briefly, 5 mL of 640 mM 2-methylimidazole was added to 5 mL of 40 mM zinc acetate dihydrate, followed by 20 s of agitation. The solution was left to incubate on the benchtop at room temperature for 16 h. After 16 h, the solution was centrifuged at 6000 $\times g$ for 10 min at room temperature. The supernatant was discarded, and the pellet washed with ultrapure water twice. The final powder was then ether used as-is or dried under vacuum.
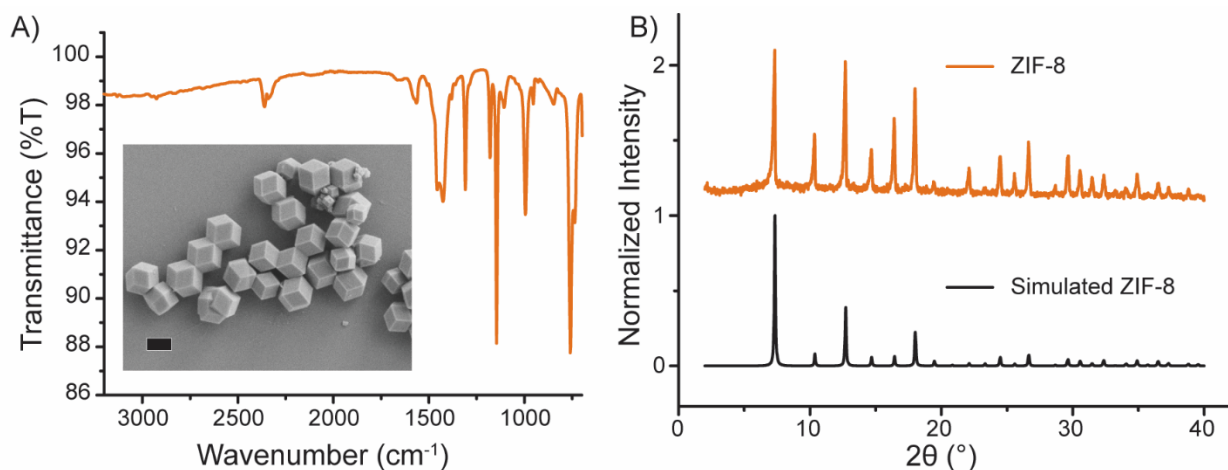
Figure B.1: The A) IR Spectroscopy of ZIF-8, the inset is an SEM micrograph of ZIF-8 (scale bar: 1 µm) and B) PXRD of simulated ZIF-8 and synthesized ZIF-8.

Time-Resolved SEM Study

Prepared ZIF-8 was incubated with the following buffers mentioned above at a concentration of 3 mg/mL, individually—water was used as a control. A total volume of 10 mL was used to ensure that enough powder would be left at the end of the study for analysis by PXRD, EDX, and SEM. The ZIF-8 in each solution was gently mixed on a rotisserie and an aliquot of sample taken at each time point. Each aliquot was washed three times with ultrapure water before loading the sample for SEM.
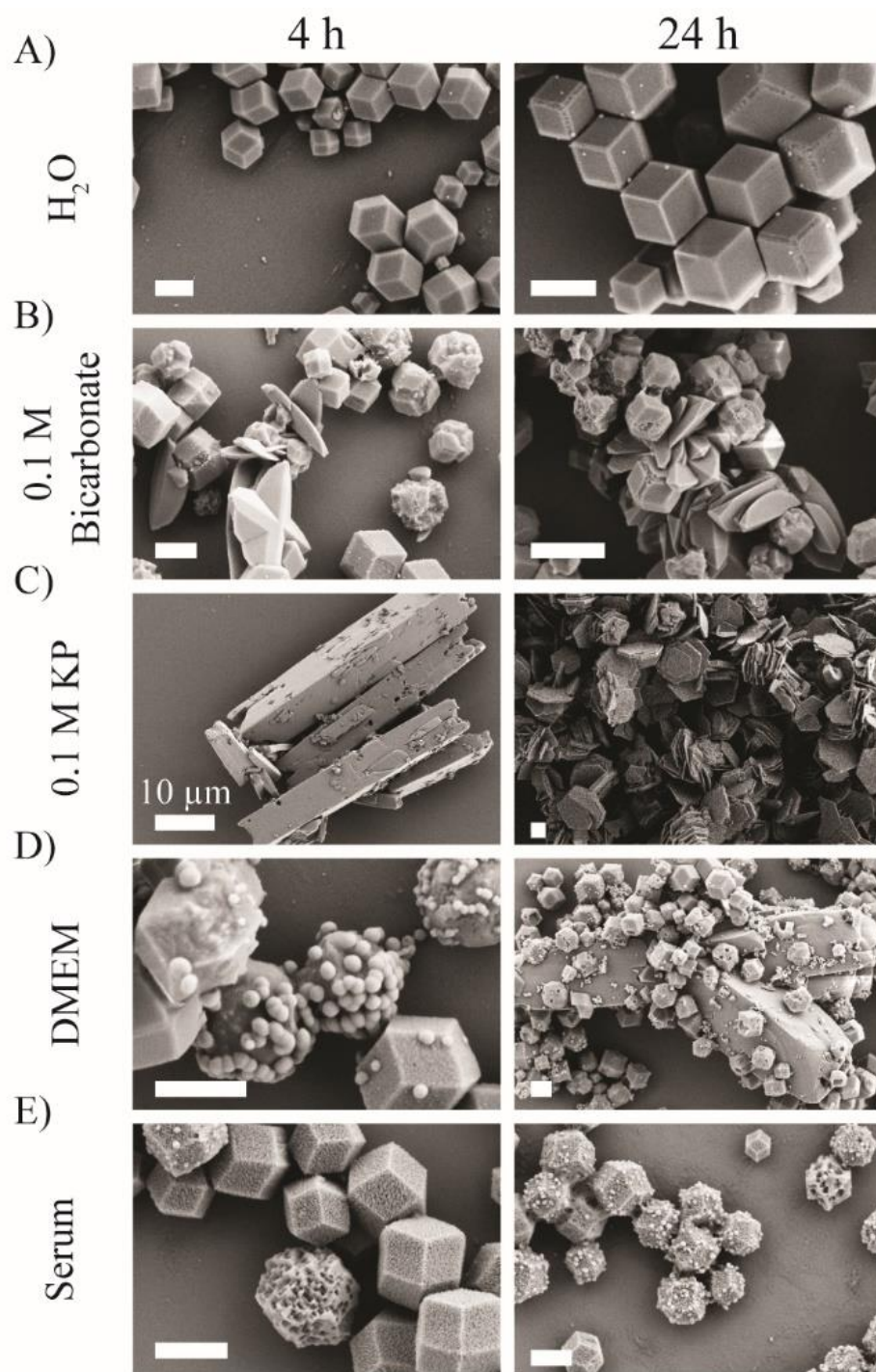
Figure B.2: Time-resolved SEM micrographs of ZIF-8 incubated in A) water, B) 0.1 M Bicarbonate buffer, C) 0.1 M KP Buffer, D) DMEM, and E) Serum. An aliquot of the ZIF-8 was taken out at 4 h and 24 h, followed by three washes with water, dried under high vacuum, and imaged by SEM. (Scale bar: 1 μm, unless otherwise stated)
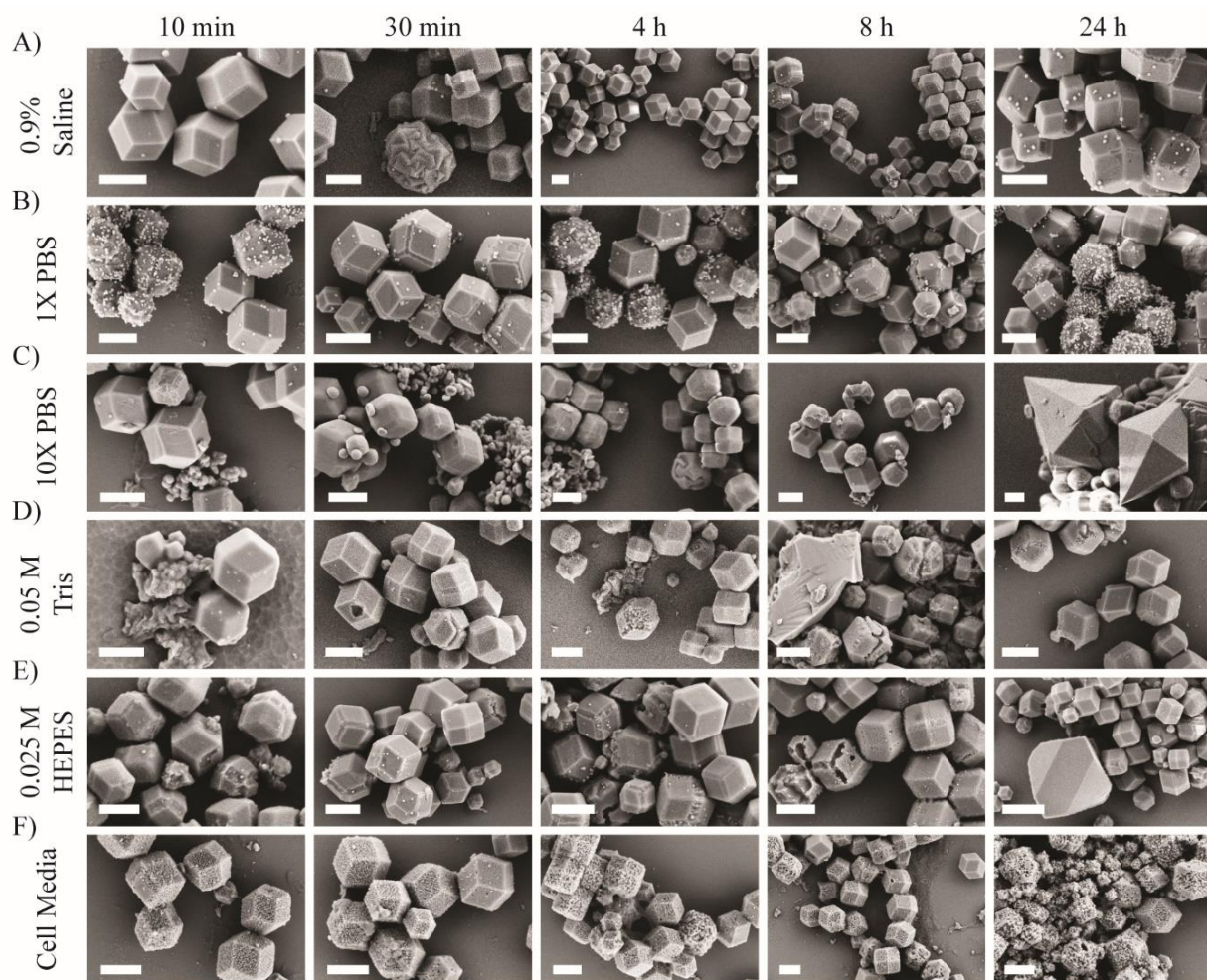
Figure B.3: Time-resolved SEM micrographs of ZIF-8 incubated in A) 0.9% saline, B) 1X PBS, C) 10X PBS, D) 0.05 M Tris buffer, E) 0.025 M HEPES, and F) Cell media. An aliquot of the ZIF-8 was taken out at 10 min, 30 min, 4 h, 8 h and 24 h, followed by three washes with water, dried under high vacuum, and imaged by SEM. (Scale bars: 1 µm)

Determination of ZIF-8 Supernatant by pH and ICP-MS

ZIF-8 was incubated with the following buffers mentioned above at a concentration of 3 mg/mL, individually—water and EDTA were used as a controls. The samples were centrifuge at 6000 ×g for 10 min at room temperature. The supernatant was transferred into a clean falcon tube to monitor change in pH. Only 2.5 mL of the supernatant was used for analysis by ICP-MS.

Table B.1: Change in pH after 24 h of incubation with ZIF-8.

Formulation	Initial pH	24 h
H_2O	7.85	9.62
0.9 % Saline	5.84	9.49
0.025 M HEPES	7.04	7.91
0.05 M Tris	7.77	8.24
0.1 M Bicarbonate	9.50	9.70
1X PBS	8.02	9.83
DMEM	7.63	8.83
Serum	7.92	8.80
Cell Media	7.87	8.61
10X PBS	7.64	9.15
0.1 M KP	7.43	8.41

Table B.2: ICP-MS of the ZIF-8 supernatant for determining the amount of released zinc.

Formulation	Control	24 h (ppb)
7.5 mg of ZIF-8	264495.8 ± 40.21	-
H_2O	0	1968.1 ± 125.1
0.9 % Saline	0	102.3 ± 12.3
0.025 M HEPES	0	32619.2 ± 28.41
0.05 M Tris	0	63291.0 ± 32.91
0.1 M Bicarbonate	0	19073.4 ± 50.40
1X PBS	0	nd
DMEM	0	2149.8 ± 104.9
Serum	0	110840.9 ± 25.29
Cell Media	0	64348.7 ± 46.44
10X PBS	0	354.5 ± 17.4
0.1 M KP	0	35.45 ± 17.37
EDTA	0	272468.2 ± 18.09

PXRD and EDX after 24 h

At the end of the SEM time resolved study, the remaining solution was centrifuged at 4300 ×g for 10 min at room temperature. The supernatant was transferred into a clean falcon tube to monitor change in pH. The pellet was washed three times with ultrapure water and dried overnight under high vacuum. The dried pellet was analyzed by PXRD and EDX to determine any changes to the ZIF-8 crystal.
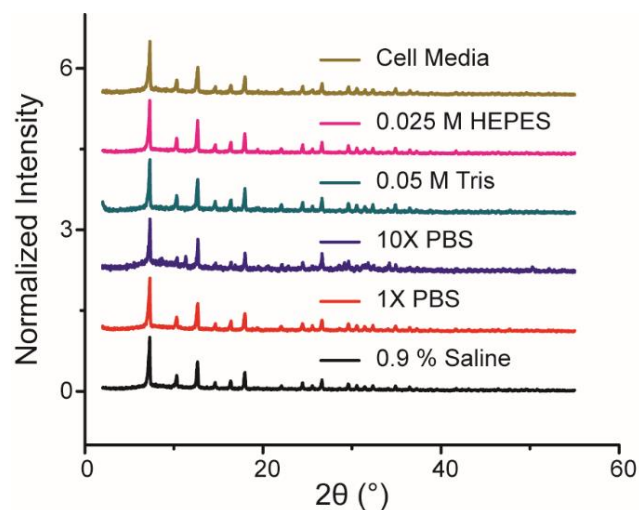
Figure B.4: PXRD of ZIF-8 after 24 h of incubation in 0.9% saline, 1X PBS, 10X PBS, 0.05 M Tris buffer, 0.025 M HEPES, and cell media.
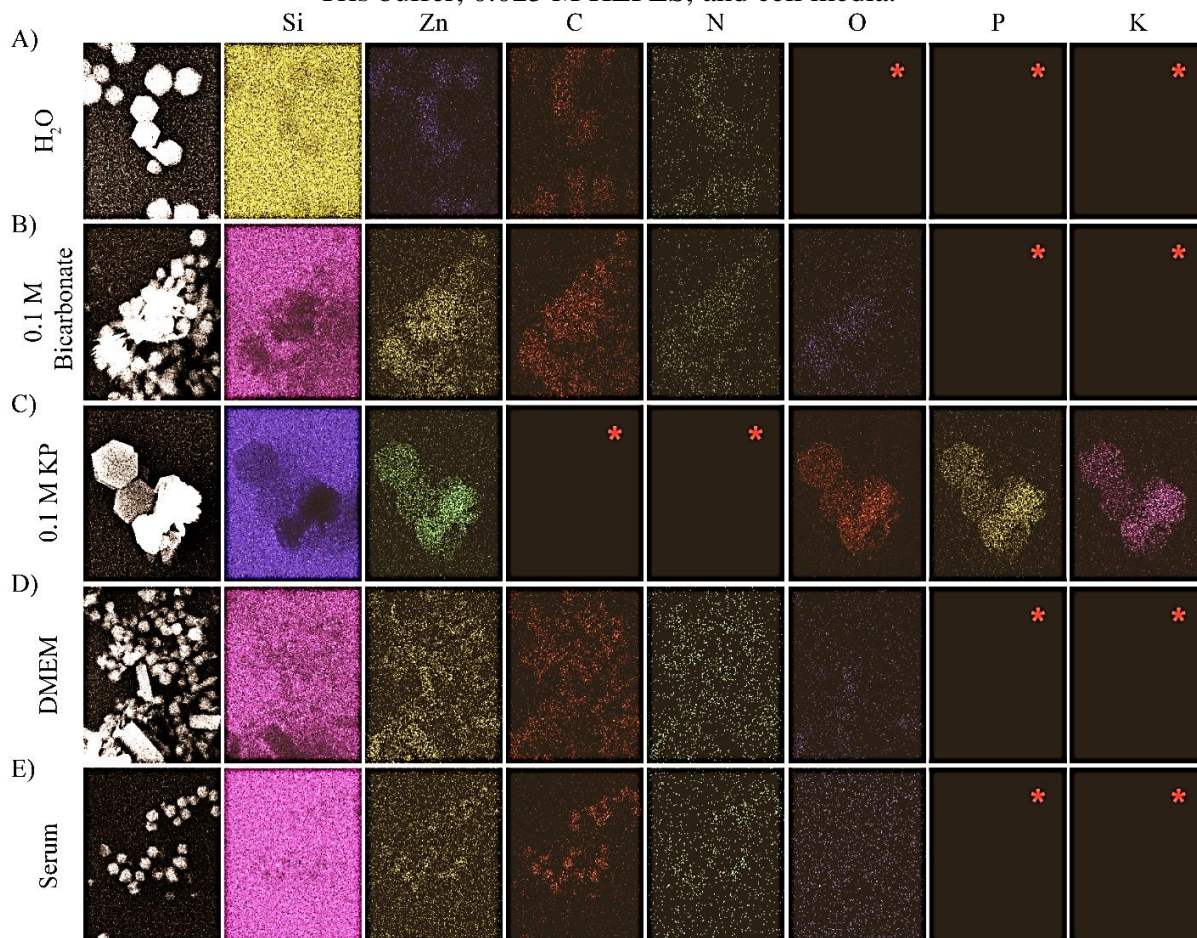
Figure B.5: EDX MAPS of ZIF-8 after incubation for 24 h in water, 0.1 M bicarbonate buffer, 0.1 M KP buffer, DMEM, and serum. (red asterisk means that the EDX spectrum in **Figure 3** did not have a signal from that element, therefore no MAP was generated)

Expression and Isolation of GFP

sfGFP-pBAD was a gift from Michael Davidson & Geoffrey Waldo (Addgene plasmid # 54519 ; http://n2t.net/addgene:54519 ; RRID:Addgene_54519) and purified using a modified protocol.[247]

Starter culture of E. coli BL21 cells harboring the plasmids were amplified SOB media supplemented with 100 µg/mL ampicillin at 37 °C. Induction was performed at OD 0.7 with 0.8% L-arabinose for a minimum of 12 hours. Cells were pelleted at 10.5K rpm for 30 mins using a Sorvall LYNX 4000 centrifuge, resuspended in 1× PBS pH 8 and lysed using a Microfluidics M-110P Microfluidizer. Cells were again centrifuges at 10.5K rpm for 1 hour to remove cell debris. The supernatant was purified using an NGC Quest 10 FPLC equipped with a 5-mL Bio-Scale Profinity IMAC cartridge. The samples were loaded using 1× PBS pH 8, washed with 10mM imidazole in 1× PBS, pH8 and eluted with 200 mM imidazole in 1× PBS, pH 8. GFP containing fractions were dialyzed against MilliQ water for 3 days and lyophilized using a Labconco Freezone 2.5 Lyophilizer. Dried GFP stored at 4°C.

GFP@ZIF

GFP@ZIF was prepared using the same protocol as ZIF-8, except GFP had a final concentration of 0.33 mg/mL. GFP@ZIF was characterized by SEM, PXRD, and IR. DLS measurements were taken to ensure that the addition of GFP would not change the size of the ZIF-8 crystals.
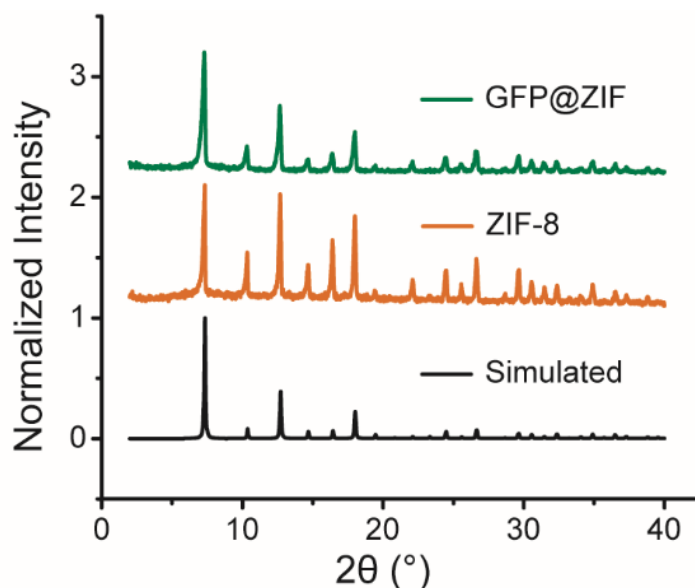
Figure B.6: PXRD of simulated ZIF-8, synthesized ZIF-8, and synthesized GFP@ZIF.
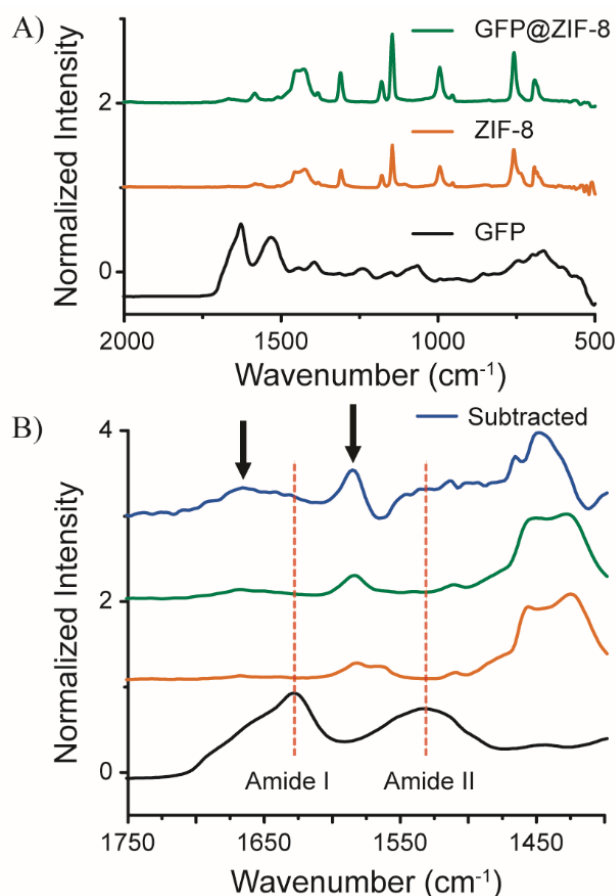
Figure B.7: A) IR absorbance of GFP, ZIF-8, and GFP@ZIF. A zoomed in spectrum from 1750-1400 cm-1 B) showing that GFP@ZIF retains the Amide I and Amide II region, but is slightly shifted to the left (depicted by the arrows). This result is similar to other proteins encapsulated in ZIF-8 and has been explained by the interaction between the amides and zinc.[149]
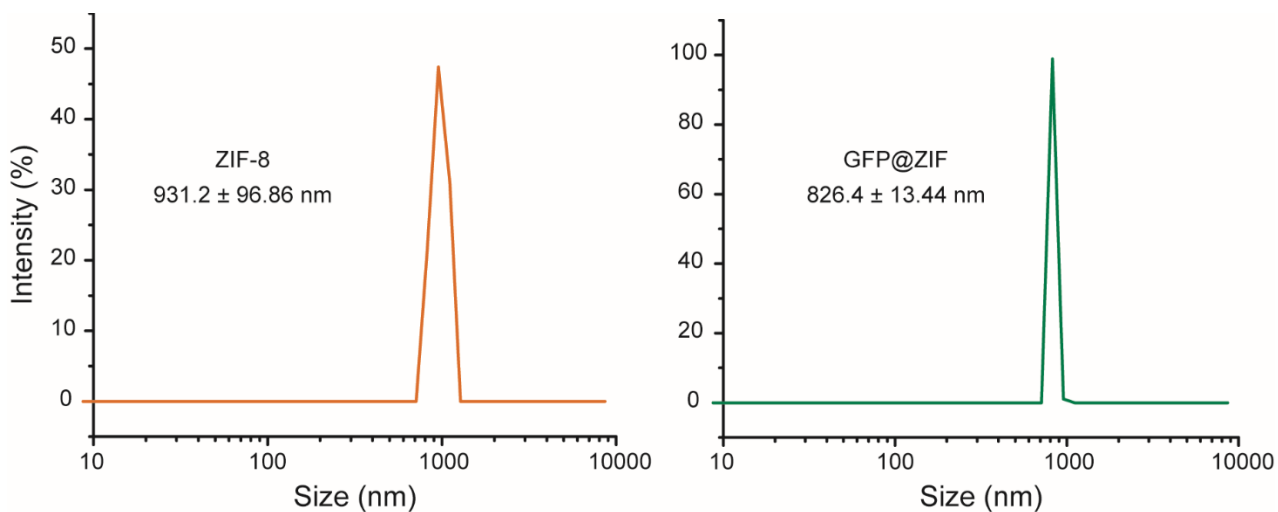
Figure B.8: DLS of ZIF-8 and GFP@ZIF

Time-Resolved Fluorescence Study

GFP@ZIF was incubated with the following buffers mentioned above at a concentration of 3 mg/mL, individually—water and EDTA were used as a controls. The release of GFP was monitored by taking the fluorescence at each time point. It should be noted that the fluorescence of each buffer was taken before incubation and used to subtract the fluorescence value at each time point.
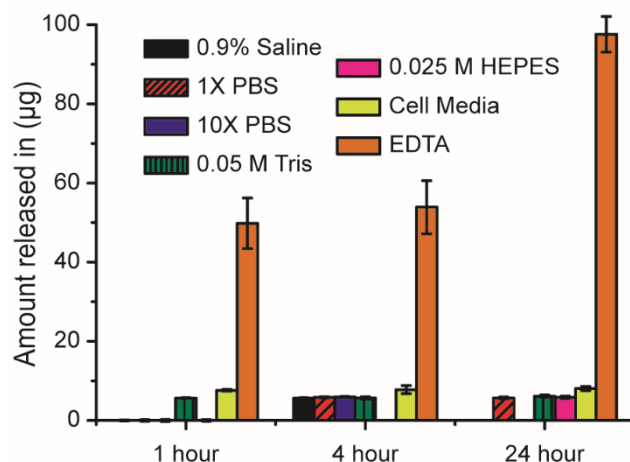
Figure B.9: The release of GFP from ZIF-8 after incubation in 0.9% saline, 1X PBS, 10X PBS, 0.05 M Tris buffer, 0.025 M HEPES, and cell media, separately. Fluorescence was taken of the supernatant at 1 h, 4 h, and 24 h.

Table B.3: Amount of GFP released over time (0 means undetectable by plate reader).

Formulation	1 h (µg)	4 h (µg)	24 h (µg)
H_2O	0 ± 0.156	0 ± 0.078	5.77 ± 0.243
0.9 % Saline	0 ± 0.135	5.61 ± 0.140	nd
0.025 M HEPES	0 ± 0.178	nd	5.88 ± 0.304
0.05 M Tris	5.63 ± 0.140	5.69 ± 0.311	6.13 ± 0.272
0.1 M Bicarbonate	0 ± 0.156	5.64 ± 0.135	5.83 ± 0.237
1X PBS	0 ± 0.206	5.84 ± 0.124	5.69 ± 0.234
DMEM	6.10 ± 0.515	5.99 ± 0.421	5.97 ± 0.337
Serum	18.2 ± 1.79	30.3 ± 1.50	36.8 ± 0.497
Cell Media	7.6 ± 0.217	7.8 ± 1.01	8.07 ± 0.539
10X PBS	0 ± 0.255	5.92 ± 0.140	nd
0.1 M KP	0 ± 0.140	9.45 ± 0.272	0 ± 0.206
EDTA	49.8 ± 6.40	53.9 ± 6.73	97.6 ± 4.52

APPENDIX C

EXTENDED DATA FOR CHAPTER 4

METHODS

Materials

Acetic acid, acetic anhydride, anti-mouse IgG (whole molecule)-alkaline phosphatase produced in goat, arabinose, bovine serum albumin, diethanolamine, magnesium chloride, β-mercatoethanol, methanol, 2-methylimidazole, paraformaldehyde, p-nitro phenyl phosphate, potassium hydroxide, potassium phosphate dibasic, potassium phosphate monobasic, poly(vinylpyrrolidone) 40k (PVP 40k), 2-propanol, sodium azide, sodium bicarbonate, sodium carbonate, sodium chloride, sodium hydroxide, sodium phosphate dibasic, sodium phosphate monobasic, Tween-20, and zinc acetate dihydrate were purchased from Sigma-Aldrich (St. Louis, MO, USA), Thermo Fisher Scientific (Waltham,

MA, USA), Chem-Impex Int'l (Wood Dale, IL, USA), or VWR (Radnor, PA, USA), and used without further modification. Anti-rat CD3-APC, anti-mouse CD4-PE/Cy7, anti-rat CD8a-APC/Cy7, anti-mouse CD44-FITC, anti-rat CD62L-BV605, ELISA MAX™ Standard Set Mouse IL-6, TNF-α, and IFN-g were from Biolegend. Ultrapure water was obtained from an ELGA PURELAB flex 2 system with resistivity measured to at least 18.2 MΩ-cm.

BACTERIAL STUDIES

Bacterial strains and growth conditions

CFT073 was obtained from ATCC and grown in Luria Bertani (LB) medium at 37°C for all experiments. pLenti-smURFP was a gift from Erik Rodriguez & Roger Tsien and was transformed into CFT073 electrocompetent cells as described: 50 µL of electrocompetent CFT073 were thawed on ice, then mixed with 100 ng of pLenti-smURFP and incubated on ice for 20 minutes. The mixture was transferred to an electroporation cuvette and electroporated at 1.8 kVs. 500 µL of SOB media was immediately added and the cells recovered for 60 minutes at 37°C. Transformants were selected on LB agar plates supplemented with 100 µg/mL ampicillin. For encapsulation experiments, CFT073-smURFP was grown to an OD_{600} of 0.9-1 and 10 mg/mL arabinose was added to induce smURFP expression. After 4 hours, cells were harvested by centrifugation at 2,000

×g for 10 min and washed three times with 0.9% saline. Pellets were weighed to ensure exactly 40 mg/mL of CFT073 would be the stock solution for all studies described. CFT@ZIF was prepared by adding 1 mg of CFT073 from the stock solution and 500 uL of 1600 mM 2-methylimidazole (HMIM) into a 1.5 mL microcentrifuge tube, followed by the addition of 500 µL of 20 mM zinc acetate dihydrate (ZnOAC). The tube was capped, swirled for 20 s, and left to incubate at RT for 20 min. HMIM and ZnOAC solution were made using 100 mM NaCl solution to keep bacteria near isotonic conditions. The solution became cloudy after a few minutes and remained colloidal throughout the incubated timeframe. Longer time frames than 20 minutes led to free ZIF-8 as seen in Extended Data Fig. 2. After 20 min, the solution was centrifuged at 4500 ×g for 10 min at 4°C. The supernatant was discarded, and the pellet was washed with ultrapure water twice. The final CFT@ZIF powder was either dried to characterize the sample or placed into 0.9% saline for *in vitro* and *in vivo* studies.

Growth Killing Assay

In a 1.5 mL microcentrifuge tube, either 0.9% saline or 500 mM acetic/acetate buffer pH 5 (Acetate buffer) at a volume of 975 µL was added to each tube. 25 µL of naked CFT073 or dried CFT@ZIF was added to each tube to obtain a 1 mg/mL concentration of bacteria. Acetate buffer can exfoliate the ZIF shell and was used as a control to show that naked CFT073 will continue to grow when incubated for the same amount of time it takes to exfoliate CFT@ZIF. CFT@ZIF must be incubated for 30 min to be fully exfoliated. The naked CFT073 or CFT@ZIF was suspended in 0.9% saline and left at 80 °C for 15 minutes. As previously stated, naked CFT073 was exposed to identical stress conditions, dilutions, and incubation in 500 mM acetic/acetate buffer pH as CFT@ZIF biocomposites. Formalin-fixed CFT073 (CFT-Fixed) was made by placing 1 mg in 5% formalin to a final volume of 1 mL and incubating overnight. CFT-Fixed was then centrifuged at 4,000 ×g and washed with 0.9% saline, twice. Each of the tested conditions was serially diluted (10^{-2} to 10^{-9}) and spotted on an LB agar plates to determine the colony-forming unit (CFU) titers formed after 12 h, individually. All experiments included n=3 per sample tested.

Macrophage Uptake by Flow CT

RAW Macrophage 264.7 cells were cultured in Dulbecco's Modified Eagle Medium supplemented with 10% FBEssence and 1% penicillin-streptomycin (50 µg/mL). Cells were seeded at ~10^5 cells/mL in a 6 well plate one day prior to testing. The cells were incubated with 25 µg/mL of indicated samples for 4 hours. The cells were washed 3× with 1× PBS, resuspended in 1 mL of 1× PBS, and transferred to a 5 mL sterile polystyrene tube. ~10,000 gated events per sample were collected using a BD LSRFortessa™ flow cytometer. Raw data were processed and analyzed using FlowJo® software Version 10.6.1. Histogram overlays were normalized to mode to compare samples that varied in number of recorded events.

Macrophage Uptake by Live Cell Imaging

RAW Macrophage 264.7 cells were as above and seeded at ~10^5 cells/mL in glass bottom dishes one day prior to testing. The cells were incubated with 25 µg/mL of indicated samples for 4 h. The cells were washed 3× with 1× PBS, stained with 10 µM Hoescht and 5 µg/mL WGA-TRITC, washed 3× with 1× PBS, and kept in 2 mL of clean supplemented media for imaging. Live cell imaging was performed with an Olympus FV3000 RS Confocal microscope. Raw images were processed using ImageJ software.

Antigen stimulation of splenic T lymphocytes

Mice were injected on days 0, 7, 14 and splenocytes were isolated from immunized mice 7 days after the third immunization. Briefly, the cells were seeded at ~ 1.0×10^6 cells per well in a 24 well plate and supplemented with RPMI 1640 medium, 10 % FBEssence, 1 % penicillin-streptomycin, and 50µm β-mercaptoethanol. Cells were re-stimulated with 10 ug naked CFT073 (10 µg/mL) for 48 hours. The supernatant was tested for cytokine production by enzyme-linked immunosorbent assay (ELISA). Then the cells were stained with anti-CD3-APC, anti-CD4-PE/Cy7, anti-CD8a-FITC, and a zombie violet viability kit and analyzed by flow cytometry. Additional cells were incubated with 10 ug/mL of live CFT073 and stained with anti-CD3-APC, anti-CD4-PE/Cy7, anti-CD8a-APC/Cy7, anti-CD44-FITC, and anti-CD62L-BV605 and analyzed by flow cytometry.

Antibody and cytokine ELISA

CFT073-specific antibody production was determined by following a previously published method.[232] Briefly, lyophilized CFT073 was resuspended in 0.05 M pH 9.6 sodium carbonate/bicarbonate buffer to a concentration of 0.31 mg/mL, 150 µL was added to each well, and was incubated at 37°C for 90 min. The plate was emptied and washed 4 times with wash buffer. 200 µL of blocking buffer was added to each well and was incubated at 37°C for 45 min. The plate was emptied and washed 4 times with wash buffer. Mouse serum was serially diluted 7 times starting at a 200× dilution using 1x PBS at ph 7.4, 150 µL added to each well, and incubated at 37°C for 90 min. The plate was emptied and washed 4 times with wash buffer. Alkaline phosphatase-conjugated goat anti-mouse IgG in conjugate buffer was added 150 µL per well and incubated at 37°C for 90 min. The plate was emptied and washed 4 times with wash buffer. 1 mg/mL p-nitrophenylphosphate in substrate buffer was added at 150 µL per well and the plate developed for 15 min at R.T. The plate was read at 405 nm and the absorbance values of the buffer blank wells averaged and subtracted from the entire plate. The blank-subtracted values of each mouse group were reported as the average ± standard deviation for each dilution. The levels of TNF-α and IFN-Ɣ were determined by ELISA following protocols recommended by the manufacturer.

ANIMAL STUDIES

Ethics Statement

Female BALB/c were obtained from Charles River Lab (Wilmington, Ma). All animal studies were done in accordance with protocol #19-06 approved by the University of Texas at Dallas Institutional Animal Care and Use Committee (IACUC).

Vaccinations

20 BALB/c mice were divided into five groups (n = 4) and injected with saline, formalin CFT-Fixed, CFT@ZIF, CFT-Heat, or CFT@ZIF-Heat suspended in saline. Heat-treated samples were placed in 80°C water for 15 minutes. CFT073 solutions were prepared such that 100 µL delivered 10 µg of CFT073. Doses of 100 µL of saline, CFT-Fixed, CFT@ZIF, CFT-Heat or CFT@ZIF-

Heat were administered subcutaneously on day 0, 7, and 14, and blood was withdrawn submandibularly on day 0, 14, 21, and 42. The blood was centrifuged to remove cells, and the anti-CFT073 IgG content of the resultant serum was determined by ELISA as described above. At the end of the study, the mice were sacrificed for histological analysis on the spleen, liver, kidney, lung, heart, and the skin at the administration site. The mice were sacrificed by carbon dioxide asphyxiation, the organs collected, and fixed in 4% formaldehyde overnight. The fixed organs were moved to a 70% ethanol solution and processed with an ASP300 S tissue processor (Leica Biosystems, Buffalo Grove, IL) for dehydration into paraffin. The organs were then embedded into paraffin wax using a HistoCore Arcadia C and H paraffin embedding station (Leica Biosystems, Buffalo Grove, IL). Each organ was sliced into 4 µm sheets using a RM2235 manual microtome (Leica Biosystems, Buffalo Grove, IL) and imaged with a DMi1 optical microscope (Leica Biosystems, Buffalo Grove, IL) at 40×magnification.

Body Clearance

10 BALB/c mice were fed a non-fluorescent diet and shaved 12 hours before imaging to reduce autofluorescence from the hair. The mice were anesthetized with isoflurane and injected with 100 µL saline (n=4), CFT(smURFP)-Fixed, or CFT(smURFP)@ZIF. The CFT073 containing solutions were prepared such that 100 µL delivered 10 µg of CFT073. A series of time points were taken after injection at 30 min, 2 h, 4 h, 8 h, 18 h, 24 h, 48 h, 72 h, 120 h, 168 h, 216 h, and 288 h. The fluorescence returned to the levels of saline at 48 hours for CFT-Fixed and 216 h for CFT@ZIF.

Survival Challenge

20 BALB/c mice were divided into five groups (n = 4) and injected with saline, formalin CFT-Fixed, CFT@ZIF, CFT-Heat, or CFT@ZIF-Heat suspended in saline. Heat treated samples were placed in 80°C water for 15 minutes. CFT073 solutions were prepared such that 100 µL of 0.9% saline delivered 10 µg of CFT073. Doses of 100 µL of saline, CFT-Fixed, CFT@ZIF, CFT-Heat or CFT@ZIF-Heat were administered subcutaneously on day 0, 7, and 14. On day 21, all mice were injected interperitoneally with a lethal dose of 3.6×10^8 CFU of CFT073 per mouse and

monitored for 48 h. All mice were euthanized when they became moribund, which is defined by lack of movement for over 15 minutes and when gently touched and shaking in place. After a mouse was euthanized, the spleen and liver were collected, homogenized, and placed on agar plates at dilutions ranging from $10^{-2} - 10^{-9}$ to determine the CFU/g. The blood was also taken from each mouse and diluted to determine the CFU/mL.
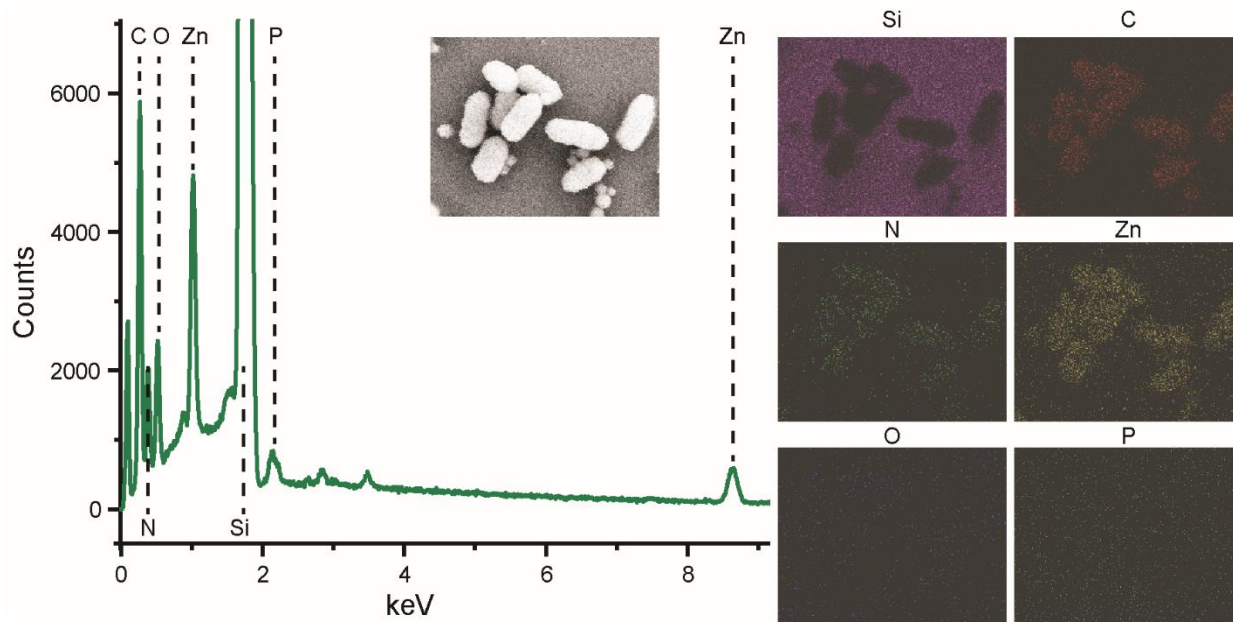
Figure C.1: The chemical analysis of CFT@ZIF was analyzed by energy dispersive X-ray. The graph shows the presence of carbon, oxygen, nitrogen, zinc, and phosphorus. In addition, image maps show zinc, oxygen, nitrogen, zinc, and phosphorus signals come from CFT@ZIF.
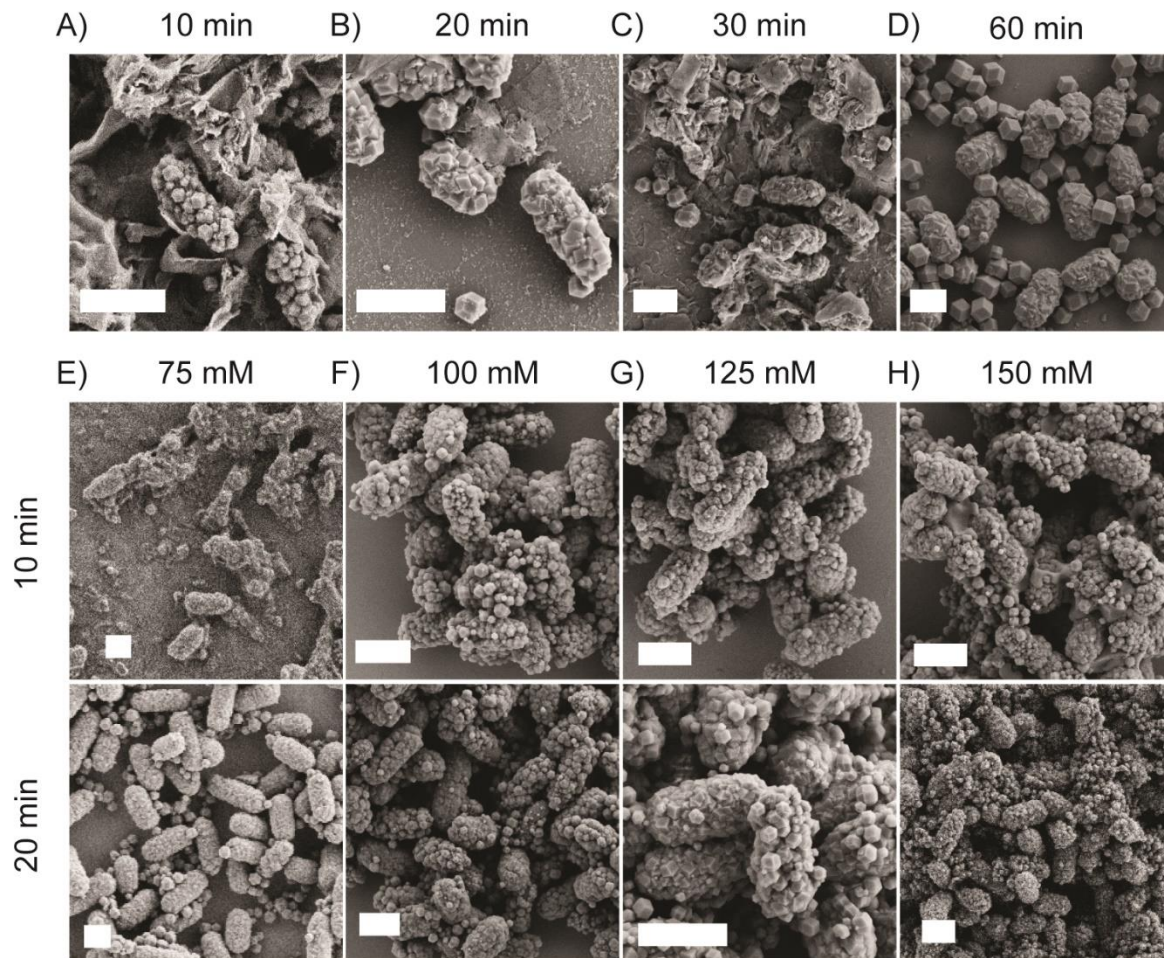
Figure C.2: Shorter incubation times and saline reduce the amount of free ZIF-8. Live CFT073 was incubated with an aqueous solution of zinc and 2-methylimidazole and left at room temperature for A) 10 minutes, B) 20 minutes, C) 30 minutes, or D) 60 minutes. After each time point, the sample was centrifuged to remove excess zinc and 2-methylimidazole and washed with water three times. CFT@ZIF encapsulation was performed with 1 mg of CFT073 in E) 75 mM, F) 100 mM, G) 125 mM, or H) 150 mM saline solutions for either 10 or 20 minutes to reduce cell bursting and the amount of free ZIF-8.
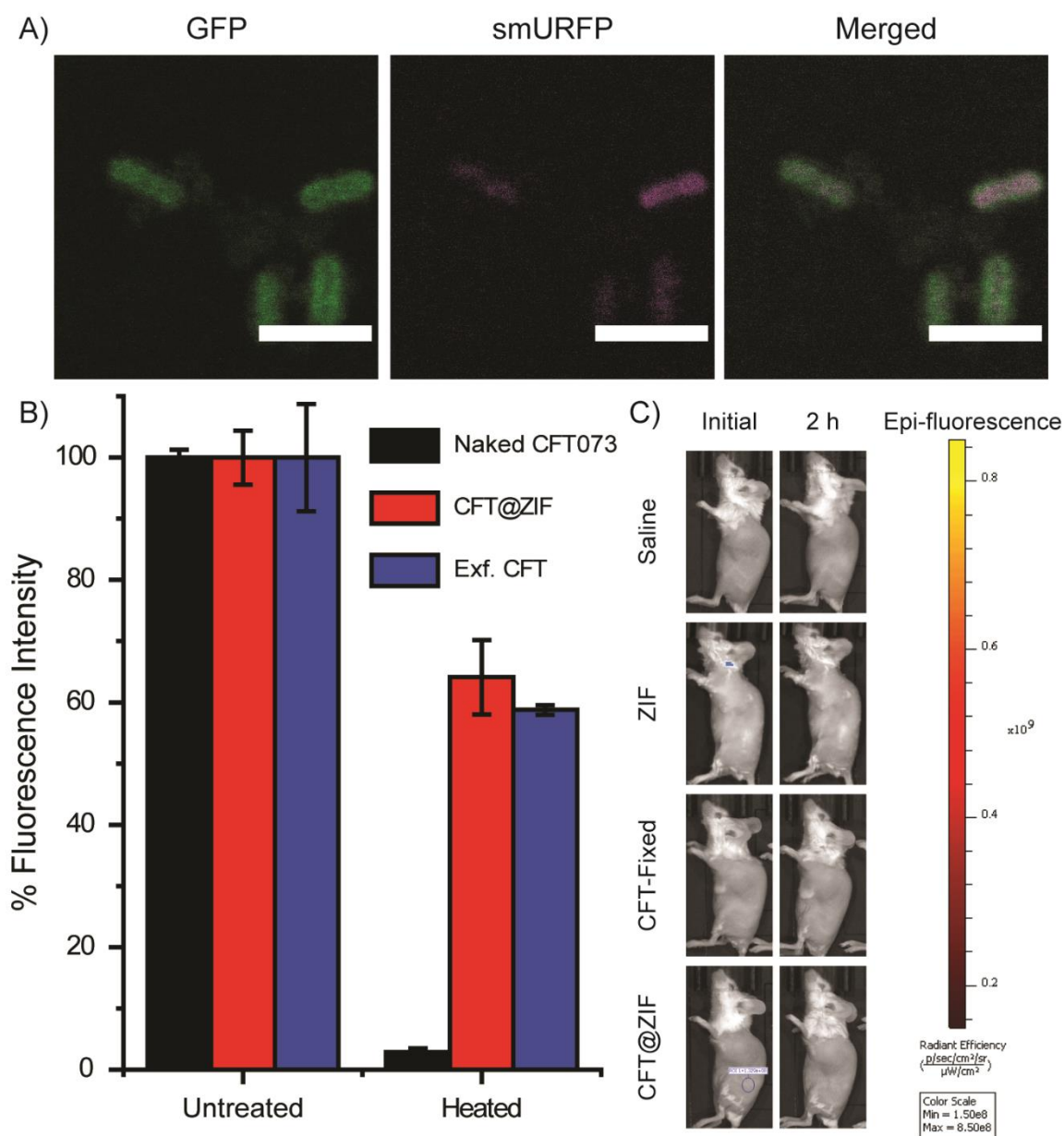
Figure C.3: ZIF-8 encapsulation protects bacterially-expressed proteins. A) CFT073 was transformed with a plasmid expressing fluorescent protein smURFP. Untreated bacteria were imaged by confocal microscopy. Each panel shows an individual fluorescent channel, in which CFT073 is within the ZIF shell. Scale bar = 5 µm B) The fluorescence intensity of naked CFT073, CFT@ZIF, or exfoliated CFT@ZIF (Exf. CFT) was measured by a fluorimeter. Sample fluorescent intensity was divided by the fluorescent intensity of untreated live CFT073 to determine percent fluorescent intensity. C) 4-6-week-old BALB/c mice (n=3) were injected with saline, ZIF, formalin-fixed CFT073, or CFT@ZIF and fluorescent intensities were measured in vivo.

REFERENCES

1. Dicker, D. et al. Global, regional, and national age-sex-specific mortality and life expectancy, 1950-2017: a systematic analysis for the Global Burden of Disease Study 2017. *The Lancet* **392**, 1684-1735 (2018).
2. Schaffner, W., Rehm, S.J. & File, T.M. Keeping our Adult Patients Healthy and Active: The Role of Vaccines across the Lifespan. *Phys. Sportsmed.* **38**, 35-47 (2010).
3. Rappuoli, R., Mandl, C.W., Black, S. & De Gregorio, E. Vaccines for the twenty-first century society. *Nat. Rev. Immunol.* **11**, 865-872 (2011).
4. Doherty, T.M., Del Giudice, G. & Maggi, S. Adult vaccination as part of a healthy lifestyle: moving from medical intervention to health promotion. *Annals of Medicine* **51**, 128-140 (2019).
5. Esparza, J. Early vaccine advocacy: Medals honoring Edward Jenner issued during the 19th century. *Vaccine* **38**, 1450-1456 (2020).
6. Jenner, E. An inquiry into the causes and effects of the variolae vaccinae, a disease discovered in some of the western counties of England, particularly Gloucestershire, and known by the name of the cow pox. (1800).
7. Gause, K.T. et al. Immunological Principles Guiding the Rational Design of Particles for Vaccine Delivery. *ACS Nano* **11**, 54-68 (2017).
8. Bogataj, M., Bogataj, L. & Vodopivec, R. Stability of perishable goods in cold logistic chains. *Int. J. Prod. Econ.* **93-94**, 345-356 (2005).
9. Karishma, M., Donna, M., Timothy, J.M. & Neena, M. Freeze-Drying of Protein-Loaded Nanoparticles for Vaccine Delivery. *Drug Delivery Lett.* **2**, 83-91 (2012).
10. Welch, R.P., Lee, H., Luzuriaga, M.A., Brohlin, O.R. & Gassensmith, J.J. Protein–Polymer Delivery: Chemistry from the Cold Chain to the Clinic. *Bioconjugate Chem.* **29**, 2867-2883 (2018).
11. Setia, S. et al. Frequency and causes of vaccine wastage. *Vaccine* **20**, 1148-1156 (2002).
12. Ashok, A., Brison, M. & LeTallec, Y. Improving cold chain systems: Challenges and solutions. *Vaccine* **35**, 2217-2223 (2017).
13. Di Pasquale, A., Preiss, S., Tavares Da Silva, F. & Garçon, N. Vaccine Adjuvants: from 1920 to 2015 and Beyond. *Vaccines (Basel)* **3**, 320-343 (2015).
14. Plotkin, S. History of vaccination. *Proc. Natl. Acad. Sci. U. S. A.* **111**, 12283 (2014).
15. Amanna, I.J. Balancing the Efficacy and Safety of Vaccines in the Elderly. *Open Longevity Sci.* **6**, 64-72 (2012).
16. Kaufmann, S.H.E. & McMichael, A.J. Annulling a dangerous liaison: vaccination strategies against AIDS and tuberculosis. *Nat. Med.* **11**, S33-S44 (2005).
17. Ruprecht, R.M. Live attenuated AIDS viruses as vaccines: promise or peril? *Immunol. Rev.* **170**, 135-149 (1999).
18. Cox, A., Baker, S.F., Nogales, A., Martínez-Sobrido, L. & Dewhurst, S. Development of a Mouse-Adapted Live Attenuated Influenza Virus That Permits In Vivo Analysis of Enhancements to the Safety of Live Attenuated Influenza Virus Vaccine. *J. Virol.* **89**, 3421-3426 (2015).

19.   Foged, C. Subunit vaccines of the future: the need for safe, customized and optimized particulate delivery systems. *Ther. delivery* **2**, 1057-1077 (2011).

20.   Gao, Q. et al. Development of an inactivated vaccine candidate for SARS-CoV-2. *Science* **369**, 77-81 (2020).

21.   Clem, A. Fundamentals of vaccine immunology. *J. Global Infect. Dis.* **3**, 73-78 (2011).

22.   Bachmann, M.F. et al. The influence of antigen organization on B cell responsiveness. *Science* **262**, 1448-1451 (1993).

23.   Vartak, A. & Sucheck, S.J.J.V. Recent advances in subunit vaccine carriers. *Vaccines (Basel)* **4**, 12 (2016).

24.   Cohen, J.J. How long do vaccines last? The surprising answers may help protect people longer. *Science* **10** (2019).

25.   Klein, N.P. et al. Waning protection following 5 doses of a 3-component diphtheria, tetanus, and acellular pertussis vaccine. *Vaccine* **35**, 3395-3400 (2017).

26.   Schwarz, T.F. et al. Ten-year immune persistence and safety of the HPV-16/18 AS04-adjuvanted vaccine in females vaccinated at 15–55 years of age. *Cancer Med,* **6**, 2723-2731 (2017).

27.   Liu, Y. et al. Trehalose glycopolymer enhances both solution stability and pharmacokinetics of a therapeutic protein. *Bioconjugate Chem.* **28**, 836-845 (2017).

28.   Schlick, T.L., Ding, Z., Kovacs, E.W. & Francis, M.B. Dual-Surface Modification of the Tobacco Mosaic Virus. *J. Am. Chem. Soc.* **127**, 3718-3723 (2005).

29.   Doonan, C., Riccò, R., Liang, K., Bradshaw, D. & Falcaro, P. Metal–organic frameworks at the biointerface: synthetic strategies and applications. *Acc. Chem. Res.* **50**, 1423-1432 (2017).

30.   Chen, T.-T., Yi, J.-T., Zhao, Y.-Y. & Chu, X. Biomineralized Metal-Organic Framework Nanoparticles Enable Intracellular Delivery and Endo-Lysosomal Release of Native Active Proteins. *J. Am. Chem. Soc.* **140**, 9912–9920 (2018).

31.   Wang, C. et al. Metal–Organic Framework Encapsulation for Biospecimen Preservation. *Chem. Mater.* **30**, 1291-1300 (2018).

32.   Riedel, S. Edward Jenner and the history of smallpox and vaccination. *Proc. (Bayl. Univ. Med. Cent.)* **18**, 21-25 (2005).

33.   Demento, S.L., Siefert, A.L., Bandyopadhyay, A., Sharp, F.A. & Fahmy, T.M. Pathogen-associated molecular patterns on biomaterials: a paradigm for engineering new vaccines. *Trends Biotechnol.* **29**, 294-306 (2011).

34.   Tsoras, A.N. & Champion, J.A. Protein and Peptide Biomaterials for Engineered Subunit Vaccines and Immunotherapeutic Applications. *Annu. Rev. Chem. Biomol. Eng.* **10**, 337-359 (2019).

35.   Black, M. et al. Self-Assembled Peptide Amphiphile Micelles Containing a Cytotoxic T-Cell Epitope Promote a Protective Immune Response In Vivo. *Adv. Mater.* **24**, 3845-3849 (2012).

36.   Vajdy, M. Immunomodulatory properties of vitamins, flavonoids and plant oils and their potential as vaccine adjuvants and delivery systems. *Expert Opin. Biol. Ther.* **11**, 1501-1513 (2011).

37.   Yang, L., Li, W., Kirberger, M., Liao, W. & Ren, J. Design of nanomaterial based systems for novel vaccine development. *Biomater. Sci.* **4**, 785-802 (2016).

38.　Irvine, D.J., Swartz, M.A. & Szeto, G.L. Engineering synthetic vaccines using cues from natural immunity. *Nat. Mater.* **12**, 978-990 (2013).

39.　Yang, J. et al. Engineered biomaterials for development of nucleic acid vaccines. *Biomater. Res.* **19**, 5 (2015).

40.　Shen, Y., Hao, T., Ou, S., Hu, C. & Chen, L. Applications and perspectives of nanomaterials in novel vaccine development. *MedChemComm* **9**, 226-238 (2018).

41.　Elmowafy, E.M., Tiboni, M. & Soliman, M.E. Biocompatibility, biodegradation and biomedical applications of poly(lactic acid)/poly(lactic-co-glycolic acid) micro and nanoparticles. *J. Pharm. Invest.* **49**, 347-380 (2019).

42.　Sahdev, P., Ochyl, L.J. & Moon, J.J. Biomaterials for nanoparticle vaccine delivery systems. *Pharm. Res.* **31**, 2563-2582 (2014).

43.　Bachelder, E.M. et al. Acid-Degradable Polyurethane Particles for Protein-Based Vaccines: Biological Evaluation and in Vitro Analysis of Particle Degradation Products. *Mol. Pharmaceutics* **5**, 876-884 (2008).

44.　Sah, H., Toddywala, R. & Chien, Y.W. Continuous release of proteins from biodegradable microcapsules and in vivo evaluation of their potential as a vaccine adjuvant. *J. Controlled Release* **35**, 137-144 (1995).

45.　Men, Y., Tamber, H., Audran, R., Gander, B. & Corradin, G. Induction of a cytotoxic T lymphocyte response by immunization with a malaria specific CTL peptide entrapped in biodegradable polymer microspheres. *Vaccine* **15**, 1405-1412 (1997).

46.　Wang, C. et al. Molecularly engineered poly(ortho ester) microspheres for enhanced delivery of DNA vaccines. *Nat. Mater.* **3**, 190-196 (2004).

47.　Singh, J., Pandit, S., Bramwell, V.W. & Alpar, H.O. Diphtheria toxoid loaded poly-(ε-caprolactone) nanoparticles as mucosal vaccine delivery systems. *Methods* **38**, 96-105 (2006).

48.　Lou, P.-J. et al. PMMA particle-mediated DNA vaccine for cervical cancer. *J. Biomed. Mater. Res., Part A* **88A**, 849-857 (2009).

49.　Su, X., Kim, B.-S., Kim, S.R., Hammond, P.T. & Irvine, D.J. Layer-by-Layer-Assembled Multilayer Films for Transcutaneous Drug and Vaccine Delivery. *ACS Nano* **3**, 3719-3729 (2009).

50.　Huang, C.-H. et al. Degradable emulsion as vaccine adjuvant reshapes antigen-specific immunity and thereby ameliorates vaccine efficacy. *Sci. Rep.* **6**, 36732 (2016).

51.　Allahyari, M. & Mohit, E. Peptide/protein vaccine delivery system based on PLGA particles. *Hum. Vaccines Immunother.* **12**, 806-828 (2016).

52.　Bose, R.J. et al. Biodegradable polymers for modern vaccine development. *J. Ind. Eng. Chem.* **77**, 12-24 (2019).

53.　Morachis, J.M., Mahmoud, E.A. & Almutairi, A. Physical and chemical strategies for therapeutic delivery by using polymeric nanoparticles. *Pharmacol. Rev.* **64**, 505-519 (2012).

54.　Gu, P. et al. Rational Design of PLGA Nanoparticle Vaccine Delivery Systems To Improve Immune Responses. *Mol. Pharmaceutics* **16**, 5000-5012 (2019).

55.　Pawar, D., Mangal, S., Goswami, R. & Jaganathan, K.S. Development and characterization of surface modified PLGA nanoparticles for nasal vaccine delivery: Effect of

mucoadhesive coating on antigen uptake and immune adjuvant activity. *Eur. J. Pharm. Biopharm.* **85**, 550-559 (2013).

56.   Silva, A.L., Soema, P.C., Slütter, B., Ossendorp, F. & Jiskoot, W. PLGA particulate delivery systems for subunit vaccines: Linking particle properties to immunogenicity. *Hum. Vaccines Immunother.* **12**, 1056-1069 (2016).

57.   Lü, J.-M. et al. Current advances in research and clinical applications of PLGA-based nanotechnology. *Expert Rev. Mol. Diagn.* **9**, 325-341 (2009).

58.   Avgoustakis, K. Pegylated poly(lactide) and poly(lactide-co-glycolide) nanoparticles: preparation, properties and possible applications in drug delivery. *Curr. Drug Delivery* **1**, 321-333 (2004).

59.   Oyewumi, M.O., Kumar, A. & Cui, Z. Nano-microparticles as immune adjuvants: correlating particle sizes and the resultant immune responses. *Expert Rev. Vaccines* **9**, 1095-1107 (2010).

60.   Shi, L. et al. Pharmaceutical and Immunological Evaluation of a Single-Shot Hepatitis B Vaccine Formulated With PLGA Microspheres. *J. Pharm. Invest.* **91**, 1019-1035 (2002).

61.   Igartua, M. et al. Enhanced immune response after subcutaneous and oral immunization with biodegradable PLGA microspheres. *J. Controlled Release* **56**, 63-73 (1998).

62.   Jia, J. et al. Adjuvanticity Regulation by Biodegradable Polymeric Nano/microparticle Size. *Mol. Pharmaceutics* **14**, 14-22 (2017).

63.   Roth, G.A. et al. Injectable Hydrogels for Sustained Codelivery of Subunit Vaccines Enhance Humoral Immunity. *ACS Cent. Sci.* (2020).

64.   Wang, Z.-B. et al. The mechanism of action of acid-soluble chitosan as an adjuvant in the formulation of nasally administered vaccine against HBV. *RSC Adv.* **6**, 96785-96797 (2016).

65.   Zhang, Y. et al. Metal-Organic-Framework-Based Vaccine Platforms for Enhanced Systemic Immune and Memory Response. *Adv. Funct. Mater.* **26**, 6454-6461 (2016).

66.   Van Der Lubben, I.M., Verhoef, J.C., van Aelst, A.C., Borchard, G. & Junginger, H.E. Chitosan microparticles for oral vaccination: preparation, characterization and preliminary in vivo uptake studies in murine Peyer's patches. *Biomaterials* **22**, 687-694 (2001).

67.   Harde, H., Agrawal, A.K. & Jain, S. Development of stabilized glucomannosylated chitosan nanoparticles using tandem crosslinking method for oral vaccine delivery. *Nanomedicine* **9**, 2511-2529 (2014).

68.   Bussio, J.I., Molina-Perea, C. & González-Aramundiz, J.V. Hyaluronic Acid Nanocapsules as a Platform for Needle-Free Vaccination. *Pharmaceutics* **11**, 246 (2019).

69.   Rydell, N., Stertman, L. & Sjöholm, I. Starch microparticles as vaccine adjuvant. *Expert Opin. Drug Delivery* **2**, 807-828 (2005).

70.   Wang, H. & Roman, M. Cellulose-based oral vaccine formulation for influenza virus. *Nanomedicine: Nanotechnology, Biology and Medicine* **12**, 489 (2016).

71.   Sarei, F., Dounighi, N.M., Zolfagharian, H., Khaki, P. & Bidhendi, S.M. Alginate nanoparticles as a promising adjuvant and vaccine delivery system. *Indian J. Pharm. Sci.* **75**, 442-449 (2013).

72.   Nagpal, P.S., Kesarwani, A., Sahu, P. & Upadhyay, P. Aerosol immunization by alginate coated mycobacterium (BCG/MIP) particles provide enhanced immune response and

protective efficacy than aerosol of plain mycobacterium against M.tb. H37Rv infection in mice. *BMC Infect. Dis.* **19**, 568 (2019).

73. Harde, H., Agrawal, A.K. & Jain, S. Tetanus Toxoids Loaded Glucomannosylated Chitosan Based Nanohoming Vaccine Adjuvant with Improved Oral Stability and Immunostimulatory Response. *Pharm. Res.* **32**, 122-134 (2015).

74. Walke, S. et al. Preparation and characterization of microencapsulated DwPT trivalent vaccine using water soluble chitosan and its in-vitro and in-vivo immunological properties. *Int. J. Biol. Macromol.* **107**, 2044-2056 (2018).

75. Jabbal-Gill, I., Watts, P. & Smith, A. Chitosan-based delivery systems for mucosal vaccines. *Expert Opin. Drug Delivery* **9**, 1051-1067 (2012).

76. Singh, B. et al. Needle-Free Immunization with Chitosan-Based Systems. *Int. J. Mol. Sci.* **19**, 3639 (2018).

77. Xing, L. et al. Chemical Modification of Chitosan for Efficient Vaccine Delivery. *Molecules* **23**, 229 (2018).

78. Gordon, S. et al. Chitosan hydrogels containing liposomes and cubosomes as particulate sustained release vaccine delivery systems. *J. Liposome Res.* **22**, 193-204 (2012).

79. Bobbala, S., Gibson, B., Gamble, A.B., McDowell, A. & Hook, S. Poloxamer 407-chitosan grafted thermoresponsive hydrogels achieve synchronous and sustained release of antigen and adjuvant from single-shot vaccines. *Immunol. Cell Biol.* **96**, 656-665 (2018).

80. Highton, A.J., Kojarunchitt, T., Girardin, A., Hook, S. & Kemp, R.A. Chitosan hydrogel vaccine generates protective CD8 T cell memory against mouse melanoma. *Immunol. Cell Biol.* **93**, 634-640 (2015).

81. Yoon, Y.M. et al. A combination hydrogel microparticle-based vaccine prevents type 1 diabetes in non-obese diabetic mice. *Sci. Rep.* **5**, 13155 (2015).

82. Luzuriaga, M.A. et al. A Whole Cell Metal-Organic Framework Encapsulated Vaccine Against Septicemic UPEC Infection. *bioRxiv* (2020).

83. Lee, A.L.Z., Yang, C., Gao, S., Hedrick, J.L. & Yang, Y.Y. Subcutaneous vaccination using injectable biodegradable hydrogels for long-term immune response. *Nanomedicine: Nanotechnology, Biology and Medicine* **21**, 102056 (2019).

84. Maghrebi, S., Jambhrunkar, M., Joyce, P. & Prestidge, C.A. Engineering PLGA–Lipid Hybrid Microparticles for Enhanced Macrophage Uptake. *ACS Appl. Bio Mater.* **3**, 4159-4167 (2020).

85. Liu, L. et al. Hyaluronic Acid-Modified Cationic Lipid–PLGA Hybrid Nanoparticles as a Nanovaccine Induce Robust Humoral and Cellular Immune Responses. *ACS Appl. Mater. Interfaces* **8**, 11969-11979 (2016).

86. Wang, N., Chen, M. & Wang, T. Liposomes used as a vaccine adjuvant-delivery system: From basics to clinical immunization. *J. Controlled Release* **303**, 130-150 (2019).

87. Corthésy, B. & Bioley, G. Lipid-Based Particles: Versatile Delivery Systems for Mucosal Vaccination against Infection. *Front. Immunol.* **9**, 431-431 (2018).

88. Salatin, S. et al. Hydrogel nanoparticles and nanocomposites for nasal drug/vaccine delivery. *Arch. Pharmacal Res.* **39**, 1181-1192 (2016).

89. Luzuriaga, M.A. et al. Enhanced Stability and Controlled Delivery of MOF-Encapsulated Vaccines and Their Immunogenic Response In Vivo. *ACS Appl. Mater. Interfaces* **11**, 9740-9746 (2019).

90.   Luzuriaga, M.A. et al. ZIF-8 degrades in cell media, serum, and some—but not all—common laboratory buffers. *Supramol. Chem.* **31**, 485-490 (2019).

91.   Wang, Y., Deng, L., Kang, S.-M. & Wang, B.-Z. Universal influenza vaccines: from viruses to nanoparticles. *Expert Rev. Vaccines* **17**, 967-976 (2018).

92.   Reddy, S.T., Swartz, M.A. & Hubbell, J.A. Targeting dendritic cells with biomaterials: developing the next generation of vaccines. *Trends Immunol.* **27**, 573-579 (2006).

93.   Yenkoidiok-Douti, L. & Jewell, C.M. Integrating Biomaterials and Immunology to Improve Vaccines Against Infectious Diseases. *ACS Biomater. Sci. Eng.* **6**, 759-778 (2020).

94.   Frangione-Beebe, M., Rose, R., Kaumaya, P. & Schwendeman, S. Microencapsulation of a synthetic peptide epitope for HTLV-1 in biodegradable poly (D, L-lactide-co-glycolide) microspheres using a novel encapsulation technique. *J. Microencapsulation* **18**, 663-677 (2001).

95.   Zhao, L. et al. Nanoparticle vaccines. *Vaccine* **32**, 327-337 (2014).

96.   Mody, K.T. et al. Mesoporous silica nanoparticles as antigen carriers and adjuvants for vaccine delivery. *Nanoscale* **5**, 5167-5179 (2013).

97.   Slütter, B. et al. Conjugation of ovalbumin to trimethyl chitosan improves immunogenicity of the antigen. *J. Controlled Release* **143**, 207-214 (2010).

98.   He, Q. et al. Calcium Phosphate Nanoparticle Adjuvant. *Clin. Diagn. Lab. Immunol.* **7**, 899-903 (2000).

99.   Bivas-Benita, M. et al. Generation of Toxoplasma gondii GRA1 protein and DNA vaccine loaded chitosan particles: preparation, characterization, and preliminary in vivo studies. *Int. J. Pharm.* **266**, 17-27 (2003).

100.   Boks, M.A. et al. Controlled release of a model vaccine by nanoporous ceramic microneedle arrays. *Int. J. Pharm.* **491**, 375-383 (2015).

101.   He, X. et al. Augmented humoral and cellular immune responses to hepatitis B DNA vaccine adsorbed onto cationic microparticles. *J. Controlled Release* **107**, 357-372 (2005).

102.   Alkie, T.N., Yitbarek, A., Taha-Abdelaziz, K., Astill, J. & Sharif, S. Characterization of immunogenicity of avian influenza antigens encapsulated in PLGA nanoparticles following mucosal and subcutaneous delivery in chickens. *PLOS ONE* **13**, e0206324 (2018).

103.   Chen, X. et al. Enhanced Humoral and Cell-Mediated Immune Responses Generated by Cationic Polymer-Coated PLA Microspheres with Adsorbed HBsAg. *Mol. Pharmaceutics* **11**, 1772-1784 (2014).

104.   Sexton, A. et al. A Protective Vaccine Delivery System for In Vivo T Cell Stimulation Using Nanoengineered Polymer Hydrogel Capsules. *ACS Nano* **3**, 3391-3400 (2009).

105.   Huang, C.-H., Huang, C.-Y. & Huang, M.-H. Impact of antigen-adjuvant associations on antigen uptake and antigen-specific humoral immunity in mice following intramuscular injection. *Biomed. Pharmacother.* **118**, 109373 (2019).

106.   Huang, M.-H. et al. Emulsified Nanoparticles Containing Inactivated Influenza Virus and CpG Oligodeoxynucleotides Critically Influences the Host Immune Responses in Mice. *PLOS ONE* **5**, e12279 (2010).

107.   Wang, S. et al. Manipulating the Selection Forces during Affinity Maturation to Generate Cross-Reactive HIV Antibodies. *Cell* **160**, 785-797 (2015).

108. Tam, H.H. et al. Sustained antigen availability during germinal center initiation enhances antibody responses to vaccination. *Proc. Natl. Acad. Sci. U. S. A.* **113**, E6639 (2016).

109. Han, S., Asoyan, A., Rabenstein, H., Nakano, N. & Obst, R. Role of antigen persistence and dose for CD4+ T-cell exhaustion and recovery. *Proc. Natl. Acad. Sci. U. S. A.* **107**, 20453 (2010).

110. Mueller, S.N. & Ahmed, R. High antigen levels are the cause of T cell exhaustion during chronic viral infection. *Proc. Natl. Acad. Sci. U. S. A.* **106**, 8623 (2009).

111. Cleland, J.L. Solvent Evaporation Processes for the Production of Controlled Release Biodegradable Microsphere Formulations for Therapeutics and Vaccines. *Biotechnol. Prog.* **14**, 102-107 (1998).

112. Guarecuco, R. et al. Immunogenicity of pulsatile-release PLGA microspheres for single-injection vaccination. *Vaccine* **36**, 3161-3168 (2018).

113. Smallshaw, J.E. & Vitetta, E.S. A lyophilized formulation of RiVax, a recombinant ricin subunit vaccine, retains immunogenicity. *Vaccine* **28**, 2428-2435 (2010).

114. Prego, C. et al. Chitosan-based nanoparticles for improving immunization against hepatitis B infection. *Vaccine* **28**, 2607-2614 (2010).

115. Bertram, U., Bernard, M.-C., Haensler, J., Maincent, P. & Bodmeier, R. In situ gelling nasal inserts for influenza vaccine delivery. *Drug Dev. Ind. Pharm.* **36**, 581-593 (2010).

116. Adams, J.R., Haughney, S.L. & Mallapragada, S.K. Effective polymer adjuvants for sustained delivery of protein subunit vaccines. *Acta Biomater.* **14**, 104-114 (2015).

117. Kim, Y.-C., Quan, F.-S., Compans, R.W., Kang, S.-M. & Prausnitz, M.R. Formulation and coating of microneedles with inactivated influenza virus to improve vaccine stability and immunogenicity. *J. Controlled Release* **142**, 187-195 (2010).

118. Dierendonck, M. et al. Nanoporous Hydrogen Bonded Polymeric Microparticles: Facile and Economic Production of Cross Presentation Promoting Vaccine Carriers. *Adv. Funct. Mater.* **24**, 4634-4644 (2014).

119. Nimtrakul, P., Atthi, R., Limpeanchob, N. & Tiyaboonchai, W. Development of Pasteurella multocida-loaded microparticles for hemorrhagic septicemia vaccine. *Drug Dev. Ind. Pharm.* **41**, 423-429 (2015).

120. Cooper, P.D. & Petrovsky, N. Delta inulin: a novel, immunologically active, stable packing structure comprising β-d-[2 → 1] poly(fructo-furanosyl) α-d-glucose polymers. *Glycobiology* **21**, 595-606 (2011).

121. Hashem, F.M., Fahmy, S.A., El-Sayed, A.M. & Al-Sawahli, M.M. Development and evaluation of chitosan microspheres for tetanus, diphtheria and divalent vaccines: a comparative study of subcutaneous and intranasal administration in mice. *Pharm. Dev. Technol.* **18**, 1175-1185 (2013).

122. Rizwan, S.B. et al. Cubosomes containing the adjuvants imiquimod and monophosphoryl lipid A stimulate robust cellular and humoral immune responses. *J. Controlled Release* **165**, 16-21 (2013).

123. Boopathy, A.V. et al. Enhancing humoral immunity via sustained-release implantable microneedle patch vaccination. *Proc. Natl. Acad. Sci. U. S. A.* **116**, 16473 (2019).

124. Demento, S.L. et al. Role of sustained antigen release from nanoparticle vaccines in shaping the T cell memory phenotype. *Biomaterials* **33**, 4957-4964 (2012).

125. O'Hagan, D.T. et al. The preparation, characterization and pre-clinical evaluation of an orally administered HIV-I vaccine, consisting of a branched peptide immunogen entrapped in controlled release microparticles. *J. Controlled Release* **36**, 75-84 (1995).

126. Gupta, R.K., Chang, A.-C., Griffin, P., Rivera, R. & Siber, G.R. In vivo distribution of radioactivity in mice after injection of biodegradable polymer microspheres containing 14C-labeled tetanus toxoid. *Vaccine* **14**, 1412-1416 (1996).

127. Cleland, J.L. et al. Development of a single-shot subunit vaccine for HIV-1. 5. Programmable in vivo autoboost and long lasting neutralizing response. *J. Pharm. Invest.* **87**, 1489-1495 (1998).

128. Raghuvanshi, R.S., Singh, O. & Panda, A.K. Formulation and Characterization of Immunoreactive Tetanus Toxoid Biodegradable Polymer Particles. *Drug Delivery* **8**, 99-106 (2001).

129. Feng, L. et al. Pharmaceutical and immunological evaluation of a single-dose hepatitis B vaccine using PLGA microspheres. *J. Controlled Release* **112**, 35-42 (2006).

130. Huang, C.-Y. et al. Polysorbasome: A Colloidal Vesicle Contoured by Polymeric Bioresorbable Amphiphiles as an Immunogenic Depot for Vaccine Delivery. *ACS Appl. Mater. Interfaces* **10**, 12553-12561 (2018).

131. Sinani, G. et al. Modified chitosan-based nanoadjuvants enhance immunogenicity of protein antigens after mucosal vaccination. *Int. J. Pharm.* **569**, 118592 (2019).

132. Liu, G. et al. Development of a single-dose recombinant CAMP factor entrapping poly(lactide-co-glycolide) microspheres-based vaccine against Streptococcus agalactiae. *Vaccine* **35**, 1246-1253 (2017).

133. Gallovic, M.D. et al. Microparticles formulated from a family of novel silylated polysaccharides demonstrate inherent immunostimulatory properties and tunable hydrolytic degradability. *J. Mater. Chem. B* **4**, 4302-4312 (2016).

134. Standley, S.M. et al. Acid-Degradable Particles for Protein-Based Vaccines: Enhanced Survival Rate for Tumor-Challenged Mice Using Ovalbumin Model. *Bioconjugate Chem.* **15**, 1281-1288 (2004).

135. Foster, S., Duvall, C.L., Crownover, E.F., Hoffman, A.S. & Stayton, P.S. Intracellular Delivery of a Protein Antigen with an Endosomal-Releasing Polymer Enhances CD8 T-Cell Production and Prophylactic Vaccine Efficacy. *Bioconjugate Chem.* **21**, 2205-2212 (2010).

136. Lv, M. et al. Redox-responsive hyperbranched poly(amido amine) and polymer dots as a vaccine delivery system for cancer immunotherapy. *J. Mater. Chem. B* **5**, 9532-9545 (2017).

137. Zhang, N.-Z. et al. Vaccination with Toxoplasma gondii calcium-dependent protein kinase 6 and rhoptry protein 18 encapsulated in poly(lactide-co-glycolide) microspheres induces long-term protective immunity in mice. *BMC Infect. Dis.* **16**, 168 (2016).

138. Leader, B., Baca, Q.J. & Golan, D.E. Protein therapeutics: a summary and pharmacological classification. *Nat. Rev. Drug Discovery* **7**, 21-29 (2008).

139. Xu, M. et al. Improved In Vitro and In Vivo Biocompatibility of Graphene Oxide through Surface Modification: Poly(Acrylic Acid)-Functionalization is Superior to PEGylation. *ACS Nano* **10**, 3267-3281 (2016).

140. Thirumalai, D. & Reddy, G. Are native proteins metastable? *Nat. Chem.* **3**, 910-911 (2011).

141. Mallamace, F. et al. Energy landscape in protein folding and unfolding. *Proc. Natl. Acad. Sci. U. S. A.* **113**, 3159-3163 (2016).

142. Carmichael, S.P. & Shell, M.S. Entropic (de) stabilization of surface-bound peptides conjugated with polymers. *J. Chem. Phys.* **143**, 243103 (2015).

143. Pisal, S., Wawde, G., Salvankar, S., Lade, S. & Kadam, S. Vacuum foam drying for preservation of LaSota virus: effect of additives. *AAPS Pharmscitech* **7**, E30-E37 (2006).

144. LeClair, D.A., Cranston, E.D., Lichty, B.D., Xing, Z. & Thompson, M.R. Consecutive spray drying to produce coated dry powder vaccines suitable for oral administration. *ACS Biomater. Sci. Eng.* **4**, 1669-1678 (2018).

145. Sridhar, B.V. et al. Thermal Stabilization of Biologics with Photoresponsive Hydrogels. *Biomacromolecules* **19**, 740-747 (2018).

146. Lee, P.W. et al. Biodegradable Viral Nanoparticle/Polymer Implants Prepared via Melt-Processing. *ACS Nano* **11**, 8777-8789 (2017).

147. Vrdoljak, A. et al. Induction of broad immunity by thermostabilised vaccines incorporated in dissolvable microneedles using novel fabrication methods. *J. Controlled Release* **225**, 192-204 (2016).

148. Alsaiari, S.K. et al. Endosomal Escape and Delivery of CRISPR/Cas9 Genome Editing Machinery Enabled by Nanoscale Zeolitic Imidazolate Framework. *J. Am. Chem. Soc.* **140**, 143-146 (2018).

149. Liang, K. et al. Biomimetic mineralization of metal-organic frameworks as protective coatings for biomacromolecules. *Nat. Commun.* **6**, 7240 (2015).

150. Li, S. et al. Template-Directed Synthesis of Porous and Protective Core–Shell Bionanoparticles. *Angew. Chem., Int. Ed.* **55**, 10691-10696 (2016).

151. Li, S. et al. Investigation of Controlled Growth of Metal–Organic Frameworks on Anisotropic Virus Particles. *ACS Appl. Mater. Interfaces* **10**, 18161-18169 (2018).

152. Wang, C. et al. Silk-Encapsulated Plasmonic Biochips with Enhanced Thermal Stability. *ACS Appl. Mater. Interfaces* **8**, 26493-26500 (2016).

153. Rosi, N.L., Eddaoudi, M., Kim, J., O'Keeffe, M. & Yaghi, O.M. Advances in the chemistry of metal-organic frameworks. *CrystEngComm* **4**, 401-404 (2002).

154. McGuire, C.V. & Forgan, R.S. The surface chemistry of metal–organic frameworks. *Chem. Commun.* **51**, 5199-5217 (2015).

155. Banerjee, R. et al. High-throughput synthesis of zeolitic imidazolate frameworks and application to CO2 capture. *Science* **319**, 939-943 (2008).

156. Hayashi, H., Côté, A.P., Furukawa, H., O'Keeffe, M. & Yaghi, O.M. Zeolite A imidazolate frameworks. *Nat. Mater.* **6**, 501-506 (2007).

157. Li, L. et al. Highly efficient separation of methane from nitrogen on a squarate-based metal-organic framework. *AIChE Journal* **64**, 3681-3689 (2018).

158. Huxley, M.T. et al. Protecting-group-free site-selective reactions in a metal–organic framework reaction vessel. *J. Am. Chem. Soc.* **140**, 6416-6425 (2018).

159. Otake, K.-I. et al. Single-Atom-Based Vanadium Oxide Catalysts Supported on Metal–Organic Frameworks: Selective Alcohol Oxidation and Structure–Activity Relationship. *J. Am. Chem. Soc.* **140**, 8652–8656 (2018).

160. Fan, C. et al. Silver Nanoclusters Encapsulated into Metal–Organic Frameworks with Enhanced Fluorescence and Specific Ion Accumulation toward the Microdot Array-Based Fluorimetric Analysis of Copper in Blood. *ACS Sens.* **3**, 441-450 (2018).

161. Zhuang, J. et al. Optimized metal–organic-framework nanospheres for drug delivery: evaluation of small-molecule encapsulation. *ACS nano* **8**, 2812-2819 (2014).

162. Adhikari, C., Das, A. & Chakraborty, A. Zeolitic imidazole framework (ZIF) nanospheres for easy encapsulation and controlled release of an anticancer drug doxorubicin under different external stimuli: a way toward smart drug delivery system. *Mol. Pharmaceutics* **12**, 3158-3166 (2015).

163. Zheng, H. et al. One-pot synthesis of metal–organic frameworks with encapsulated target molecules and their applications for controlled drug delivery. *J. Am. Chem. Soc.* **138**, 962-968 (2016).

164. Abánades Lázaro, I. et al. Surface-Functionalization of Zr-Fumarate MOF for Selective Cytotoxicity and Immune System Compatibility in Nanoscale Drug Delivery. *ACS Appl. Mater. Interfaces* **10**, 31146-31157 (2018).

165. Majewski, M.B. et al. Enzyme encapsulation in metal–organic frameworks for applications in catalysis. *CrystEngComm* **19**, 4082-4091 (2017).

166. Riccò, R. et al. Metal–Organic Frameworks for Cell and Virus Biology: A Perspective. *ACS Nano* **12**, 13-23 (2018).

167. Nadar, S.S. & Rathod, V.K. Encapsulation of lipase within metal-organic framework (MOF) with enhanced activity intensified under ultrasound. *Enzyme Microb. Technol.* **108**, 11-20 (2018).

168. Li, P. et al. Encapsulation of a nerve agent detoxifying enzyme by a mesoporous zirconium metal–organic framework engenders thermal and long-term stability. *J. Am. Chem. Soc.* **138**, 8052-8055 (2016).

169. Hoop, M. et al. Biocompatibility characteristics of the metal organic framework ZIF-8 for therapeutical applications. *Appl. Mater. Today* **11**, 13-21 (2018).

170. Maddigan, N.K. et al. Protein surface functionalisation as a general strategy for facilitating biomimetic mineralisation of ZIF-8. *Chem. Sci.* **9**, 4217-4223 (2018).

171. Liao, F.-S. et al. Shielding against Unfolding by Embedding Enzymes in Metal–Organic Frameworks via a de Novo Approach. *J. Am. Chem. Soc.* **139**, 6530-6533 (2017).

172. Duan, Y. et al. One-pot synthesis of a metal–organic framework-based drug carrier for intelligent glucose-responsive insulin delivery. *Chem. Commun.* **54**, 5377-5380 (2018).

173. Zhu, Q. et al. Nano-Biocatalysts of Cyt c@ZIF-8/GO Composites with High Recyclability via a de Novo Approach. *ACS Appl. Mater. Interfaces* **10**, 16066-16076 (2018).

174. Deng, H. et al. Large-pore apertures in a series of metal-organic frameworks. *science* **336**, 1018-1023 (2012).

175. Chen, Y., Li, P., Modica, J.A., Drout, R.J. & Farha, O.K. Acid-Resistant Mesoporous Metal–Organic Framework toward Oral Insulin Delivery: Protein Encapsulation, Protection, and Release. *J. Am. Chem. Soc.* **140**, 5678-5681 (2018).

176. Li, P. et al. Toward design rules for enzyme immobilization in hierarchical mesoporous metal-organic frameworks. *Chem* **1**, 154-169 (2016).

104

177. Lyu, F., Zhang, Y., Zare, R.N., Ge, J. & Liu, Z. One-Pot Synthesis of Protein-Embedded Metal–Organic Frameworks with Enhanced Biological Activities. *Nano Letters* **14**, 5761-5765 (2014).

178. Xu, A.-W., Ma, Y. & Cölfen, H. Biomimetic mineralization. *J. Mater. Chem.* **17**, 415-449 (2007).

179. Maurer, P. et al. A therapeutic vaccine for nicotine dependence: preclinical efficacy, and phase I safety and immunogenicity. *Eur. J. Immunol.* **35**, 2031-2040 (2005).

180. Stephanopoulos, N. & Francis, M.B. Choosing an effective protein bioconjugation strategy. *Nat. Chem. Biol.* **7**, 876-884 (2011).

181. Rybicki, E.P. Plant-based vaccines against viruses. *Virol. J.* **11**, 205 (2014).

182. Banik, S. et al. Development of a multivalent subunit vaccine against tularemia using tobacco mosaic virus (TMV) based delivery system. *PloS one* **10**, e0130858 (2015).

183. Gasanova, T.V., Petukhova, N.V. & Ivanov, P.A. Chimeric particles of tobacco mosaic virus as a platform for the development of next-generation nanovaccines. *Nanotechnol. Russ.* **11**, 227-236 (2016).

184. Masarapu, H. et al. Physalis mottle virus-like particles as nanocarriers for imaging reagents and drugs. *Biomacromolecules* **18**, 4141-4153 (2017).

185. Dharmarwardana, M. et al. Nitroxyl Modified Tobacco Mosaic Virus as a Metal-Free High-Relaxivity MRI and EPR Active Superoxide Sensor. *Mol. Pharmaceutics* **15**, 2973–2983 (2018).

186. Bäcker, M. et al. Tobacco mosaic virus as enzyme nanocarrier for electrochemical biosensors. *Sens. Actuators, B* **238**, 716-722 (2017).

187. Anderson, C.E. et al. Dual Contrast-Magnetic Resonance Fingerprinting (DC-MRF): A Platform for Simultaneous Quantification of Multiple MRI Contrast Agents. *Sci. Rep.* **7**, 8431 (2017).

188. Pitek, A.S. et al. Elongated Plant Virus-Based Nanoparticles for Enhanced Delivery of Thrombolytic Therapies. *Mol. Pharmaceutics* **14**, 3815-3823 (2017).

189. Finbloom, J.A. et al. Stable disk assemblies of a tobacco mosaic virus mutant as nanoscale scaffolds for applications in drug delivery. *Bioconjugate Chem.* **27**, 2480-2485 (2016).

190. Cossé, A., König, C., Lamprecht, A. & Wagner, K.G. Hot Melt Extrusion for Sustained Protein Release: Matrix Erosion and In Vitro Release of PLGA-Based Implants. *AAPS Pharmscitech* **18**, 15-26 (2017).

191. Ren, Y., Shi, X., Sun, Q. & Sun, L. Dual-controlled oral colon-targeted delivery of bovine insulin based on mesoporous phosphonate. *Mater. Res. Bull.* **48**, 4850-4855 (2013).

192. Majewski, M., Noh, H., Islamoglu, T. & Farha, O.K. NanoMOFs: little crystallites for substantial applications. *J. Mater. Chem. A* **6**, 7338-7350 (2018).

193. Jha, S.K. & Marqusee, S. Kinetic evidence for a two-stage mechanism of protein denaturation by guanidinium chloride. *Proc. Natl. Acad. Sci. U. S. A.* **111**, 4856-4861 (2014).

194. Zhang, H., Chen, W., Gong, K. & Chen, J. Nanoscale Zeolitic Imidazolate Framework-8 as Efficient Vehicles for Enhanced Delivery of CpG Oligodeoxynucleotides. *ACS Appl. Mater. Interfaces* **9**, 31519-31525 (2017).

195. Schade, D.S. THE TIMING OF MEAL INSULIN ADMINISTRATION. *Endocr. Pract.* **23**, 1482-1484 (2017).

196. Barter, M. et al. Simultaneous neutron powder diffraction and microwave dielectric studies of ammonia absorption in metal–organic framework systems. *Phys. Chem. Chem. Phys.* **20**, 10460-10469 (2018).

197. Wang, Y. et al. Photoelectrochemical biosensor for protein kinase A detection based on carbon microspheres, peptide functionalized Au-ZIF-8 and TiO2/g-C3N4. *Talanta* **196**, 197-203 (2019).

198. Abánades Lázaro, I., Abánades Lázaro, S. & Forgan, R.S. Enhancing anticancer cytotoxicity through bimodal drug delivery from ultrasmall Zr MOF nanoparticles. *Chem. Commun.* **54**, 2792-2795 (2018).

199. Teplensky, M.H. et al. Temperature Treatment of Highly Porous Zirconium-Containing Metal–Organic Frameworks Extends Drug Delivery Release. *J. Am. Chem. Soc.* **139**, 7522-7532 (2017).

200. Bellido, E. et al. Understanding the Colloidal Stability of the Mesoporous MIL-100(Fe) Nanoparticles in Physiological Media. *Langmuir* **30**, 5911-5920 (2014).

201. Oettl, K. & Stauber, R.E. Physiological and pathological changes in the redox state of human serum albumin critically influence its binding properties. *Br. J. Pharmacol.* **151**, 580-590 (2007).

202. Lu, J., Stewart, Alan J., Sadler, Peter J., Pinheiro, Teresa J.T. & Blindauer, Claudia A. Albumin as a zinc carrier: properties of its high-affinity zinc-binding site. *Biochem. Soc. Trans.* **36**, 1317-1321 (2008).

203. Cui, S.-F. et al. Novel hybrids of metronidazole and quinolones: synthesis, bioactive evaluation, cytotoxicity, preliminary antimicrobial mechanism and effect of metal ions on their transportation by human serum albumin. *Eur. J. Med. Chem.* **86**, 318-334 (2014).

204. Stewart, A.J., Blindauer, C.A., Berezenko, S., Sleep, D. & Sadler, P.J. Interdomain zinc site on human albumin. *Proc. Natl. Acad. Sci. U. S. A.* **100**, 3701 (2003).

205. Hink, M.A. et al. Structural dynamics of green fluorescent protein alone and fused with a single chain Fv protein. *J. Biol. Chem.* **275**, 17556-17560 (2000).

206. Liang, W. et al. Control of Structure Topology and Spatial Distribution of Biomacromolecules in Protein@ZIF-8 Biocomposites. *Chem. Mater.* **30**, 1069-1077 (2018).

207. Abánades Lázaro, I. et al. Selective Surface PEGylation of UiO-66 Nanoparticles for Enhanced Stability, Cell Uptake, and pH-Responsive Drug Delivery. *Chem* **2**, 561-578 (2017).

208. Sugianli, A.K. et al. Antimicrobial resistance in uropathogens and appropriateness of empirical treatment: a population-based surveillance study in Indonesia. *J. Antimicrob. Chemother.* **72**, 1469-1477 (2017).

209. Terlizzi, M.E., Gribaudo, G. & Maffei, M.E. UroPathogenic Escherichia coli (UPEC) Infections: Virulence Factors, Bladder Responses, Antibiotic, and Non-antibiotic Antimicrobial Strategies. *Front. Microbiol.* **8**, 1566 (2017).

210. Foxman, B. Epidemiology of urinary tract infections: Incidence, morbidity, and economic costs. *Dis.-Mon.* **49**, 53-70 (2003).

211. Neugent, M.L., Hulyalkar, N.V., Nguyen, V.H., Zimmern, P.E. & De Nisco, N.J. Advances in Understanding the Human Urinary Microbiome and Its Potential Role in Urinary Tract Infection. *mBio* **11**, e00218-00220 (2020).

212. Majeed, A., Alarfaj, S., Darouiche, R. & Mohajer, M. An update on emerging therapies for urinary tract infections. *Expert Opin. Emerging Drugs* **22**, 53-62 (2017).

213. Hooton, T.M. Recurrent urinary tract infection in women. *Int. J. Antimicrob. Agents* **17**, 259-268 (2001).

214. Mellata, M., Mitchell, N.M., Schödel, F., Curtiss, R. & Pier, G.B. Novel vaccine antigen combinations elicit protective immune responses against Escherichia coli sepsis. *Vaccine* **34**, 656-662 (2016).

215. Artero, A. et al. Prognostic factors of mortality in patients with community-acquired bloodstream infection with severe sepsis and septic shock. *J. Crit. Care* **25**, 276-281 (2010).

216. Labelle, A. et al. The determinants of hospital mortality among patients with septic shock receiving appropriate initial antibiotic treatment*. *Crit. Care Med.* **40**, 2016-2021 (2012).

217. Foxman, B. Urinary tract infection syndromes: occurrence, recurrence, bacteriology, risk factors, and disease burden. *Infect. Dis. Clin. North Am.* **28**, 1-13 (2014).

218. Asadi Karam, M.R., Oloomi, M., Mahdavi, M., Habibi, M. & Bouzari, S. Vaccination with recombinant FimH fused with flagellin enhances cellular and humoral immunity against urinary tract infection in mice. *Vaccine* **31**, 1210-1216 (2013).

219. Farajzadah Sheikh, A. et al. Virulence-associated genes and drug susceptibility patterns of uropathogenic Escherichia coli isolated from patients with urinary tract infection. *Infect. Drug Resist.* **12**, 2039-2047 (2019).

220. Blackburn, N.K. & Besselaar, T.G. A study of the effect of chemical inactivants on the epitopes of Rift Valley fever virus glycoproteins using monoclonal antibodies. *J. Virol. Methods* **33**, 367-374 (1991).

221. Tsen, S.-W.D. et al. Chemical-free inactivated whole influenza virus vaccine prepared by ultrashort pulsed laser treatment. *J. Biomed. Opt.* **20**, 051008 (2014).

222. Frey, J. Biological safety concepts of genetically modified live bacterial vaccines. *Vaccine* **25**, 5598-5605 (2007).

223. Astria, E. et al. Carbohydrates@MOFs. *Mater. Horiz.* **6**, 969-977 (2019).

224. Liang, K. et al. Metal–Organic Framework Coatings as Cytoprotective Exoskeletons for Living Cells. *Adv. Mater.* **28**, 7910-7914 (2016).

225. Li, S. et al. Hierarchical Porous Carbon Arising from Metal–Organic Framework-Encapsulated Bacteria and Its Energy Storage Potential. *ACS Appl. Mater. Interfaces* **12**, 11884-11889 (2020).

226. Kaper, J.B., Nataro, J.P. & Mobley, H.L.T. Pathogenic Escherichia coli. *Nat. Rev. Microbiol.* **2**, 123-140 (2004).

227. Spurbeck, R.R. et al. Fimbrial Profiles Predict Virulence of Uropathogenic Escherichia coli Strains: Contribution of Ygi and Yad Fimbriae. *Infect. Immun.* **79**, 4753-4763 (2011).

228. Alteri, C.J., Hagan, E.C., Sivick, K.E., Smith, S.N. & Mobley, H.L.T. Mucosal Immunization with Iron Receptor Antigens Protects against Urinary Tract Infection. *PLoS Pathog.* **5**, e1000586 (2009).

229. Moriel, D.G. et al. Identification of protective and broadly conserved vaccine antigens from the genome of extraintestinal pathogenic Escherichia coli. *Proc. Natl. Acad. Sci. U. S. A.* **107**, 9072-9077 (2010).

230. Jalava, K., Hensel, A., Szostak, M., Resch, S. & Lubitz, W. Bacterial ghosts as vaccine candidates for veterinary applications. *J. Controlled Release* **85**, 17-25 (2002).

231. Torres, J.F., Lyerly, D.M., Hill, J.E. & Monath, T.P. Evaluation of formalin-inactivated *Clostridium difficile* vaccines administered by parenteral and mucosal routes of immunization in hamsters. *Infect. Immun.* **63**, 4619-4627 (1995).

232. Sunwoo, H.H., Lee, E.N., Menninen, K., Suresh, M.R. & Sim, J.S. Growth Inhibitory Effect of Chicken Egg Yolk Antibody (IgY) on Escherichia coli O157:H7. *J. Food Sci.* **67**, 1486-1494 (2002).

233. Couñago, R.M. et al. Imperfect coordination chemistry facilitates metal ion release in the Psa permease. *Nat. Chem. Biol.* **10**, 35-41 (2014).

234. Velasco, E. et al. A new role for Zinc limitation in bacterial pathogenicity: modulation of α-hemolysin from uropathogenic Escherichia coli. *Sci. Rep.* **8**, 6535 (2018).

235. McDevitt, C.A. et al. A Molecular Mechanism for Bacterial Susceptibility to Zinc. *PLoS Pathog.* **7**, e1002357 (2011).

236. Pape, K.A., Catron, D.M., Itano, A.A. & Jenkins, M.K. The Humoral Immune Response Is Initiated in Lymph Nodes by B Cells that Acquire Soluble Antigen Directly in the Follicles. *Immunity* **26**, 491-502 (2007).

237. Tanaka, T., Narazaki, M. & Kishimoto, T. IL-6 in inflammation, immunity, and disease. *Cold Spring Harbor Perspect. Biol.* **6**, a016295 (2014).

238. Sun, C.-Y. et al. Zeolitic imidazolate framework-8 as efficient pH-sensitive drug delivery vehicle. *Dalton Trans.* **41**, 6906-6909 (2012).

239. Durymanov, M. et al. Cellular Uptake, Intracellular Trafficking, and Stability of Biocompatible Metal-Organic Framework (MOF) Particles in Kupffer Cells. *Mol. Pharmaceutics* **16**, 2315-2325 (2019).

240. Zhong, X. et al. An aluminum adjuvant-integrated nano-MOF as antigen delivery system to induce strong humoral and cellular immune responses. *J. Controlled Release* **300**, 81-92 (2019).

241. Obst, R. et al. Sustained antigen presentation can promote an immunogenic T cell response, like dendritic cell activation. *Proc. Natl. Acad. Sci. U. S. A.* **104**, 15460-15465 (2007).

242. Spellberg, B. & Edwards, J.E., Jr. Type 1/Type 2 Immunity in Infectious Diseases. *Clin. Infect. Dis.* **32**, 76-102 (2001).

243. Natarajan, K. et al. The Role of Molecular Flexibility in Antigen Presentation and T Cell Receptor-Mediated Signaling. *Front. Immunol.* **9**, 1657 (2018).

244. Durant, L. et al. Identification of Candidates for a Subunit Vaccine against Extraintestinal Pathogenic Escherichia coli. *Infect. Immun.* **75**, 1916-1925 (2007).

245. Sidjabat, H.E. et al. Colonisation dynamics and virulence of two clonal groups of multidrug-resistant Escherichia coli isolated from dogs. *Microbes Infect.* **11**, 100-107 (2009).

246. Park, J.W., Kim, Y., Lee, K.-J. & Kim, D.J. Novel Cyanine Dyes with Vinylsulfone Group for Labeling Biomolecules. *Bioconjugate Chem.* **23**, 350-362 (2012).

247. Pédelacq, J.-D., Cabantous, S., Tran, T., Terwilliger, T.C. & Waldo, G.S. Engineering and characterization of a superfolder green fluorescent protein. *Nat. Biotechnol.* **24**, 79-88 (2006).

BIOGRAPHICAL SKETCH

Michael A. Luzuriaga was born May 24, 1992 at the La Habra Hospital in La Habra, California. His family has lived in Hacienda Heights, California and his mother moved to Riverside, CA in 2006 after his parents got divorced. Michael is of Peruvian descent, is the oldest of three brothers and is very family oriented. After graduating from Wilson High School in 2010, Michael enrolled to Fullerton College in Fullerton, California to pursue a major in electrical engineering. In 2012, he transferred to the California State Polytechnic University in Pomona, California and in 2013 switched his major to chemistry after taking organic chemistry with Dr. Michael Page. In 2014, he joined Dr. Page's lab to do research in the field of green chemistry that focused in developing new polymers from seed oils. In March 2016, Michael received his Bachelor of Science in Chemistry and worked at Dunn-Edwards Paints Company for 3 months. In August 2016, he entered the Chemistry graduate program at The University of Texas at Dallas in Richardson, Texas and joined Dr. Jeremiah J. Gassensmith's Lab in October. From 2016 - 2020, he has devoted his time to investigating ZIF-8 as a new biomaterial to protect antigens from denaturation and as an adjuvant to enhance the immune activation. As of October 2020, he has published 10 peer reviewed articles with three being first author. His time spent with Dr. Gassensmith has made him a better writer, researcher, and mentor. In October 2020, He accepted a postdoc position at Harvard Medical School in Boston, Massachusetts to conduct research for Dr. Malley on multiple antigen presenting system (MAPS).

Michael A. Luzuriaga

CurriculumVitae

Linkedin: https://www.linkedin.com/in/michael-luzuriaga-95bb38185/
Email: mal161930@utdallas.edu
Twitter: https://twitter.com/Luzuriaga_24

Education

Candidate for Doctor of Philosophy in Chemistry (Expected 2020)
University of Texas at Dallas, Richardson, TX, USA
Advisor: Professor Jeremiah. J. Gassensmith
Thesis Title: A New Biomaterial for Vaccination: An Aqueous ZIF-8 Crystal Growth to Preserve and Enhance the Immune Activation

Bachler of Science in Chemistry (2016)
California State Polytechnic University (Cal Poly Pomona), Pomona, CA, USA
Advisor: Prof. Michael Page
Thesis Title: "Purification of Poly-hydroxylated Biodiesel: Green Plastics from Renewable Sources"

Awards, Scholarships, and Fellowships

Minnie K. Patton Scholarship, 2020
Dissertation Research Award, 2020
Minnie K. Patton Endowed Scholarship, 2019
Julia William Van Ness Merit Scholarship, 2019
David Daniel Thesis Award, 2019
Hispanic scholarship funds (HSF) Scholar (2017-2019)
University of Texas at Dallas Graduate Studies Scholarship (2016 - Present)
Society of Adv. Chicanos and Native Americans in Science Travel Scholarship (SACNAS), 2017
Hispanic Scholarship Foundation Scholar (2017 - Present)
Louis Stokes Alliances for Minority Participation Program (2015-2016)

Professional Memberships

American Chemical Society	Member (2016 – Present)
SACNAS National Chapter	Member (2017 – Present)
SACNAS The University of Texas at Dallas Chapter	Officer: National Liaison (2017-2018)
Chemistry Graduate Student Association	Officer: Marketing Manager (2017-2018)
SACNAS The University of Texas at Dallas Chapter	Officer: Vice President (2017-2018)
SACNAS The University of Texas at Dallas Chapter	Officer: Vice President (2017-2018)

Research Experiences

University of Texas at Dallas, Aug 2016 - Present
Department of Chemistry and Biochemistry; Advisor: Prof. Jeremiah. J. Gassensmith
Graduate student researches a new fabrication method to make microneedles, improving the storage of vaccines and the efficiency of drugs to reach its target site. Projects focus is with Tobacco Mosaic Virus as the carrier for delivering drugs and using the 3D printer to fabricate biomedical applications.
Dunn-Edwards Paints, Los Angeles, CA, USA, Mar. 2016 – July 2016
Research contract on paint development and optimization of existing paint formulations.
University of Cal Poly Pomona, Sept. 2014 - Mar. 2016
Department of Chemistry, Pomona, CA, USA; Advisor: Prof. Michael Page
Undergraduate Researcher worked on the analysis of poly-hydroxylated biodiesel via GC-MS. Separated chemical compounds using Normal Phase column chromatography. These compounds were used to make green polyurethanes. The analysis via GC-MS determined the abundance of the compounds used to make the polyurethanes.

Publications

1. **M. A. Luzuriaga**, F. C. Herbert, O. R. Brohlin, A. Shahrivarkevishahi, Y. H. Wijesundara, K. Veera, C. E. Benjamin, S. Popal, M. D. Burton, M. A. Ingersoll, N. J. D. Nisco, J. J. Gassensmith*. "A Whole Cell Metal-Organic Framework Encapsulated Vaccine Against Septicemic UPEC Infection" bioRxiv, **2020**. DOI: 10.1101/2020.06.14.148452. Submitted for Review

2. F. C. Herbert, O. R. Brohlin, T. Galbraith, C. E. Benjamin, C. A. Reyes, **M. A. Luzuriaga**, A. Shahrivarkevishahi, J. J. Gassensmith*. "Supramolecular Encapsulation of Small-Ultrared Fluorescent Proteins in Virus-Like Nanoparticles for Noninvasive In Vivo Imaging Agents" *Bioconjugate Chem.* **2020**, *31*, 1529-1536. DOI: 10.1021/acs.bioconjchem.0c00190

3. S. Li, X. Zhou, Z. Chen, F. C. Herbert, R. Jayawickramage, S. D. Panangala, **M. A. Luzuriaga**, S. B. Alahakoon, S. D. Diwakara, X. Meng, L. Fei, J. Ferraris, R. A. Smaldone, J. J. Gassensmith*. "Hierarchical Porous Carbon Arising from Metal–Organic Framework-Encapsulated Bacteria and Its Energy Storage Potential" *ACS Appl. Mater. Interfaces* **2020**, *12*, 11884-11889. DOI: 10.1039/C9SC05510J

4. H. Lee, A. Shahrivarkevishahi, J. L. Lumata, **M. A. Luzuriaga**, L. M. Hagge, C. E. Benjamin, O. R. Brohlin, C. R. Parish, H. R. Firouzi, S. O. Nielsen, L. L. Lumata, J. J. Gassensmith*. "Supramolecular and Biomacromolecular Enhancement of Metal-Free Magnetic Resonance Imaging Contrast Agents" *Chemical Science* **2020**, *11*, 2045-2050. DOI: 10.1039/C9SC05510J

5. **M. A. Luzuriaga**, C. E. Benjamin, M. W. Gaertner, H. Lee, F. C. Herbert, S. Mallick, J. J. Gassensmith*. "ZIF-8 Degrades in Cell Media, Serum, and Some—but Not All—Common Laboratory Buffers" *Supramolecular Chemistry* **2019**, *31*, 485-490. DOI: 10.1080/10610278.2019.1616089

6. **M. A. Luzuriaga**, R. P. Welch, M. Dharmarwardana, C. E. Benjamin, S. Li, A. Shahrivarkevishahi, S. Popal, L. H. Tuong, C. T. Creswell, J. J. Gassensmith*. "Enhanced Stability and Controlled Delivery of MOF-Encapsulated Vaccines and Their Immunogenic Response In Vivo." *ACS Appl. Mater. Interfaces* **2019**, *11*, 9740-9746. DOI: 10.1021/acsami.8b20504

7. G. A. Appuhamillage, D. R. Berry, C. E. Benjamin, **M. A. Luzuriaga**, J. C. Reagan, J. J. Gassensmith, R. A. Smaldone*. "A Biopolymer Based 3D Printable Hydrogel for Toxic Metal Adsorption from Water." *Poly. Int.* **2019**, In Press. DOI: 10.1002/pi.5787

8. R. P. Welch, H. Lee, **M. A. Luzuriaga**, O. R. Brohlin, and J. J. Gassensmith*. "Protein-Polymer Delivery: Chemistry from the Cold Chain to the Clinic." Bioconjugate Chem. **2018**, *29*, 2867-2883. DOI: 10.1021/acs.bioconjchem.8b00483

9. M. Dharmarwardana,‡ B. S. Arimilli,‡ **M. A. Luzuriaga**, S. Kwon, H. Lee, G. A. Appuhamillage, G. T. McCandless, R. A. Smaldone, J. J. Gassensmith*. "The Thermo-Responsive Behavior in Molecular Crystals of Naphthalene Diimides and their 3D Printed Thermochromic Composites." *CrystEngComm* **2018**, *20*, 6054-6060. ‡co-first authors DOI: 10.1039/c8ce00798e

10. M. Dharmarwardana, A. F. Martins, Z. Chen, P. M. Palacios, C. M. Nowak, R. P. Welch, S. Li, **M. A. Luzuriaga**, L. Bleris, B. S. Pierce, A. D. Sherry, J. J. Gassensmith*."Nitroxyl Modified Tobacco Mosaic Virus as a Metal-Free High-Relaxivity MRI and EPR Active Superoxide Sensor." *Mol. Pharm.*, **2018**, *15*, 2973-2983. DOI: 10.1021/acs.molpharmaceut.8b00262

11. **M. A. Luzuriaga**; D.R. Berry, J.C. Reagan, R.A. Smaldone, J.J. Gassensmith*. "Biodegradable 3D printed polymer microneedles for transdermal drug delivery." *Lab Chip* **2018**, *18*, 1223-1230. DOI: 10.1039/C8LC00098K

Meeting and Conferences

1. **M. A. Luzuriaga**, S. Popal, A. Shahrivarkevishahi, J. J. Gassensmith, **Contributed** Poster on "*MOF-Based Vaccine Enhances Immunity in Vaccinated Mice*" SACNAS National Meeting, Virtual Conference. October 20, **2020**.

2. **M. A. Luzuriaga**, S. Popal, A. Shahrivarkevishahi, J. J. Gassensmith, **Contributed** Poster on "*MOF-Based Vaccine Enhances Immunity in Vaccinated Mice*" National Organization for the Professional Advancement of Black Chemists and Chemical Engineers (NOBCChe) National Meeting, Virtual Conference. September 24, **2020**.

3. **M. A. Luzuriaga**, R. P. Welch, M. Dharmarwardana, C. E. Benjamin, S. Popal, J. J. Gassensmith, **Contributed** Lecture on "*Enhanced Immunogenic Response of Biomimetic Mineralized Vaccines*" ACS National Meeting, San Diego, CA, USA. August 28, **2019**.

4. **M. A. Luzuriaga**, R. P. Welch, M. Dharmarwardana, C. E. Benjamin, S. Popal, L. H. Tuong, J. J. Gassensmith, **Contributed** Lecture on "*Enhanced Immunogenic Response of Biomimetic Mineralized Vaccines*" University of North Texas 52nd DFW/ACS Meeting-in-Miniature, Denton, TX, USA. April 27, **2019**. Awarded first place prize for Best Talk.

5. **M. A. Luzuriaga**, R. P. Welch, M. Dharmarwardana, C. E. Benjamin, S. Popal, L. H. Tuong, J. J. Gassensmith, **Contributed** Poster on "Enhanced Immunogenic Response of Biomimetic Mineralized Vaccines." The Physical Virology Gordon Research Conference, Ventura Beach, CA, USA. January 20, **2019**.

6. **M.A. Luzuriaga**, D.R. Berry, R.A. Smaldone, J. J. Gassensmith, **Contributed** lecture on " Microneedles Produced via 3D Printing for Transdermal Drug Delivery." <u>Southern Methodist University meeting in miniature</u>, Dallas, TX, USA. April 21, **2018**.
7. **M.A. Luzuriaga**, D.R. Berry, J.C. Reagan, R.A. Smaldone, J. J. Gassensmith, **Contributed** poster on " Low Cost 3D Printed Microneedles for Transdermal Drug Delivery." <u>American Chemical Society National Conference</u>, New Orleans, LA, USA. March 21, **2018**. Presented at Sci-Mix event. Awarded Poster Nomination.
8. **M.A. Luzuriaga**, D.R. Berry, J.C. Reagan, R.A. Smaldone, J. J. Gassensmith, **Contributed** lecture on " Low Cost 3D Printed Microneedles for Transdermal Drug Delivery." <u>UT Dallas Alumni Association</u>, Dallas, TX, USA. September 22, **2017**.
9. **M.A. Luzuriaga**, D.R. Berry, J.C. Reagan, R.A. Smaldone, J. J. Gassensmith, **Contributed** lecture on " Microneedles Produced via Fused Filament Fabrication 3D Printing for Transdermal Drug Delivery." <u>SACNAS National Conference</u>, Salt Lake City, UT, USA. October 20, **2017**.
10. **M.A. Luzuriaga**, M.F.Z. Page, **Contributed** Lecture on "*Analysis of Poly-hydroxylated Biodiesel Through GC-MS.*" <u>Student Research Conference</u> at Cal Poly Pomona, CA, USA. March 4, **2016.**
11. **M.A. Luzuriaga**, M.F.Z. Page, **Contributed** Poster on "*Purification of Poly-hydroxylated Biodiesel: Green Plastics from Renewable Sources.*" <u>Southern California Conference for Undergraduate Research</u> at Harvey Mudd College, CA, USA. November 23, **2015**.

Technical Proficiency

Laboratory Skills
Mice handling and Injection, Tissue harvesting, flow cytometry, ELISA (antibodies and cytokines), MOF synthesis, Cell techniques, Chromatographic methods, Organic synthesis, Virus Isolations, and Chemical Etching.

Instrumentation Methods
Animal Imager, Circular Dichroism, Atomic Force Microscopy, ESI-MS, FT-IR spectroscopy, Fluorescence spectroscopy, GC-MS, HPLC, NMR spectroscopy (1D, 2D), Single crystal and powder X-ray diffraction, SEM, TEM, UV-Vis, 3D printing, MRI, DSC, and TGA.

Computer/ IT
Adobe Illustrator, Chemdraw, Blender, Cura, Microsoft office (Word, Excel, PowerPoint, One Note), Origin, Nano Drop, Top Spin, Image J, Graphpad, and Chimera.

Teaching Experience

Teaching Assistant (TA) for CHEM 2123 "Organic Chemistry Lab I"   **Aug 2017 - Present**
University of Texas at Dallas
TA for CHEM 2125 "Organic Chemistry Lab II"   **Aug 2016 – Aug 2017**
University of Texas at Dallas
Chemistry Tutor for General Chemistry   **Aug 2015 - Mar 2016**
Cal Poly Pomona